Ministry of Higher Education
and Scientific Research
University of Kerbala
College of Education for Pure Sciences

Pure Sciences International Journal of Kerbala

Year:2025
Volume : 2
ISSUE : 7

ISSN: 6188-2789 Print
3005 -2394 Online

PURE
SCIENCES
International Journal of Kerbala

Pure Sciences International Journal of Kerbala

(PSIJK) is published in four issues annually

A quarterly peer-reviewed scientific journal issued by the College of Education for Pure Sciences at the University of Kerbala, specializing in pure sciences, accredited for the purposes of scientific promotion Pursuant to Ministerial Resolution No. **B.T 7575** Dated **14 /9 /2023**

Licensed by

Ministry of Higher Education
and Scientific Research and Scientific Research

Issued by

University of Kerbala
College of Education for Pure Sciences

2025 , Volume 2 , Issue 7
30 September

Ministry of Higher Education and Scientific Research

College of Education for Pure Sciences

University of Kerbala

Print ISSN: 6188-2789

Online ISSN: 3005 -2394

Consignment Number in the Housebook and Iraqi

Documents: 2515, 2021

Postal Code: 56001

Mailbox: 232

Mobile: +964 7769920165

https://journals.uokerbala.edu.iq

Iraq - Holy Karbala

Workflow by OJS/PKP

About the Journal

The "Pure Sciences International Journal of Kerbala", published quarterly and distributed internationally by the College of Education for Pure Sciences provides a forum for publication of significant science advancements and developments in chemistry, biology, computer, physics, mathematics and interdisciplinary areas of science. All prospective authors are invited to submit their original contributions on new theoretical and applied aspects of growing research. All manuscripts submitted, including symposium papers, will be peer reviewed by qualified scholars assigned by the editorial board.

You are cordially encouraged to use this journal as a means of dissemination of information on the various facets of science and technical problems; and to impart specialized knowledge, quality and excellence to strengthen the perception of technological resources and needs of the world. The PSIJK is looking forward to receiving your assistance to working together to develop a worthwhile, high quality journal.

Aims and Scope

Pure Sciences International Journal of Kerbala is an open-access, interdisciplinary, single-blind peer-reviewed journal that consolidates research activities in the experimental and theoretical aspects of modern sciences. The journal aims to make significant contributions to applied research and knowledge globally through the publication of original high-quality research papers and review articles on recent advances and frontier achievements in Biology, Mathematics, Chemistry, Physics, and Computer Science, as well as their related and subfields.

Scope of Research

The journal encompasses both fundamental and applied investigations across a wide range of interdisciplinary topics. Articles of an interdisciplinary nature are particularly welcome. Any paper reporting scientifically accurate and valuable research that adheres to accepted ethical and scientific publishing standards will be considered for publication.

Publication Ethics

Pure Sciences International Journal of Kerbala is committed to upholding the highest standards of publication ethics. We adhere to the principles and policies outlined by the Committee on Publication Ethics (COPE).

Duties of Editors

- Editors have full authority to reject or accept manuscripts.
- Editors maintain the confidentiality of submitted manuscripts under review until they are published.
- Editors preserve the anonymity of reviewers.
- Editors disclose and try to avoid any conflict of interest.
- Editors comment on ethical questions and possible misconduct raised by submissions.

Duties of Reviewers

- Reviewers assist the editorial board in making editorial decisions.
- Reviews should be conducted objectively, and observations should be formulated clearly with supporting arguments.
- Reviewers should not consider manuscripts in which they have conflicts of interest.
- Reviewers should treat the manuscript as a confidential document.

Duties of Authors

- The submitted manuscript should not be submitted to more than one journal for simultaneous consideration.
- The submitted work should be original and should not have been published elsewhere.
- Authors should adhere to discipline-specific rules for acquiring, selecting, and processing data.
- Authors should properly cite all content referenced from other materials.

Research Involving Humans, Animals, and Plants

- Research involving humans must be conducted in accordance with the Declaration of Helsinki.
- Research involving animals must adhere to international, national, and institutional guidelines for the humane treatment of animals.
- Studies on plants must be carried out within the guidelines provided by the authors› institution and national or international regulations.

Consent for Publication

- Written informed consent must be obtained from individuals who are featured in the manuscript.
- The consent form must state that the details/images will be freely available on the internet.

Fundamental Errors in Published Works

- Authors are obligated to promptly notify the journal editor of any significant errors or inaccuracies in the published work.

Plagiarism

- Plagiarism in any form constitutes a serious violation of publication ethics and is not acceptable.
- All submitted manuscripts are checked for plagiarism using professional plagiarism-checking software.

Complaints/Appeals

- All complaints, concerns, or appeals regarding authorship issues or the peer-review process should be addressed to the Editor-in-Chief.

Conflicts of Interest/Competing Interests

- Authors must disclose any conflicts of interest they may have with the publication of the manuscript.

Confidentiality

- A submitted manuscript is a confidential material.
- The journal will not disclose submitted manuscripts to anyone except individuals who partake in the processing and preparation of the manuscript for publication.

Misconduct

- Misconduct constitutes a violation of this editorial policy, journal policies, publication ethics, or any applicable guidelines/policies specified by COPE, WAME, and ICMJE.

Correction and Retraction of Articles

- Corrections may be made to a published article with the authorization of the editor of the journal.
- When necessary, the retraction of articles will be done according to COPE retraction guidelines.

Acknowledgment

- Individuals who participated in the development of a manuscript but do not qualify as an author should be acknowledged.
- Organizations that provided support in terms of funding and/or other resources should also be acknowledged.

Editorial board

Saly Naser Abbasa **Maha Jassim Manshad** **Ahmed Essam Sultan**	A Review: The Impact of Viral Mutations on theTtransmission Dynamics of the Monkeypox Virus	10
Hazha Zirar Hussain	Use the q-Integral Operator that Implicitly Contain the q-Ruscheweyh Derivative in a New Class of Analytic Univalent Functions Described by Some of their Finite Negative Invariant Coefficients	16
Mustafa K. Mushatet **Asaad Abbas khalaf**	The Preventive Effect of Pomegranate Peel Powder (Punica Granatum) Against Ethanol-Induced Oxidative Stress on Various Biochemical Parameters in Albino Rats	23
Noorulhuda Hussein Qandeel	The Multi-Attribute Decision-Making Problem Using Single-Valued Neutrosophic Numbers	29
Jihan Hussein AL-Masoudi **Neepal Imtair Al Garaawi**	Phytochemicals Screening and Antimicrobial Activity of Veronica Agrastis Extract	35
Mahasen Abid –Ali Alkafaji **Neepal Imtair Al Garaawi** **Fatima Karim Khudair**	The Phytochemical Compounds and the Antimicrobial Activity of Portulaca grandiflora Aqueous & Methanol Extracts in Iraq	40
Imad Kadhim Khudhair	Synthesis and Characterization of Indium Phosphide by Electrochemical Deposition Method	46
Ruaa Hussain Ali Ali Hassan Mohammed	R-Al Tememe Transformation for Solving Ordinary Differential Equations with Constant Coeffecients	53
Ihsan Mezher Rasheed **Kawthar Abdulabbas Hassoon**	A Secure Hybrid Symmetric Cryptosystem Combining Huffman Coding, Affine Transformation, and Cartesian Graphs	58

PURE SCIENCES
International Journal of Kerbala

Pure Sciences International Journal of Kerbala

Year: 2025 Volume : 2 Issue : 7 ISSN: 6188-2789 Print 3005 -2394 Online

Pure Sciences International Journal of Kerbala

A Review: The Impact of Viral Mutations on theTtransmission Dynamics of the Monkeypox Virus

Saly Naser Abbasa [a] , Maha Jassim Manshad [b *], Bassam Maytham Oleiwi [b]

[a] *Department of Biology , College of Education for Pure Sciences, University of Kerbala , Karbala, Iraq*
[b] *Department of Chemistry, College of Education for Pure Sciences, University of Kerbala , Karbala, Iraq*

P A P E R I N F O

Received :16.03.2025
Received :29.06.2025
Accepted :30.09.2025

Keywords:
monkeypox virus,
immune response, fear,
viral mutations

A B S T R A C T

Monkeypox virus (MPXV) is an emerging zoonotic pathogen under the Orthopoxvirus genus, primarily found in Central and West Africa. It shares similarities with the variola virus, responsible for smallpox, and causes symptoms such as fever, rash, and swollen lymph nodes. The virus spreads through direct contact with infected animals, people, or contaminated objects. The recent rise in monkeypox cases beyond its usual regions has raised global health concerns. Understanding its epidemiology, clinical symptoms, and transmission is crucial for effective prevention and control. Research on vaccines and treatments is essential to mitigate future outbreaks.Viral mutations play a significant role in the evolution and behavior of MPXV, affecting transmission, virulence, and immune system interactions. This review examines how genetic changes influence the virus's spread, enhance its pathogenicity, and alter immune responses. Mutations in surface proteins may improve viral attachment to host cells, facilitating transmission. Additionally, changes in key viral genes can help evade immune detection, leading to more severe outcomes. These mutations pose public health challenges, potentially reducing vaccine and diagnostic effectiveness.Understanding the impact of viral mutations on monkeypox is crucial for effective surveillance, prevention, and treatment strategies. This analysis emphasizes the importance of continuous genomic monitoring to anticipate changes in monkeypox epidemiology and adapt public health responses accordingly.

DOI: 10.53851/psijk.v2.i7.10-15

1. INTRODUCTION

Belonging to the Orthopoxvirus genus of the Poxviridae family, the Monkeypox virus (MPXV) was first discovered in 1970 in a 9-month-old infant in the Democratic Republic of the Congo. (Berche, 2022) (Huang et al., 2022) (Reed et al., 2004) Interest in MPXV resurged after the cessation of smallpox vaccinations in the 1970s, (Likos et al., 2005) leading to increased susceptibility (McCollum & Damon, 2014). The virus is zoonotic, mainly found in rodents and small mammals, with occasional spillovers to humans. Monkeypox manifests through Elevated body temperature, cephalalgia, and enlarged lymphatic glands (Letafati & Sakhavarz, 2023) (Stanford et al., 2007) and a rash that progresses to fluid-filled lesions (Moss, 2012) (Okyay et al., 2022) .Although it is usually milder than smallpox, it may result in complications such as pneumonia and sepsis (Petersen et al., 2019). There is no specific treatment, but smallpox vaccines provide partial protection (Moss, 2013) (Tolonen et al., 2001) (World Health Organization, 2022)

Monkeypox is the organism which is categorized into two genetic clades: the Central African clade, prevalent in the Congo Basin and known for its greater virulence, and the West African clade, which is correlated with a less severe disease presentation (Reynolds & Damon, 2012) (Simpson et al., 2020). The virus spreads via respiratory droplets, direct contact with
infected fluids, and contaminated surfaces. In the 2003 U.S (Bartlett, 2002) (Thornhill et al., 2022) outbreak, infected prairie dogs were the primary source of human infections, demonstrating its potential for transmission across species (Di Giulio & Eckburg, 2004) (Kieser et al., 2020) (Rao, 2022). The increasing human-to-human transmission highlights the need for effective monitoring and containment strategies (Vaccines, W.H.O., 2022) (Afshar et al., 2022) (Kmiec & Kirchhoff, 2022).

The purpose of this review is to evaluate and consolidate existing knowledge regarding the impact of genetic mutations in the monkeypox virus (MPXV) on its transmission dynamics. This involves investigating the

*Corresponding Author Institutional Email:
maha.j@uokerbala.edu.iq (Maha Jassim Manshad)

molecular alterations noted in recent outbreaks, assessing their influence on viral fitness, transmissibility, and interactions with hosts, as well as considering the implications for public health responses and future surveillance initiatives.

2. GENOMIC CHARACTERIZATION OF MPXV

MPXV is a double-stranded DNA virus with a genome size of approximately 197 kilobases (Kmiec & Kirchhoff, 2022). It comprises a central region that is preserved, bordered by variable terminal regions that encode virulence factors. The genome contains inverted terminal repeats, open reading frames, and genes linked to immune evasion. Genetic diversity within MPXV enhances its adaptability to new hosts and environments (Beer & Rao, 2019) (Alakunle et al., 2020). The Central African clade exhibits mutations that suppress T-cell activation and inflammatory cytokine production, leading to higher virulence. Studies show that the West African clade has deletions in specific genes, correlating with lower pathogenicity (Kugelman et al., 2014).

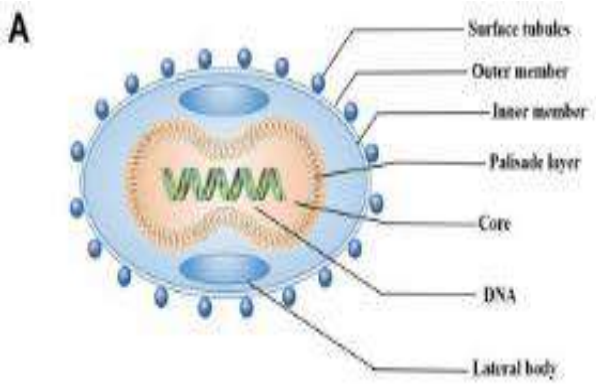

Figure 1. This illustration presents the structural and genomic attributes of the monkeypox virus (MPXV). (Kugelman et al., 2014) .(A) The composition of MPXV consists of five unique elements: Key elements consist of the core, the palisade layer, the outer and inner membranes, surface tubules, and nucleic acids, specifically DNA (Beer & Rao, 2019).

Electron microscopy reveals that MPXV particles are large, brick-shaped, and contain essential enzymes for transcription and replication. The virus exists in two forms: mature virions (MVs) with a single membrane, responsible for initial host attachment, and extracellular enveloped virions (EVs), which aid in viral spread. These structural characteristics impact the capability of a virus to infect host entities while successfully evading immune reactions. (Di Giulio & Eckburg, 2004) (Berthet et al., 2021)

3. PATHOGENESIS AND IMMUNE RESPONS

MPXV infects hosts via respiratory droplets, direct contact, or through skin lesions (Durski, 2018) (Doshi et al., 2019) (Smith & Kotwa, 2002) .The virus enters through mucosal surfaces, replicates in local tissues, and spreads to lymph nodes, leading to systemic infection (Alzhanova & Früh, 2010) (Realegeno et al., 2020) (Weinstein et al., 2005).The incubation period ranges from 7 to 21 days. During early infection, the virus remains non-transmissible (Stanford et al., 2007) (Cann et al., 2013) (Elwood, 1989)However, once symptoms appear, particularly skin lesions, transmission risk increases (Liu et al., 2005) (MacLeod et al., 2015).

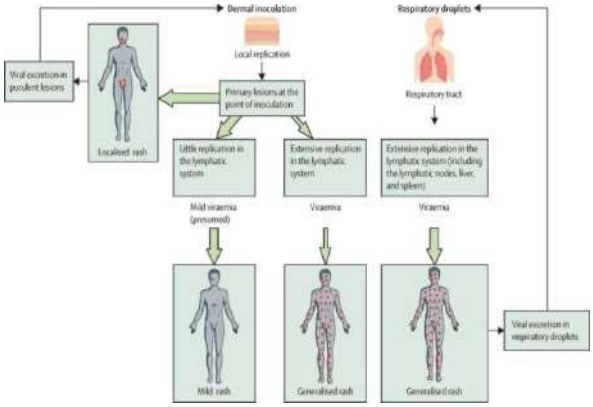

Figure 2. Recommended framework for understanding the distribution the spread of the monkeypox virus throughout the organism and its consequences. association with the modes of transmission.

The immune system responds to MPXV through humoral and cellular mechanisms (Realegeno et al., 2017) (Karem et al., 2007)Natural infection or vaccination induces IgM and IgG antibody production, promoting immunity (Shao et al., 2009) (Zaeck et al., 2023) (Verreault et al., 2013). CD4+ and CD8+ T cells also play a role in viral clearance. Some studies suggest that smallpox vaccination provides long-lasting immunity against MPXV, (Edghill-Smith et al., 2005) (Hammarlund et al., 2008) though vaccine-derived immunity has declined over time. Research indicates that the monkeypox virus can persist in antigen-presenting cells, allowing prolonged immune evasion (Hammarlund et al., 2003).

4. TRANSMISSION AND SYMPTOMS

Monkeypox is primarily zoonotic but can spread between humans. Transmission occurs through contact with infected animals (e.g., rodents, monkeys) or through contaminated materials. The occurrence of human-to-human transmission is relatively rare. It remains a possibility through respiratory secretions, skin-to-skin contact, and fomites (WHO, 2022)as shown in Figure (3) (Islam et al., 2022).

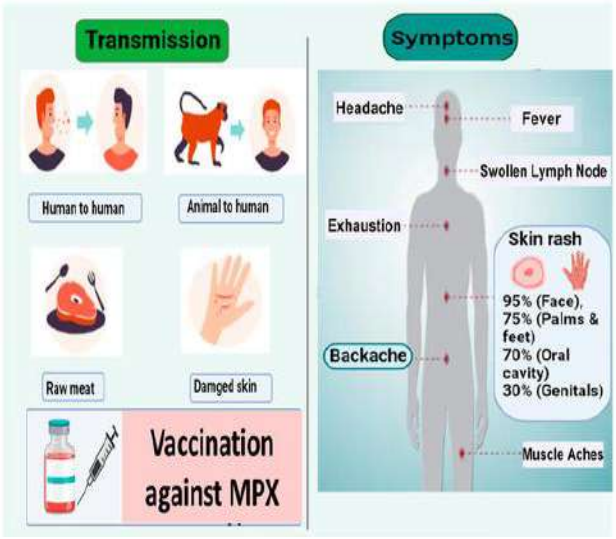

Figure 3. Symptoms resemble those of smallpox and include fever, swollen lymph nodes, muscle aches, and rashes (Reynolds et al., 2007). The rash develops in stages, starting with macules, advancing to papules, and subsequently forming Prior to this, the presence of vesicles, pustules, and scabs was noted. healing. Children and immunocompromised individuals are at higher risk of severe disease. (Reynolds et al., 2006) (Huhn et al., 2005).

5.THE IMPACT OF FEAR ON MPXV TRANSMISSION

Public perception and fear influence the spread of monkeypox (Islam et al., 2022) (Gross & Canteras, 2012) (Mobbs et al., 2010).Psychological responses to outbreaks can drive panic and misinformation (Davis et al., 2010) (Schmidt-Sane et al., 2022) .Studies from previous epidemics, such as COVID-19, show that fear disproportionately affects certain demographics, particularly healthcare workers and socially vulnerable populations (Nimbi et al., 2023) (Fitzpatrick et al., 2020). Media coverage plays a crucial role in shaping public attitudes and adherence to preventive measures. Effective risk communication, avoiding stigma, and promoting accurate information are essential in controlling the outbreak (Schmidt-Sane et al., 2022) (Nimbi et al., 2021).

6. FACTORS INFLUENCING MPXV TRANSMISSION

6.1 Ecological Sustainability

MPXV persists in the environment under specific conditions (Breman et al., 1980) (Titanji et al., 2022) .Studies indicate that the virus remains viable for weeks on contaminated surfaces, particularly in low-temperature, low-humidity settings (Pan et al., 2023) (Huq, 1976) .PCR analyses of household and hospital surfaces show MPXV DNA contamination (Verreault et al., 2013) underscoring the need for stringent disinfection practices (Pfeiffer, 2022).

6.2 Host and Viral Factors

MPXV is transmitted 1. Transmission occurs through direct contact with lesions, via respiratory droplets, and through other means.

2. The spread of infection can happen through direct interaction with lesions, through respiratory droplets, and by additional methods.

3. Infection can be transmitted through direct contact with lesions, through respiratory droplets, and by various other routes. contaminated surfaces (Nörz et al., 2022) (Morgan et al., 2022) (Gould et al., 2022). Studies suggest that the current outbreak strain exhibits higher transmission rates due to mutations affecting viral attachment and immune evasion (Chen et al., 2005) (Weaver & Isaacs, 2008). The 2022 outbreak primarily have affected individuals identified as men and they have sexual encounters with other men (MSM), (Mitjà et al., 2023) (Yinka-Ogunleye et al., 2019) (UK Health Security Agency, 2022) suggesting transmission through close physical contact, including sexual activity (Isidro et al., 2022) (Kaler et al., 2022) (Pan et al., 2022).

6.3 Cross-Species Transmission and Human-to-Human Transmission.

Animal reservoirs, including rodents and primates, play a key role in maintaining MPXV circulation. Evidence has emerged regarding the spread of illnesses from humans to animal populations (Jezek et al., 1986) (Vivancos et al., 2022)such as a case involving a dog in France, indicates that infected pets could contribute to viral spread (Hutson et al., 2009) (Ježek et al., 1988). Additionally, It has been observed that transmission occurs from the mother to the fetus. (Learned et al., 2005) with severe outcomes such as fetal demise (Cudmore et al., 1995) (Peiró-Mestres et al., 2022)

7. POPULATION DYNAMICS AND OUTBREAK PATTERNS

Mathematical models suggest that MPXV transmission is influenced by social and behavioral factors (Lapa et al., 2022) Studies on sexual networks indicate that a small group of highly connected individuals may drive outbreaks, explaining the rapid spread within specific communities (Lapa et al., 2022) (Parker & Buller, 2013). Differences in median age and transmission dynamics between outbreaks in Africa and recent global cases suggest evolutionary changes in MPXV (Seang et al., 2022).

8. CONCLUSION

Monkeypox continues to spread globally, presenting challenges similar to COVID-19. Viral mutations play a critical role in transmission, virulence, and immune evasion. The ability of MPXV to adapt to new hosts underscores the need for continuous genomic surveillance. Understanding these mutations is essential

for developing effective vaccines, treatments, and public health interventions. Future research should focus on monitoring viral evolution and improving outbreak response strategies.

REFERENCES

Afshar, Z. M., Rostami, H. N., Hosseinzadeh, R., Janbakhsh, A., Pirzaman, A. T., Babazadeh, A., ... & Ebrahimpour, S. (2022). The reemergence of monkeypox as a new potential health challenge: a critical review. Authorea Preprints.

Alakunle, E., Moens, U., Nchinda, G., & Okeke, M. I. (2020). Monkeypox virus in Nigeria: infection biology, epidemiology, and evolution. Viruses, 12(11), 1257.

Alzhanova, D., & Früh, K. (2010). Modulation of the host immune response by cowpox virus. Microbes and infection, 12(12-13), 900-909.

Bartlett, J. G. (2002). Review of literature: general infectious diseases. Infect Dis Clin Pract, 11(9), 579-582.

Beer, E. M., & Rao, V. B. (2019). A systematic review of the epidemiology of human monkeypox outbreaks and implications for outbreak strategy. PLoS neglected tropical diseases, 13(10), e0007791.

Berche, P. (2022). Life and death of smallpox. La Presse Médicale, 51(3), 104117.

Berthet, N., Descorps-Declère, S., Besombes, C., Curaudeau, M., Nkili Meyong, A. A., Selekon, B., ... & Nakoune, E. (2021). Genomic history of human monkeypox infections in the Central African Republic between 2001 and 2018. Scientific reports, 11(1), 13085.

Breman, J. G., Steniowski, M. V., Zanotto, E., Gromyko, A. I., & Arita, I. (1980). Human monkeypox, 1970–79. Bulletin of the World Health Organization, 58(2), 165.

Cann, J. A., Jahrling, P. B., Hensley, L. E., & Wahl-Jensen, V. (2013). Comparative pathology of smallpox and monkeypox in man and macaques. Journal of comparative pathology, 148(1), 6–21.

Chen, N., Li, G., Liszewski, M. K., Atkinson, J. P., Jahrling, P. B., Feng, Z., ... & Buller, R. M. L. (2005). Virulence differences between monkeypox virus isolates from West Africa and the Congo basin. Virology, 340(1), 46–63.

Cudmore, S., Cossart, P., Griffiths, G., & Way, M. (1995). Actin-based motility of vaccinia virus. Nature, 378(6557), 636–638.

Davis, M., Walker, D. L., Miles, L., & Grillon, C. (2010). Phasic vs sustained fear in rats and humans: role of the extended amygdala in fear vs anxiety. Neuropsychopharmacology, 35(1), 105–135.

Di Giulio, D. B., & Eckburg, P. B. (2004). Human monkeypox: an emerging zoonosis. The Lancet infectious diseases, 4(1), 15–25.

Doshi, R. H., Guagliardo, S. A. J., Doty, J. B., et al. (2019). Epidemiologic and ecologic investigations of monkeypox, Likouala Department, Republic of the Congo, 2017. Emerg Infect Dis, 25, 281–289.

Durski, K. N. (2018). Emergence of monkeypox—West and Central Africa, 1970–2017. MMWR. Morbidity and mortality weekly report, 67.

Edghill-Smith, Y., Golding, H., Manischewitz, J., King, L. R., Scott, D., Bray, M., ... & Franchini, G. (2005). Smallpox vaccine–induced antibodies are necessary and sufficient for protection against monkeypox virus. Nature medicine, 11(7), 740–747.

Elwood, J. M. (1989). Smallpox and its eradication. J Epidemiol Community Health, 43, 92.

Fitzpatrick, K. M., Harris, C., & Drawve, G. (2020). Fear of COVID-19 and the mental health consequences in America. Psychological trauma: theory, research, practice, and policy, 12(S1), S17.

Gould, S., Atkinson, B., Onianwa, O., Spencer, A., Furneaux, J., Grieves, J., ... & Sinha, R. (2022). Air and surface sampling for monkeypox virus in a UK hospital: an observational study. The Lancet Microbe, 3(12), e904–e911.

Gross, C. T., & Canteras, N. S. (2012). The many paths to fear. Nature Reviews Neuroscience, 13(9), 651–658.

Hammarlund, E., Dasgupta, A., Pinilla, C., Norori, P., Früh, K., & Slifka, M. K. (2008). Monkeypox virus evades antiviral CD4+ and CD8+ T cell responses by suppressing cognate T cell activation. Proceedings of the National Academy of Sciences, 105(38), 14567–14572.

Hammarlund, E., Lewis, M. W., Hansen, S. G., Strelow, L. I., Nelson, J. A., Sexton, G. J., ... & Slifka, M. K. (2003). Duration of antiviral immunity after

smallpox vaccination. Nature medicine, 9(9), 1131–1137.

Huang, Y. A., Howard-Jones, A. R., Durrani, S., Wang, Z., & Williams, P. C. (2022). Monkeypox: A clinical update for paediatricians. Journal of paediatrics and child health, 58(9), 1532–1538.

Huq, F. (1976). Effect of temperature and relative humidity on variola virus in crusts. Bulletin of the World Health Organization, 54(6), 710.

Huhn, G. D., Bauer, A. M., Yorita, K., Graham, M. B., Sejvar, J., Likos, A., ... & Kuehnert, M. J. (2005). Clinical characteristics of human monkeypox, and risk factors for severe disease. Clinical infectious diseases, 41(12), 1742–1751.

Hutson, C. L., Olson, V. A., Carroll, D. S., Abel, J. A., Hughes, C. M., Braden, Z. H., ... & Regnery, R. L. (2009). A prairie dog animal model of systemic orthopoxvirus disease using West African and Congo Basin strains of monkeypox virus. Journal of General Virology, 90(2), 323–333.

Isidro, J., Borges, V., Pinto, M., Sobral, D., Santos, J. D., Nunes, A., ... & Gomes, J. P. (2022). Phylogenomic characterization and signs of microevolution in the 2022 multi-country outbreak of monkeypox virus. Nature medicine, 28(8), 1569–1572.

Islam, M. A., Sangkham, S., Tiwari, A., Vadiati, M., Hasan, M. N., Noor, S. T. A., ... & Sherchan, S. P. (2022). Association between global monkeypox cases and meteorological factors. International journal of environmental research and public health, 19(23), 15638.

Ježek, Z., Grab, B., Szczeniowski, M. V., Paluku, K. M., & Mutombo, M. (1988). Human monkeypox: secondary attack rates. Bulletin of the World Health Organization, 66(4), 465.

Jezek, Z., Marennikova, S. S., Mutumbo, M., Nakano, J. H., Paluku, K. M., & Szczeniowski, M. (1986). Human monkeypox: a study of 2,510 contacts of 214 patients. Journal of infectious diseases, 154(4), 551–555.

Kaler, J., Hussain, A., Flores, G., Kheiri, S., & Desrosiers, D. (2022). Monkeypox: a comprehensive review of transmission, pathogenesis, and manifestation. Cureus, 14(7).

Karem, K. L., Reynolds, M., Hughes, C., Braden, Z., Nigam, P., Crotty, S., ... & Damon, I. K. (2007). Monkeypox-induced immunity and failure of childhood smallpox vaccination to provide complete protection. Clinical and Vaccine Immunology, 14(10), 1318–1327.

Kmiec, D., & Kirchhoff, F. (2022). Monkeypox: a new threat? International journal of molecular sciences, 23(14), 7866.

Kugelman, J. R., Johnston, S. C., Mulembakani, P. M., Kisalu, N., Lee, M. S., Koroleva, G., ... & Rimoin, A. W. (2014). Genomic variability of monkeypox virus among humans, Democratic Republic of the Congo. Emerging infectious diseases, 20(2), 232.

Lapa, D., Carletti, F., Mazzotta, V., Matusali, G., Pinnetti, C., Meschi, S., ... & Maggi, F. (2022). Monkeypox virus isolation from a semen sample collected in the early phase of infection in a patient with prolonged seminal viral shedding. The Lancet Infectious Diseases, 22(9), 1267–1269.

Learned, L. A., Reynolds, M. G., Wassa, D. W., Li, Y. U., Olson, V. A., Karem, K., ... & Damon, I. K. (2005). Extended interhuman transmission of monkeypox in a hospital community in the Republic of the Congo, 2003. The American journal of tropical medicine and hygiene, 73(2), 428–434.

Letafati, A., & Sakhavarz, T. (2023). Monkeypox virus: A review. Microbial pathogenesis, 176, 106027.

Likos, A. M., Sammons, S. A., Olson, V. A., Frace, A. M., Li, Y., Olsen-Rasmussen, M., ... & Damon, I. K. (2005). A tale of two clades: monkeypox viruses. Journal of General Virology, 86(10), 2661–2672.

Liu, L., Xu, Z., Fuhlbrigge, R. C., Pena-Cruz, V., Lieberman, J., & Kupper, T. S. (2005). Vaccinia virus induces strong immunoregulatory cytokine production in healthy human epidermal keratinocytes: a novel strategy for immune evasion. Journal of virology, 79(12), 7363–7370.

MacLeod, D. T., Nakatsuji, T., Wang, Z., Di Nardo, A., & Gallo, R. L. (2015). Vaccinia virus binds to the scavenger receptor MARCO on the surface of keratinocytes. Journal of Investigative Dermatology, 135(1), 142–150.

McCollum, A. M., & Damon, I. K. (2014). Human monkeypox. Clinical infectious diseases, 58(2), 260–267.

Mitjà, O., Ogoina, D., Titanji, B. K., Galvan, C., Muyembe, J. J., Marks, M., & Orkin, C. M. (2023). Monkeypox. The Lancet, 401(10370), 60–74.

Mobbs, D., Yu, R., Rowe, J. B., Eich, H., FeldmanHall, O., & Dalgleish, T. (2010). Neural activity associated with monitoring the oscillating threat value of a tarantula. Proceedings of the National Academy of Sciences, 107(47), 20582–20586.

Morgan, C. N., Whitehill, F., Doty, J. B., Schulte, J., Matheny, A., Stringer, J., ... & McCollum, A. M. (2022). Environmental persistence of monkeypox virus on surfaces in household of person with travel-associated infection, Dallas, Texas, USA, 2021. Emerging infectious diseases, 28(10), 1982.

Moss, B. (2012). Poxvirus cell entry: how many proteins does it take? Viruses, 4(5), 688–707.

Moss, B. (2013). Poxvirus DNA replication. Cold Spring Harbor perspectives in biology, 5(9), a010199.

Nimbi, F. M., Baiocco, R., Giovanardi, G., Tanzilli, A., & Lingiardi, V. (2023). Who is afraid of monkeypox? Analysis of psychosocial factors associated with the first reactions of fear of monkeypox in the Italian population. Behavioral Sciences, 13(3), 235.

Nörz, D., Pfefferle, S., Brehm, T., Franke, G., Grewe, I., Knobling, B., ... & Knobloch, J. K. (2022). Evidence of surface contamination in hospital rooms occupied by patients infected with monkeypox, Germany, June 2022. Eurosurveillance, 27(26), 2200477.

Okyay, R. A., Bayrak, E., Kaya, E., Şahin, A. R., Koçyiğit, B. F., Taşdoğan, A. M., ... & Sümbül, H. E. (2022). Another epidemic in the shadow of COVID-19 pandemic: a review of monkeypox. Proteins, 7(10), 10–14744.

Pan, D., Nazareth, J., Sze, S., Martin, C. A., Decker, J., Fletcher, E., ... & Tang, J. W. (2023). Transmission of monkeypox/mpox virus: a narrative review of environmental, viral, host, and population factors in relation to the 2022 international outbreak. Journal of Medical Virology, 95(2), e28534.

Parker, S., & Buller, R. M. (2013). A review of experimental and natural infections of animals with monkeypox virus between 1958 and 2012. Future virology, 8(2), 129–157.

Petersen, E., Kantele, A., Koopmans, M., Asogun, D., Yinka-Ogunleye, A., Ihekweazu, C., & Zumla, A. (2019). Human monkeypox: epidemiologic and clinical characteristics, diagnosis, and prevention. Infectious disease clinics of North America, 33(4), 1027.

Pfeiffer, J. A. (2022). High-contact object and surface contamination in a household of persons with monkeypox virus infection—Utah, June 2022. MMWR. Morbidity and Mortality Weekly Report, 71.

Rao, A. K. (2022). Use of JYNNEOS (smallpox and monkeypox vaccine, live, nonreplicating) for preexposure vaccination of persons at risk for occupational exposure to orthopoxviruses: recommendations of the Advisory Committee on Immunization Practices—United States, 2022. MMWR. Morbidity and mortality weekly report, 71.

Realegeno, S., Priyamvada, L., Kumar, A., Blackburn, J. B., Hartloge, C., Puschnik, A. S., ... & Satheshkumar, P. S. (2020). Conserved Oligomeric Golgi (COG) complex proteins facilitate orthopoxvirus entry, fusion and spread. Viruses, 12(7), 707.

Reed, K. D., Melski, J. W., Graham, M. B., Regnery, R. L., Sotir, M. J., Wegner, M. V., ... & Damon, I. K. (2004). The detection of monkeypox in humans in the Western Hemisphere. New England Journal of Medicine, 350(4), 342–350.

Reynolds, M. G., & Damon, I. K. (2012). Outbreaks of human monkeypox after cessation of smallpox vaccination. Trends in microbiology, 20(2), 80–87.

Reynolds, M. G., Davidson, W. B., Curns, A. T., Conover, C. S., Huhn, G., Davis, J. P., ... & Damon, I. K. (2007). Spectrum of infection and risk factors for human monkeypox, United States, 2003. Emerging infectious diseases, 13(9), 1332.

Reynolds, M. G., Yorita, K. L., Kuehnert, M. J., Davidson, W. B., Huhn, G. D., Holman, R. C., & Damon, I. K. (200

PURE SCIENCES
International Journal of Kerbala

Pure Sciences International Journal of Kerbala

Year: 2025 Volume : 2 Issue : 7 ISSN: 6188-2789 Print 3005 -2394 Online

2025,Volume 2 , Issue 7 , PSIJK (16-22)

Pure Sciences International Journal of Kerbala

Use the q-Integral Operator that Implicitly Contain the q-Ruscheweyh Derivative in a New Class of Analytic Univalent Functions Described by Some of their Finite Negative Invariant Coefficients

Hazha Zirar Hussain [a*]

[a] Department of Mathematics, College of Sciences, Salahaddin University-Erbil, Iraq

P A P E R I N F O

Received: 09.04.2025
Accepted: 23.06.2025
Published: 30.09.2025

Keywords:
Analytic Functions, Univalent Functions, q-Ruscheweyeh Derivative Operator, q-Integral Operator,Convolution.

A B S T R A C T

In this article, we study some of the basic geometric properties involved in finding an estimate or determining the value of the coefficients on the basis that the function is characterized by the starlike and convexity of the order ϑ, respectively. In addition to other properties, all this is done by defining a new class of analytic univalent functions by applying a quantum integral that implicitly contains a Ruscheweyh's quantum derivative to this special class, described by some of its non-variable coefficients.

DOI: 10.53851/psijk.v2.i7.16 -22

1. INTRODUCTION

The research starts by assuming the class $\mathfrak{A}$, which is the set of all the analytic univalent functions that have the following natural form:

$$f(z) = z + \sum_{k=2}^{\infty} a_k \, z^k. \qquad (1.1)$$

By fulfilling the normalized conditions $f(0) = 0, f'(0) = 1$, all of this is in the famous unit disc $\mathcal{U} = \{z \in \mathbb{C}: |z| < 1\}$.

Now we will take a subclass $\mathfrak{A}^*$of our original class such that each function has the following form:

$$f(z) = z - \sum_{k=n+1}^{\infty} a_k \, z^k, (a_k \geq 0). \qquad (1.2)$$

Since the quantum derivative operator or Jackson derivative operator plays an important and effective role in this field of complex analysis, especially recently, many researchers have used this operator in their research and obtained important and interesting results such as (Illafe, Mohd, Yousef, & Supramaniam, 2024) (Bangi, 2024) (Alsoboh & Oros, 2024) (Al-Rawashdeh, 2025) (Abubaker, Matarneh, Khan, Suha, & Kamal, 2024) (Delphi, 2024)

Let us not forget that the first person who defined this operator was Jackson in his researches (Jackson, 1905) (Jackson, 1909) (Jackson, 1910a) (Jackson, Fukuda, Dunn, et al., 1910b) where he studied the q calculation and its applications in his researches.

Let us remember the definition of the involutional product of two functions f defined by (1.1) and j defined as follows:

$$j(z) = z + \sum_{k=2}^{\infty} b_k \, z^k, \qquad (1.3)$$

in class $\mathfrak{A}$, it is symbolized by the symbol $f * j$ and is known as follows:

$$(f * j)(z) = z + \sum_{k=2}^{\infty} a_k \, b_k z^k. \qquad (1.4)$$

Now I need to recall the concept of the q-number $[\zeta]_q$ as follows:

$$[\zeta]_q = \frac{1 - q^{\zeta}}{1 - q}, \qquad (1.5)$$

*Corresponding Author Institutional Email:
hazha.hussain@su.edu.krd (Hazha Zirar Hussain)

if ζ is complex number, and

$$[\zeta]_{\mathfrak{q}} = 1 + \sum_{k=1}^{m-1} \mathfrak{q}^k, \qquad (1.6)$$

if $\zeta = m$ is natural number.

Based on what we have mentioned $[0]_{\mathfrak{q}} = 0$, on condition $0 < \mathfrak{q} < 1$.

Under the same condition we take the definition of the q-factorial $[k]_{\mathfrak{q}}!$ as

$$[k]_{\mathfrak{q}}! = \begin{cases} 1 & if\ k = 0 \\ \prod_{m=1}^{k} [m]_{\mathfrak{q}} & if\ k \in \mathbb{N} \end{cases}$$

$[s]_{\mathfrak{q},k}!$ is also known as

$$[s]_{\mathfrak{q},k}! = \begin{cases} 1 & if\ k = 0 \\ \prod_{m=s}^{s+k-1} [m]_{\mathfrak{q}} & if\ k \in \mathbb{N} \end{cases}$$

and that is when $s \in \{0, 1, 2, \dots.\}$.

Likewise, Jackson's quantum derivative for a function belonging to the class $\mathfrak{A}$ under the same condition is usually written in the following form:

$$\mathfrak{D}_{\mathfrak{q}} f(z) = \begin{cases} \dfrac{f(z) - f(\mathfrak{q}z)}{(1-\mathfrak{q})z} & if\ z \neq 0 \\ f'(z) & if\ z = 0 \end{cases}$$

it is certainly true when $f'(z)$ exists.In addition we have:

$$(\mathfrak{D}_{\mathfrak{q}}^2 f)(z) = \big(\mathfrak{D}_{\mathfrak{q}}(\mathfrak{D}_{\mathfrak{q}} f)\big)(z). \qquad (1.7)$$

In Source No. [11], Ruscheweyh's q-derivative of a function in the class $\mathfrak{A}$ is defined in the following way:

$$\mathcal{R}_{\mathfrak{q},\zeta} f(z) = f(z) * \left(z + \sum_{k=2}^{\infty} \frac{[\zeta+1]_{\mathfrak{q},k-1}}{[k-1]_{\mathfrak{q}}!}\, z^k \right), \quad \zeta > -1. \qquad (1.8)$$

More over, in the research in sources No. (Srivastava, Wanas, & Srivastava, 2021) (Srivastava, Ahmad, Khan, Khan, & Khan, 2019) the q integration operator for a function in the class $\mathfrak{A}$ was defined by:

$$\mathcal{R}_{\mathfrak{q},\zeta}^{-1} f(z) + \mathcal{R}_{\mathfrak{q},\zeta}(z) = z\big(\mathfrak{D}_{\mathfrak{q}} f(z)\big), \qquad (1.9)$$

$$\mathcal{R}_{\mathfrak{q},\zeta}^{-1} f(z) = z + \sum_{k=2}^{\infty} \frac{[k]_{\mathfrak{q}}!}{[\zeta+1]_{\mathfrak{q},k-1}}\, z^k, k \geq 2. \qquad (1.10)$$

A special case of it was studied in source No. (Noor, 1999) when $\mathfrak{q} \to 1^-$.

The q integral operator $\mathfrak{J}_{\mathfrak{q}}^{\zeta}$ in source [13] was defined by the following formula:

$$\mathfrak{J}_{\mathfrak{q}}^{\zeta} f(z) = f(z) * \mathcal{R}_{\mathfrak{q},\zeta}^{-1} f(z) = z + \sum_{k=2}^{\infty} \frac{[k]_{\mathfrak{q}}!}{[\zeta+1]_{\mathfrak{q},k-1}}\, a_k z^k. \qquad (1.11)$$

The following relations are also true.

$$\mathfrak{J}_{\mathfrak{q}}^{\zeta} f(z) = z\big(\mathfrak{D}_{\mathfrak{q}} f(z)\big), \qquad (1.12)$$

$$\mathfrak{J}_{\mathfrak{q}}^{1} f(z) = f(z). \qquad (1.13)$$

Now we come to the heart of the article, which is defining our class as a first step, as follows:

Definition 1.1: If we determine or prove the conditions , $\zeta > -1, 0 < \mathfrak{q} < 1,\ \chi \in \mathbb{C}\setminus\{0\}, 0 < \upsilon \leq 1,\ \phi \leq 1$, in the light of this, the function $f \in \mathfrak{A}^*$, is an element of the class $\mathfrak{H}_{\mathfrak{q}}^{\zeta}(\chi, \phi, \nu)$ if the following inequality is satisfied:

$$\left| \frac{1}{\chi} \left(\frac{z\mathfrak{D}_{\mathfrak{q}}\left(\mathfrak{J}_{\mathfrak{q}}^{\zeta} f(z)\right)}{\mathfrak{J}_{\mathfrak{q}}^{\zeta} f(z)} - \phi \right) \right| < \nu, \qquad (1.14)$$

and don't forget that z is in the open unit disk.

2. DISCUSSION OF THE EMERGING RESULTS

In this part of the article, we present and discuss the most important results and facts that have been reached and proven by first studying the characteristics and determining the values of the coefficients in the following theorem:

Theorem 2.1: The function f, which is formulated in the form (1.2), is an element of the distinct class $\mathfrak{H}_{\mathfrak{q}}^{\zeta}(\chi, \phi, \nu)$ if and only if the following condition is met:

$$\sum_{k=2}^{\infty} \frac{\big([k]_{\mathfrak{q}} - \phi + \upsilon|\chi|\big)\,[k]_{\mathfrak{q}}!}{[\zeta+1]_{\mathfrak{q},k-1}}\, a_k \leq (1 - \phi + \upsilon|\chi|), \qquad (2.1)$$

that's when $\zeta > -1, 0 < \mathfrak{q} < 1,\ \chi \in \mathbb{C}\setminus\{0\}, 0 < \upsilon \leq 1,\ \phi \leq 1$.

Proof: The first step to start the proof is to take f in the defined class $\mathfrak{H}_{\mathfrak{q}}^{\zeta}(\chi, \phi, \nu)$. So

$$\mathcal{R}e\left(\frac{z\mathfrak{D}_{\mathfrak{q}}\left(\mathfrak{J}_{\mathfrak{q}}^{\zeta} f(z)\right)}{\mathfrak{J}_{\mathfrak{q}}^{\zeta} f(z)} - \phi \right) > -\upsilon|\chi|. \qquad (2.2)$$

Let's take the quantity on the left side of the previous equation and simplify it as follows:

$$\frac{z\mathfrak{D}_{\mathfrak{q}}\left(\mathfrak{J}_{\mathfrak{q}}^{\zeta} f(z)\right)}{\mathfrak{J}_{\mathfrak{q}}^{\zeta} f(z)} = \frac{z - \sum_{k=2}^{\infty} [k]_{\mathfrak{q}} \frac{[k]_{\mathfrak{q}}!}{[\zeta+1]_{\mathfrak{q},k-1}}\, a_k z^k}{z - \sum_{k=2}^{\infty} \frac{[k]_{\mathfrak{q}}!}{[\zeta+1]_{\mathfrak{q},k-1}}\, a_k z^k}. \qquad (2.3)$$

Consequently,

$$\mathcal{R}e\left(\frac{(1-\phi)z - \sum_{k=2}^{\infty} \big([k]_{\mathfrak{q}} - \phi\big) \frac{[k]_{\mathfrak{q}}!}{[\zeta+1]_{\mathfrak{q},k-1}}\, a_k z^k}{z - \sum_{k=2}^{\infty} \frac{[k]_{\mathfrak{q}}!}{[\zeta+1]_{\mathfrak{q},k-1}}\, a_k z^k} \right) > -\upsilon|\chi|. \qquad (2.4)$$

Now we give the variable z only the real value, i.e. on the real axis and approaching one from the left, and thus we complete the proof of the first step.

The second step of the proof is to prove the fact that inequality (2.1) is true and we start by taking

$$\left|\frac{z\mathfrak{D}_{\mathfrak{q}}\left(\mathfrak{I}_{\mathfrak{q}}^{\zeta}f(z)\right)}{\mathfrak{I}_{\mathfrak{q}}^{\zeta}f(z)}-\phi\right|$$
$$=\left|\frac{(1-\phi)z-\sum_{k=2}^{\infty}\left([k]_{\mathfrak{q}}-\phi\right)\frac{[k]_{\mathfrak{q}}!}{[\zeta+1]_{\mathfrak{q},k-1}}a_kz^k}{z-\sum_{k=2}^{\infty}\frac{[k]_{\mathfrak{q}}!}{[\zeta+1]_{\mathfrak{q},k-1}}a_kz^k}\right|$$
$$\leq\frac{(1-\phi+\upsilon|\chi|)\left(1-\sum_{k=2}^{\infty}[k]_{\mathfrak{q}}\frac{[k]_{\mathfrak{q}}!}{[\zeta+1]_{\mathfrak{q},k-1}}a_k\right)}{1-\sum_{k=2}^{\infty}\frac{[k]_{\mathfrak{q}}!}{[\zeta+1]_{\mathfrak{q},k-1}}a_k}$$
$$\leq 1-\phi+\upsilon|\chi|. \qquad (2.5)$$

Here lies the importance of the maximum modulus theorem in its application and obtaining that f is an element of the distinct class $\mathfrak{H}_{\mathfrak{q}}^{\zeta}(\chi,\phi,\nu)$.

Thus, we have successfully demonstrated the proof of the theorem.

We note that for the extreme functions in the special class $\mathfrak{H}_{\mathfrak{q}}^{\zeta}(\chi,\phi,\nu)$, it can be written in the form:

$$f(z)=z-\frac{(1-\phi+\upsilon|\chi|)\,[\zeta+1]_{\mathfrak{q},k-1}}{\left([k]_{\mathfrak{q}}-\phi+\upsilon|\chi|\right)[k]_{\mathfrak{q}}!}\,z^k,k\geq 2. \qquad (2.6)$$

That is, the theorem is sharp for them, and thus we obtain the following clear result.

Corollary: If we take the function f, which has the formula (1.2), in the special class $\mathfrak{H}_{\mathfrak{q}}^{\zeta}(\chi,\phi,\nu)$, its coefficients satisfy the following condition:

$$a_k\leq\frac{(1-\phi+\upsilon|\chi|)\,[\zeta+1]_{\mathfrak{q},k-1}}{\left([k]_{\mathfrak{q}}-\phi+\upsilon|\chi|\right)[k]_{\mathfrak{q}}!},k\geq 2. \qquad (2.7)$$

As we have previously noted, the extreme functions achieve the equality condition for inequality (2.7).

Now we come to the main goal of this article, which is to define a basic subclass of the class $\mathfrak{H}_{\mathfrak{q}}^{\zeta}(\chi,\phi,\nu)$, by fixing a finite number of coefficients of its functions defined in the form (1.2), i.e. with a finite number of fixed coefficients in the following form:

Definition 2.3: Let $\mathfrak{HB}_{\mathfrak{q}}^{\zeta}(\chi,\phi,\nu,\tau_m)$ be a subclass of the distinct class $\mathfrak{H}_{\mathfrak{q}}^{\zeta}(\chi,\phi,\nu)$, each of its elements or rather its functions, is written in the following form:

$$f(z)=z-\sum_{l=2}^{m}\frac{(1-\phi+\upsilon|\chi|)\,[\zeta+1]_{\mathfrak{q},k-1}\tau_l}{\left([l]_{\mathfrak{q}}-\phi+\upsilon|\chi|\right)[l]_{\mathfrak{q}}!}\,z^l-\sum_{k=m+1}^{\infty}a_k\,z^k. \qquad (2.8)$$

The class $\mathfrak{HB}_{\mathfrak{q}}^{\zeta}(\chi,\phi,\nu,\tau_m)$ is equivalent to the class $\mathfrak{H}_{\mathfrak{q}}^{\zeta}(\chi,\phi,\nu)$ when$\tau_m=1$.

As we see in sources (Lashin, Badghaish, & Alshehri, 2024) (Maran, Juma, & Al-Saphory, 2025) (Al-Saleem, 2025) (Akyar, 2025) (Al-Hawary, Frasin, & Salah, 2025) various classes of univalent functions that have the property of negative coefficients and fixing a finite number of them have been studied.This is an important step in serving the development of geometric field in mathematics, the queen of sciences.

From the series of results, we have the following theorem.

Theorem 2.4: The function f of the form (1.2) is an element of the class $\mathfrak{HB}_{\mathfrak{q}}^{\zeta}(\chi,\phi,\nu,\tau_m)$ if and only if the following condition is met:

$$\sum_{k=m+1}^{\infty}\frac{\left([k]_{\mathfrak{q}}-\phi+\upsilon|\chi|\right)[k]_{\mathfrak{q}}!}{[\zeta+1]_{\mathfrak{q},k-1}}\,a_k\leq(1-\phi+\upsilon|\chi|)\left(1-\sum_{l=2}^{m}\tau_l\right). \qquad (2.9)$$

Proof: We use the important fact in Theorem 2.1 . In addition, we take

$$a_k=\frac{(1-\phi+\upsilon|\chi|)\,[\zeta+1]_{\mathfrak{q},k-1}\tau_l}{\left([k]_{\mathfrak{q}}-\phi+\upsilon|\chi|\right)[k]_{\mathfrak{q}}!},k=2,3,\dots m \qquad (2.10)$$

to arrive at

$$\sum_{l=2}^{m}\tau_l-\sum_{k=m+1}^{\infty}\frac{(1-\phi+\upsilon|\chi|)\,[\zeta+1]_{\mathfrak{q},k-1}}{\left([k]_{\mathfrak{q}}-\phi+\upsilon|\chi|\right)[k]_{\mathfrak{q}}!}\,a_k\leq 1, \qquad (2.11)$$

which leads us to the proof of the theorem easily and simply.

The result in the inequality (2.9) is strict for a function of the form

$$f(z)=z-\sum_{l=2}^{m}\frac{(1-\phi+\upsilon|\chi|)\,[\zeta+1]_{\mathfrak{q},k-1}\tau_l}{\left([l]_{\mathfrak{q}}-\phi+\upsilon|\chi|\right)[l]_{\mathfrak{q}}!}\,z^l-\frac{(1-\phi+\upsilon|\chi|)\,[\zeta+1]_{\mathfrak{q},k-1}(1-\sum_{l=2}^{m}\tau_l)}{\left([k]_{\mathfrak{q}}-\phi+\upsilon|\chi|\right)[k]_{\mathfrak{q}}!}\,z^k, \qquad (2.12)$$

while the value of k starts from $m+1$ and larger.

Corollary 2.5: If f is an element of the class $\mathfrak{HB}_{\mathfrak{q}}^{\zeta}(\chi,\phi,\nu,\tau_m)$, then its coefficients are met:

$$a_k\leq\frac{(1-\phi+\upsilon|\chi|)\,[\zeta+1]_{\mathfrak{q},k-1}(1-\sum_{l=2}^{m}\tau_l)}{\left([k]_{\mathfrak{q}}-\phi+\upsilon|\chi|\right)[k]_{\mathfrak{q}}!}, \qquad (2.13)$$

as we mentioned when $k\geq m+1$.

Let us pause for a moment and observe and test the convexity of the class $\mathfrak{HB}_{\mathfrak{q}}^{\zeta}(\chi,\phi,\nu,\tau_m)$ by studying and applying the convexity theories and thus stating and proving the validity and truth of the opposite of the case, all within proposal of the following theorem.

Theorem 2.6: A function f is an element of the class $\mathfrak{HB}_{\mathfrak{q}}^{\zeta}(\chi,\phi,\nu,\tau_m)$ if and only if it can be written in the form

$$f(z)=\sum_{k=m}^{\infty}\eta_k f_k, \qquad (2.14)$$

under the condition

$$\sum_{k=m}^{\infty}\eta_k=1,\ \ \eta_k\geq 0 \qquad (2.15)$$

and take the functions

$$f_m(z)=z-\sum_{l=2}^{m}\frac{(1-\phi+\upsilon|\chi|)\,[\zeta+1]_{\mathfrak{q},l-1}\tau_l}{\left([l]_{\mathfrak{q}}-\phi+\upsilon|\chi|\right)[l]_{\mathfrak{q}}!}\,z^l\ . \qquad (2.16)$$

$$f_k(z)=z-\sum_{l=2}^{m}\frac{(1-\phi+\upsilon|\chi|)\,[\zeta+1]_{\mathfrak{q},l-1}\tau_l}{\left([l]_{\mathfrak{q}}-\phi+\upsilon|\chi|\right)[l]_{\mathfrak{q}}!}\,z^l-\frac{(1-\phi+\upsilon|\chi|)\,[\zeta+1]_{\mathfrak{q},k-1}(1-\sum_{l=2}^{m}\tau_l)}{\left([k]_{\mathfrak{q}}-\phi+\upsilon|\chi|\right)[k]_{\mathfrak{q}}!}\,z^k, \qquad (2.17)$$

for all values of k starting from $m+1$ onwards.

Proof: First, we prove the first part by taking the function f, which can be written as follows:

$$f(z)=\sum_{k=m}^{\infty}\eta_k f_k. \qquad (2.18)$$

So, in other words, it can be written as

$$f(z)=z-\sum_{l=2}^{m}\frac{(1-\phi+\upsilon|\chi|)\,[\zeta+1]_{\mathfrak{q},k-1}\tau_l}{\left([l]_{\mathfrak{q}}-\phi+\upsilon|\chi|\right)[l]_{\mathfrak{q}}!}\,z^l-\sum_{k=m+1}^{\infty}\frac{(1-\phi+\upsilon|\chi|)\,[\zeta+1]_{\mathfrak{q},k-1}(1-\sum_{l=2}^{m}\tau_l)}{\left([k]_{\mathfrak{q}}-\phi+\upsilon|\chi|\right)[k]_{\mathfrak{q}}!}z^k\ . \qquad (2.19)$$

We call Theorem 2.4 and conclude the following

$$\sum_{k=m+1}^{\infty}\frac{(1-\phi+\upsilon|\chi|)\,[\zeta+1]_{\mathfrak{q},k-1}(1-\sum_{l=2}^{m}\tau_l)\,\eta_k}{\left([k]_{\mathfrak{q}}-\phi+\upsilon|\chi|\right)[k]_{\mathfrak{q}}!}\cdot\frac{\left([k]_{\mathfrak{q}}-\phi+\upsilon|\chi|\right)[k]_{\mathfrak{q}}!}{[\zeta+1]_{\mathfrak{q},k-1}}$$

$$=\left(1-\sum_{l=2}^{m}\tau_l\right)(1-\phi+\upsilon|\chi|)(1-\eta_m)\leq\left(1-\sum_{l=2}^{m}\tau_l\right)(1-\phi+\upsilon|\chi|), \qquad (2.20)$$

This gives us our desired goal, which is the truth that f is an element of the class $\mathfrak{HB}_{\mathfrak{q}}^{\zeta}(\chi,\phi,\nu,\tau_m)$.

To complete the proof, we come to the second part and take $f\in\mathfrak{HB}_{\mathfrak{q}}^{\zeta}(\chi,\phi,\nu,\tau_m)$. Now since we are in Corollary 2.6, we proved that:

$$a_k\leq\frac{(1-\phi+\upsilon|\chi|)\,[\zeta+1]_{\mathfrak{q},k-1}(1-\sum_{l=2}^{m}\tau_l)}{\left([k]_{\mathfrak{q}}-\phi+\upsilon|\chi|\right)[k]_{\mathfrak{q}}!}, \qquad (2.21)$$

when $k\geq m+1$.

$$\eta_k=\frac{\left([k]_{\mathfrak{q}}-\phi+\upsilon|\chi|\right)[k]_{\mathfrak{q}}!}{(1-\phi+\upsilon|\chi|)\,[\zeta+1]_{\mathfrak{q},k-1}(1-\sum_{l=2}^{m}\tau_l)}. \qquad (2.22)$$

We also put

$$\eta_m=\left(1-\sum_{k=m+1}^{\infty}\eta_k\right).$$

Consequently, it can be written

$$f(z)=\sum_{k=m}^{\infty}\eta_k f_k,$$

and once we complete the proof of this part, we have completed the proof of the theorem.

The proof of the previous theorem lies in our ability to determine the extreme points of the wonderful class $\mathfrak{HB}_{\mathfrak{q}}^{\zeta}(\chi,\phi,\nu,\tau_m)$ and thus study the properties of these distinctive points. In fact , they are the same functions shown in equations (2.16}) and (2.17) in the statement of the theorem, which we will clearly shown in the following result.

Theorem 2.7: The functions

$$f_m(z)=z-\sum_{l=2}^{m}\frac{(1-\phi+\upsilon|\chi|)\,[\zeta+1]_{\mathfrak{q},l-1}\tau_l}{\left([l]_{\mathfrak{q}}-\phi+\upsilon|\chi|\right)[l]_{\mathfrak{q}}!}\,z^l\ . \qquad (2.23)$$

$$f_k(z)=z-\sum_{l=2}^{m}\frac{(1-\phi+\upsilon|\chi|)\,[\zeta+1]_{\mathfrak{q},l-1}\tau_l}{\left([l]_{\mathfrak{q}}-\phi+\upsilon|\chi|\right)[l]_{\mathfrak{q}}!}\,z^l-\frac{(1-\phi+\upsilon|\chi|)\,[\zeta+1]_{\mathfrak{q},k-1}(1-\sum_{l=2}^{m}\tau_l)}{\left([k]_{\mathfrak{q}}-\phi+\upsilon|\chi|\right)[k]_{\mathfrak{q}}!}\,z^k, \qquad (2.24)$$

for all values of k starting from $m+1$ onwards, are exactly the extreme points of the wonderful class $\mathfrak{HB}_{\mathfrak{q}}^{\zeta}(\chi,\phi,\nu,\tau_m)$.

I would like to point out that I have noticed through my review of previous research that some of them take the summation from m to ∞ when determining the extreme points $f(k)$, and this is wrong. At first I decided to point out some of this research, but I eventually backed down and wrote it as note only.

3. IDENTIFICATION OF Q-STARLIKE AND Q-CONVEX REGIONS OF ORDER $\psi(0\leq\psi<1)$ FOR THE CHARACTERISTIC CLASS $\mathfrak{HB}_{\mathfrak{q}}^{\zeta}(\chi,\phi,\nu,\tau_m)$ WITHIN THE UNIT DISK $\mathcal{U}$

In this part of the article we show the regions where the functions of the defined class $\mathfrak{HB}_{\mathfrak{q}}^{\zeta}(\chi,\phi,\nu,\tau_m)$ are q-starlike and q-curved in our attempt to derive and

determine the radius of these regions shown in the following two theorems.

Theorem 3.1: If we take the function f in the class $\mathfrak{HB}_{\mathfrak{q}}^{\zeta}(\chi,\phi,\nu,\tau_m)$, it has a q-starlike property of order $\psi(0\le\psi<1)$ in the disk $|z|<\mathfrak{r}^*(\chi,\phi,\nu,\tau_m,\psi)$, and $\mathfrak{r}^*(\chi,\phi,\nu,\tau_m,\psi)$ is the largest value that satisfies the property

$$\sum_{l=2}^{m}([l-1]_{\mathfrak{q}}+1-\psi)\frac{(1-\phi+\upsilon|\chi|)\,[\zeta+1]_{\mathfrak{q},l-1}\tau_l}{([l]_{\mathfrak{q}}-\phi+\upsilon|\chi|)\,[l]_{\mathfrak{q}}!}\,\mathfrak{r}^{l-1}+\frac{(1-\phi+\upsilon|\chi|)\,[\zeta+1]_{\mathfrak{q},k-1}(1-\sum_{l=2}^{m}\tau_l)([k]_{\mathfrak{q}}-\psi+1)}{([k]_{\mathfrak{q}}-\phi+\upsilon|\chi|)\,[k]_{\mathfrak{q}}!}\,\mathfrak{r}^{k-1}\le 1-\psi. \quad (3.1)$$

The extreme functions is

$$f(z)=z-\sum_{l=2}^{m}\frac{(1-\phi+\upsilon|\chi|)\,[\zeta+1]_{\mathfrak{q},l-1}\tau_l}{([l]_{\mathfrak{q}}-\phi+\upsilon|\chi|)\,[l]_{\mathfrak{q}}!}\,z^l-\frac{(1-\phi+\upsilon|\chi|)\,[\zeta+1]_{\mathfrak{q},k-1}(1-\sum_{l=2}^{m}\tau_l)}{([k]_{\mathfrak{q}}-\phi+\upsilon|\chi|)\,[k]_{\mathfrak{q}}!}\,z^k. \quad (3.2)$$

The theorem acquires the limiting property in it.

Proof: In order for the function $f\in\mathfrak{HB}_{\mathfrak{q}}^{\zeta}(\chi,\phi,\nu,\tau_m)$ have the q-starlike property of order $\psi(0\le\psi<1)$, we start by taking the quantity

$$\left|\frac{zf'(z)}{f(z)}-1\right|\le\frac{\sum_{l=2}^{m}[l-1]_{\mathfrak{q}}\frac{(1-\phi+\upsilon|\chi|)\,[\zeta+1]_{\mathfrak{q},l-1}\tau_l}{([l]_{\mathfrak{q}}-\phi+\upsilon|\chi|)\,[l]_{\mathfrak{q}}!}\,\mathfrak{r}^{k-1}+\sum_{k=m+1}^{\infty}[k-1]_{\mathfrak{q}}a_k\mathfrak{r}^{k-1}}{1-\sum_{l=2}^{m}\frac{(1-\phi+\upsilon|\chi|)\,[\zeta+1]_{\mathfrak{q},l-1}\tau_l}{([l]_{\mathfrak{q}}-\phi+\upsilon|\chi|)\,[l]_{\mathfrak{q}}!}\,\mathfrak{r}^{k-1}-\sum_{k=m+1}^{\infty}a_k\mathfrak{r}^{k-1}}. \quad (3.3)$$

It must be

$$\le 1-\psi,$$

by setting $|z|\le\mathfrak{r}$, so we have

$$\sum_{l=2}^{m}([l-1]_{\mathfrak{q}}+1-\psi)\frac{(1-\phi+\upsilon|\chi|)\,[\zeta+1]_{\mathfrak{q},l-1}\tau_l}{([l]_{\mathfrak{q}}-\phi+\upsilon|\chi|)\,[l]_{\mathfrak{q}}!}\,\mathfrak{r}^{l-1}+\sum_{k=m+1}^{\infty}([k-1]_{\mathfrak{q}}-\psi+1)a_k\mathfrak{r}^{k-1}\le 1-\psi. \quad (3.4)$$

By referring to Theorem 2.4, we have the important fact

$$a_k=\frac{(1-\phi+\upsilon|\chi|)\,[\zeta+1]_{\mathfrak{q},k-1}(1-\sum_{l=2}^{m}\tau_l)\eta_k}{([k]_{\mathfrak{q}}-\phi+\upsilon|\chi|)\,[k]_{\mathfrak{q}}!}, \quad (3.5)$$

that's when $\eta_k\ge 0,\sum_{k=3}^{\infty}\eta_k\le 1,k\ge 3$.

We determine the value of $k^*=k^*(\mathfrak{r})$ so that the quantity

$$\frac{(1-\phi+\upsilon|\chi|)\,[\zeta+1]_{\mathfrak{q},k^*-1}([k^*]_{\mathfrak{q}}-\psi+1)}{([k^*]_{\mathfrak{q}}-\phi+\upsilon|\chi|)\,[k^*]_{\mathfrak{q}}!}\,\mathfrak{r}^{k^*-1}, \quad (3.6)$$

has its highest value by fixing the value of $\mathfrak{r}$ in it.

After that we have

$$\sum_{k=m+1}^{\infty}([k-1]_{\mathfrak{q}}-\psi+1)a_k\mathfrak{r}^{k-1}\le\frac{(1-\phi+\upsilon|\chi|)\,[\zeta+1]_{\mathfrak{q},k-1}(1-\sum_{l=2}^{m}\tau_l)([k^*]_{\mathfrak{q}}-\psi+1)}{([k^*]_{\mathfrak{q}}-\phi+\upsilon|\chi|)\,[k^*]_{\mathfrak{q}}!}\,\mathfrak{r}^{k^*-1}. \quad (3.7)$$

Finally, we have determined the region where the functions in the class $\mathfrak{HB}_{\mathfrak{q}}^{\zeta}(\chi,\phi,\nu,\tau_m)$ are q-starlike of order $\psi(0\le\psi<1)$ which is $|z|<r\,(\chi,\phi,\nu,\tau_m,\psi)$, provided that

$$\sum_{l=2}^{m}([l-1]_{\mathfrak{q}}+1-\psi)\frac{(1-\phi+\upsilon|\chi|)\,[\zeta+1]_{\mathfrak{q},l-1}\tau_l}{([l]_{\mathfrak{q}}-\phi+\upsilon|\chi|)\,[l]_{\mathfrak{q}}!}\,\mathfrak{r}^{l-1}+\frac{(1-\phi+\upsilon|\chi|)\,[\zeta+1]_{\mathfrak{q},k^*-1}(1-\sum_{l=2}^{m}\tau_l)([k^*]_{\mathfrak{q}}-\psi+1)}{([k^*]_{\mathfrak{q}}-\phi+\upsilon|\chi|)\,[k^*]_{\mathfrak{q}}!}\,\mathfrak{r}^{k^*-1}\le 1-\psi. \quad (3.8)$$

We can now determine the value of $\mathfrak{r}^*=\mathfrak{r}^*(\chi,\phi,\nu,\tau_m,\psi)$ and the value of $k^*(\mathfrak{r}^*)$ associated with it by

$$\sum_{l=2}^{m}([l-1]_{\mathfrak{q}}+1-\psi)\frac{(1-\phi+\upsilon|\chi|)\,[\zeta+1]_{\mathfrak{q},l-1}\tau_l}{([l]_{\mathfrak{q}}-\phi+\upsilon|\chi|)\,[l]_{\mathfrak{q}}!}\,\mathfrak{r}^{*l-1}+\frac{(1-\phi+\upsilon|\chi|)\,[\zeta+1]_{\mathfrak{q},k^*-1}(1-\sum_{l=2}^{m}\tau_l)([k^*]_{\mathfrak{q}}-\psi+1)}{([k^*]_{\mathfrak{q}}-\phi+\upsilon|\chi|)\,[k^*]_{\mathfrak{q}}!}\,\mathfrak{r}^{*k^*-1}\le 1-\psi. \quad (3.9)$$

Which is the q-starlike radius of the functions in the class $\mathfrak{HB}_{\mathfrak{q}}^{\zeta}(\chi,\phi,\nu,\tau_m)$.

Since the concepts of ψ-starlike and ψ-curvature radii are related to each other.As we have found or defined the first, it is natural to think about defining the region of the ψ -curvature in the unit disk $\mathcal{U}$ for the functions in our special class $\mathfrak{HB}_{\mathfrak{q}}^{\zeta}(\chi,\phi,\nu,\tau_m)$ by proposing the following theorem:

Theorem 3.2: If we take the function f in the class $\mathfrak{HB}_{\mathfrak{q}}^{\zeta}(\chi,\phi,\nu,\tau_m)$, it has a q-convex property of order $\psi(0\le\psi<1)$ in the disk $|z|<\mathfrak{r}^{**}(\chi,\phi,\nu,\tau_m,\psi)$, and $\mathfrak{r}^{**}(\chi,\phi,\nu,\tau_m,\psi)$ is the largest value that satisfies the property

$$\sum_{l=2}^{m}[l]_{\mathfrak{q}}([l-1]_{\mathfrak{q}}+1-\psi)\frac{(1-\phi+\upsilon|\chi|)\,[\zeta+1]_{\mathfrak{q},l-1}\tau_l}{([l]_{\mathfrak{q}}-\phi+\upsilon|\chi|)\,[l]_{\mathfrak{q}}!}\,\mathfrak{r}^{l-1}+\frac{(1-\phi+\upsilon|\chi|)\,[\zeta+1]_{\mathfrak{q},k-1}(1-\sum_{l=2}^{m}\tau_l)([k]_{\mathfrak{q}}-\psi+1)}{([k]_{\mathfrak{q}}-\phi+\upsilon|\chi|)\,[k]_{\mathfrak{q}}!}\,\mathfrak{r}^{k-1}\le 1-\psi. \quad (3.10)$$

The extreme functions is

$$f(z)=z-\sum_{l=2}^{m}\frac{(1-\phi+\upsilon|\chi|)\,[\zeta+1]_{\mathfrak{q},l-1}\tau_l}{([l]_{\mathfrak{q}}-\phi+\upsilon|\chi|)\,[l]_{\mathfrak{q}}!}\,z^l-\frac{(1-\phi+\upsilon|\chi|)\,[\zeta+1]_{\mathfrak{q},k-1}(1-\sum_{l=2}^{m}\tau_l)}{([k]_{\mathfrak{q}}-\phi+\upsilon|\chi|)\,[k]_{\mathfrak{q}}!}\,z^k. \quad (3.11)$$

The theorem acquires the limiting property

Proof: To prove the theorem, we take

$$\left|\frac{zf''(z)}{f'(z)}\right|\le\left[\sum_{l=2}^{m}[l]_{\mathfrak{q}}([l-1]_{\mathfrak{q}}+1-\psi)\frac{(1-\phi+\upsilon|\chi|)\,[\zeta+1]_{\mathfrak{q},l-1}\tau_l}{([l]_{\mathfrak{q}}-\phi+\upsilon|\chi|)\,[l]_{\mathfrak{q}}!}\,\mathfrak{r}^{k-1}+\sum_{k=m+1}^{\infty}[k]_{\mathfrak{q}}[k-1]_{\mathfrak{q}}a_k\mathfrak{r}^{k-1}\right]/$$

$$\left[1-\sum_{l=2}^{m}[l]_{\mathfrak{q}}\frac{(1-\phi+\upsilon|\chi|)\,[\zeta+1]_{\mathfrak{q},l-1}\tau_l}{\left([l]_{\mathfrak{q}}-\phi+\upsilon|\chi|\right)[l]_{\mathfrak{q}}!}\,\mathfrak{r}^{k-1}-\sum_{k=m+1}^{\infty}[k]_{\mathfrak{q}}a_k\mathfrak{r}^{k-1}\right]. \quad (3.12)$$

$$\sum_{l=2}^{m}[l]_{\mathfrak{q}}\left([l-1]_{\mathfrak{q}}+1-\psi\right)\frac{(1-\phi+\upsilon|\chi|)\,[\zeta+1]_{\mathfrak{q},l-1}\tau_l}{\left([l]_{\mathfrak{q}}-\phi+\upsilon|\chi|\right)[l]_{\mathfrak{q}}!}\,\mathfrak{r}^{l-1}+\sum_{k=m+1}^{\infty}[k]_{\mathfrak{q}}\left([k-1]_{\mathfrak{q}}-\psi+1\right)a_k\mathfrak{r}^{k-1}\leq 1-\psi. \quad (3.13)$$

We determine the value of $k^*=k^*(\mathfrak{r})$ so that the quantity

$$\frac{(1-\phi+\upsilon|\chi|)\,[\zeta+1]_{\mathfrak{q},k^*-1}\left([k^*]_{\mathfrak{q}}-\psi+1\right)}{\left([k^*]_{\mathfrak{q}}-\phi+\upsilon|\chi|\right)[k^*]_{\mathfrak{q}}!}\,\mathfrak{r}^{k^*-1}, \quad (3.14)$$

has its highest value by fixing the value of $\mathfrak{r}$ in it.

After that we have

$$\sum_{k=m+1}^{\infty}[k]_{\mathfrak{q}}\left([k-1]_{\mathfrak{q}}-\psi+1\right)a_k\mathfrak{r}^{k-1}\leq\frac{(1-\phi+\upsilon|\chi|)\,[\zeta+1]_{\mathfrak{q},k-1}(1-\sum_{l=2}^{m}\tau_l)\left([k^*]_{\mathfrak{q}}-\psi+1\right)}{\left([k^*]_{\mathfrak{q}}-\phi+\upsilon|\chi|\right)[k^*]_{\mathfrak{q}}!}\,\mathfrak{r}^{k^*-1}. \quad (3.15)$$

Finally, we have determined the region where the functions in the class $\mathfrak{HB}_{\mathfrak{q}}^{\zeta}(\chi,\phi,\nu,\tau_m)$ are q-convex of order $\psi(0\leq\psi<1)$ which is $|z|<r\,(\chi,\phi,\nu,\tau_m,\psi)$, provided that

$$\sum_{l=2}^{m}[l]_{\mathfrak{q}}\left([l-1]_{\mathfrak{q}}+1-\psi\right)\frac{(1-\phi+\upsilon|\chi|)\,[\zeta+1]_{\mathfrak{q},l-1}\tau_l}{\left([l]_{\mathfrak{q}}-\phi+\upsilon|\chi|\right)[l]_{\mathfrak{q}}!}\,\mathfrak{r}^{l-1}+\frac{(1-\phi+\upsilon|\chi|)\,[\zeta+1]_{\mathfrak{q},k^*-1}(1-\sum_{l=2}^{m}\tau_l)\left([k^*]_{\mathfrak{q}}-\psi+1\right)}{\left([k^*]_{\mathfrak{q}}-\phi+\upsilon|\chi|\right)[k^*]_{\mathfrak{q}}!}\,\mathfrak{r}^{k^*-1}\leq 1-\psi. \quad (3.16)$$

We can now determine the value of $\mathfrak{r}^{**}=\mathfrak{r}^{**}(\chi,\phi,\nu,\tau_m,\psi)$ and the value of $k^*(\mathfrak{r}^{**})$ associated with it by

$$\sum_{l=2}^{m}[l]_{\mathfrak{q}}\left([l-1]_{\mathfrak{q}}+1-\psi\right)\frac{(1-\phi+\upsilon|\chi|)\,[\zeta+1]_{\mathfrak{q},l-1}\tau_l}{\left([l]_{\mathfrak{q}}-\phi+\upsilon|\chi|\right)[l]_{\mathfrak{q}}!}\,\mathfrak{r}^{**l-1}+\frac{(1-\phi+\upsilon|\chi|)\,[\zeta+1]_{\mathfrak{q},k^*-1}(1-\sum_{l=2}^{m}\tau_l)\left([k^*]_{\mathfrak{q}}-\psi+1\right)}{\left([k^*]_{\mathfrak{q}}-\phi+\upsilon|\chi|\right)[k^*]_{\mathfrak{q}}!}\,\mathfrak{r}^{**k^*-1}\leq 1-\psi, \quad (3.17)$$

which is the q-convex radius of the functions in the class $\mathfrak{HB}_{\mathfrak{q}}^{\zeta}(\chi,\phi,\nu,\tau_m)$.

4. CONCLUSION

Using the q-integral operator that implicitly contain the q-Ruscheweyh derivative, a new class of analytic univalent functions has been defined.They are distinguished by some of their finite negative invariant coefficients, and their most interesting fundumental geometric properties have been studied. In the future, the study of geometric properties can be extended to include other interesting properties. Researchers can also draw inspiration from this work to study other distinct classes, serving the field of geometry and complex analysis. The results we have reached can also be studied and analyzed on classes of multivalent functions.

REFERENCES

Abubaker, A. A., Matarneh, K., Khan, M. F. A., Suha, B., & Kamal, M. (2024). Study of quantum calculus for a new subclass of q-starlike bi-univalent functions connected with vertical strip domain. *AIMS Mathematics, 9*, 11789–11804. https://doi.org/10.3934/math.2024577

Akyar, A. (2025). On the sufficient conditions for the univalence of definite integral operators involving certain functions in S class. *Fundamentals of Contemporary Mathematical Sciences, 6*(1), 34–46. https://doi.org/10.54974/fcmathsci.1409461

Al-Hawary, T., Frasin, B. A., & Salah, J. (2025). Necessary and sufficient conditions for functions defined by binomial distribution to be in a general class of analytic functions. *Results in Nonlinear Analysis, 8*(1), 131–140. https://doi.org/10.31838/rna/2025.08.01.013

Al-Rawashdeh, W. (2025). On certain classes of bi-Bazilevic functions defined by q-Ruscheweyh differential operator. *WSEAS Transactions on Mathematics, 24*, 144–156. https://doi.org/10.37394/23206.2025.24.15

AL-Saleem, A. B. I. (2025). Certain class of analytic and univalent function with respect to symmetric. *Nonlinear Functional Analysis and Applications*, 99–111. https://doi.org/10.22771/nfaa.2025.30.01.07

Alsoboh, A., & Oros, G. I. (2024). A class of bi-univalent functions in a leaf-like domain defined through subordination via q-calculus. *Mathematics, 12*(10), 1594. https://doi.org/10.3390/math12101594

Delphi, A. M. (2024). A new subclass of analytic functions on unit disk defined by using integral operator. *Pure Sciences International Journal of Kerbala, 1*(4), 70–77.

Illafe, M., Mohd, M. H., Yousef, F., & Supramaniam, S. (2024). A subclass of bi-univalent functions defined by a symmetric q-derivative operator and Gegenbauer polynomials. *European Journal of Pure and Applied Mathematics, 17*(4), 2467–2480. https://doi.org/10.29020/nybg.ejpam.v17i4.5408

Jackson, F. H. (1905). The application of basic numbers to Bessel's and Legendre's functions (second paper). *Proceedings of the London Mathematical Society, 2*(1), 1–23. https://doi.org/10.1112/plms/s2-3.1.1

Jackson, F. H. (1909). On q-functions and a certain difference operator. *Earth and Environmental Science Transactions of the Royal Society of Edinburgh, 46*(2), 253–281. http://dx.doi.org/10.1017/S0080456800002751

Jackson, F. H. (1910a). q-difference equations. *American Journal of Mathematics, 32*(4), 305–314. https://doi.org/10.2307/2370183

Jackson, F. H., Fukuda, T., Dunn, O., et al. (1910b). On q-definite integrals. *Quarterly Journal of Pure and Applied Mathematics, 41*(15), 193–203.

Kanas, S., & Răducanu, D. (2014). Some class of analytic functions related to conic domains. *Mathematica Slovaca, 64*(5), 1183–1196. https://doi.org/10.2478/s12175-014-0268-9

Lashin, A. M. Y., Badghaish, A. O. A., & Alshehri, F. A. (2024). A study on two subclasses of analytic and univalent functions with negative coefficients involving the Poisson distribution series. *Kyungpook Mathematical Journal, 64*(1), 47–55. https://doi.org/10.5666/KMJ.2024.64.1.47

Maran, A. H., Juma, A. R. S., & Al-Saphory, R. A. (2025). On a subclass of univalent functions with negative coefficients associated to linear Srivastava–Attiya operator. *AIP Conference Proceedings, 3264*(1). https://doi.org/10.1063/5.0258978

Noor, K. I. (1999). On new classes of integral operators. *Journal of Natural Geometry, 16*(1–2), 71–80.

Srivastava, H. M., Ahmad, Q. Z., Khan, N., Kahn, N., & Khan, B. (2019). Hankel and Toeplitz determinants for a subclass of q-starlike functions associated with a general conic domain. *Mathematics, 7*(2), 181. https://doi.org/10.3390/math7020181

Srivastava, H. M., Wanas, A. K., & Srivastava, R. (2021). Applications of the q-Srivastava–Attiya operator involving a certain family of bi-univalent functions associated with the Horadam polynomials. *Symmetry, 13*(7), 1230. https://doi.org/10.3390/sym13071230

Universiti Kebangsaan Malaysia (UKM), Bangi. (2024). Properties for certain class of p-valent functions related to Jackson's operator. *Sains Malaysiana, 55*(1), 231–238. http://doi.org/10.17576/jsm-2024-5301

PURE SCIENCES
International Journal of Kerbala

Pure Sciences International Journal of Kerbala

Year: 2025 Volume : 2 Issue : 7 ISSN: 6188-2789 Print 3005 -2394 Online

2025,Volume 2 , Issue 7 , PSIJK (23-28)

Pure Sciences International Journal of Kerbala

The Preventive Effect of Pomegranate Peel Powder (Punica Granatum) Against Ethanol-Induced Oxidative Stress on Various Biochemical Parameters in Albino Rats

Mustafa K. Mushatet [a*], Asaad Abbas khalaf [a]

[a] *Branch of basic sciences, College of Nursing, University of Kerbala, Kerbala, Iraq*

P A P E R I N F O

Received: 27.04.2025
Accepted: 19.05.2025
Published: 30.09.2025

Keywords:
ethanol, GSH, MDA, oxidative stress, pomegranate

A B S T R A C T

The point of this study was to find out if pomegranate (Punica granatum) peel powder (PPP), could protect against liver oxidative stress caused by ethanol (E) in rats. We randomly divided 24 Wistar rats, weighing 190–250 g, into four groups 6 rats for each. The negative control group fed a basic diet (pellet), the positive control (ethanolic) group was given 70% ethanol at a dose of 0.005 ml/g to cause oxidative stress. Group III (E&PPP 50%) was orally treated with PPP 50% in addition to a basal diet after one hour of dosing with 70% ethanol for 0.005 ml/g, and group IV (E&PPP 80%) was orally treated with PPP 75% in addition to a basal diet after one hour of dosing with 70% ethanol for 0.005 ml/g. After 30 days, the rats were euthanized, and prior to this, blood samples were collected in specialized tubes to isolate the serum for the intended tests. In the ethanolic group of rats, serum total protein, globulin, albumin, AST, ALP, ALT, and MDA levels went up significantly, while glutathione GSH levels went down significantly. PPP diminished ethanol-induced amounts of total protein, globulin, albumin, AST, ALP, ALT, and MDA in treatment group E&PPP 80%, decreased less than the ethanolic group in E&PPP 50%, compared to the control group. Consequently, the study shows that PPP protects liver from ethanol's toxicity by scavenging free radicals and reducing ROS levels, thereby mitigating hepatocyte damage.

DOI: 10.53851/psijk.v2.i7.23 -28

1. INTRODUCTION

The pomegranate, *Punica granatum* (family: Punicaceae), is a delectable fruit recognized for its powerful antioxidant attributes. *P.granatum* is extensively farmed for the manufacturing of pomegranate juice. However, the pomegranate peel powder (PPP), a byproduct of the pomegranate industry, constitutes roughly 77% of the entire fruit(Hamed et al.,2021) . PP possesses elevated antioxidant levels compared to pomegranate juice, indicating its potential utility as a nutritional supplement in animal feed(Badawi M. E.& Gomaa A. M, 2016). PPP has numerous natural antioxidant components, including polyphenols and polysaccharides(Ibrahium M.,2010)(Bachoual R.et al.,2011) that yield antioxidative, anti-infective, antibacterial, hepatoprotective, antiatherogenic, antidiarrheal, and antimutagenic effects(El-Houseiny W. et al.,2021). PPP demonstrated anti-inflammatory and anti-atherogenic properties relative to HFD controls(Salama A. A. et al.,2019).It has an anti-ulcer activity (Abdulzahra A. & Al-Salih, H. ,2022). Pomegranate flowers contain polyphenols that can protect liver enzymes and prevent NAFLD. Punicalagin, an ellagitannin, can reduce hyperlipidemia and hepatic lipid accumulation in rats. Pomegranate extracts have antioxidant, anti-inflammatory, hypoglycemic, and hepatoprotective properties, potentially aiding in the prevention and management of NAFLD (Zamanian M. et al.,2023). Consumption of alcohol, non-steroidal anti-inflammatory medications, tobacco, an inadequate diet, and both physical and psychological stress typically result in gastric ulcers (Ajibo D. et al. ,2023). These factors may induce oxidative stress (Suzuki H. et al.,2021) . Ethanol induces ulceration of the stomach mucosa by generating highly deleterious free radicals that act as necrotic agents(Ofusori A. et al., 2019) . Ethanol disrupts stomach mucus secretion, modifies the permeability of endothelial cells (mucosa), and diminishes mucus production, rendering gastric mucosal cells more susceptible to free radicals (Hossen M. et al. ,2021). Oxidative stress (OS) refers to the imbalance between pro-oxidant processes induced by reactive

*Corresponding Author Institutional Email:
mustafa.k@uokerbala.edu.iq (Mustafa K. Mushatet)

oxygen species (ROS) and an organism's capacity to mitigate their overproduction or manage the resultant damage. Multiple studies have shown that increased reactive oxygen species (ROS) production in gastrointestinal illnesses leads to inflammation and further enhances ROS synthesis (Ghazizadeh H. et al.,2020) (Caliri A. et al., 2021). The present work may provide a rapid and secure method to mitigate oxidative stress induced by high doses of ethanol in rats through the application of three distinct quantities of pomegranate (Punica granatum) peel powder (PPP).

2. MATERIALS AND METHODS

2.1. Peel Collection and Preparation

Pomegranate fruit was brought from local suq, which lies in Karbala city. The pomegranate's external part (husk) was collected, dried, grounded with an electrical grinder, and then saved within 25 C ± 2 for later use.

2.2. Research Design and Methods

Twenty-four male growing albino rats (*Rattus norvegicus*) aged between 8 - 10 weeks, weighing 190–250 g was utilized for the study. The present study sourced animals from the animal house at the College of Pharmacy, University of Karbala. The procedure adheres to the requirements set forth by the National Institutes of Health (NIH), and the research design received approval from the local committee. The animals are contained in groups within enclosures, with unimpeded access to sustenance and hydration. Following two-weeks acclimatization period, the animals were partitioned into three equal groups:

- Group I (control) Animals of this group fed on basal diet (pellet).
- Group II (Ethanolic) 70% ethanol for 0.005 ml/g to induce oxidative stress (Beiranvand M. et al., 2021)(Abdel-Kawi S. et al.,2023).
- Group III (E&PPP 50%) was orally treated with PPP 30% in addition to basal diet (Abd Elsabor R. et al., 2018)(Hanani Z. et al.,2018) after one hour of dosing with 70% ethanol for 0.005 ml/g.
- Group IV (E&PPP 80%) was orally treated with PPP 75% in addition to basal diet, after one hour of dosing with 70% ethanol for 0.005 ml/g.

Daily food consumption was documented, while body weight was measured weekly. Upon the conclusion of the experiment (30 days).

2.3. Data Analysis

All results are shown as the mean ± standard deviation. ANOVA was employed to assess the statistical significance of the experimental data, with a significance level of $P < .05$. We may utilize the Excel 2013 software as a quantitative tool to conduct this statistical analysis.

3. RESULTS AND DISCUSSION

3.1. The Effects of Ethanol on the Biochemical Parameter Levels

Table 1 showed significant differences in all biochemical parameter levels, i.e., there was a significant increase ($P < 0.05$) in all of (Total protein, Globulin, Albumin, AST, ALP, ALT, MDA) in Ethanol group compared to control and treatment E&PPP 30%, E&PPP 75% groups. While there was a significant decrease in and GSH in Ethanol group compared to control and treatment E&PPP 30%, E&PPP 75% groups, may be altered by ethanol action in this group (Preedy V. et al.,1988) This may be elucidated by the elevated levels of ethanol-induced inflammation in the ethanol group (Xu H. et al.,2024) , Ethanol induces oxidative stress through the generation of reactive oxygen species (ROS)(Gugliandolo E. et al.,2021). It has a pivotal role in various illnesses, including stomach ulcers (Yoo J. et al., 2018) . Because of ethanol-induced hepatotoxicity (Yoo J. et al., 2018), the AST level was increased in the ethanol group compared to control, and increase level of ALP, ALT in this group. It goes back to the same reason (Liu Q. et al., 2024) (Arumugam M. K. et al., 2022).

ALT is predominantly located in non-mitochondrial regions of liver cells, whereas roughly 80% of AST is in the mitochondria of liver cells. Damage to liver cells releases ALT and AST into the serum, leading to an increase in serum AST and ALT levels. The invasion of cancer cells damages normal liver cells in liver cancer patients, leading to a rise in ALT and AST levels (Yang J., 2010). Ethanol induced oxidative stress (Jedidi S. et al., 2022), and destroyed mitochondria (Zhao H. et al., 2021).Therefore, it decreases the hepatic GSH and SOD (Schlorff E. et al., 1999), in addition to increasing hepatic MDA leve (Alsaif M. A., 2007) there for the levels of GSH in the second group reduced to 14.10 ± 0.30 compared to normal level in the control group 16.78 ± 0.40.

Table 1. The values are evidently average ± SD value, n = 6 in each group, [a] show the difference in statistics. With a control group, [b] statistical disparity according to CRG group, ($P < 0.05$).

Parameters	Control	Ethanol	E&PPP 50%	E&PPP 75%
Total protein (mg/dL)	05.85 ± 0.20	08.11 ± 0.14 [a]	07.50 ± 0.10 [a]	06.28 ± 0.12 [b]
Globulin (mg/dL)	01.83 ± 0.10	03.05 ± 0.10 [a]	02.49 ± 0.30 [a]	02.02 ± 0.15 [b]
Albumin (mg/dL)	04.02 ± 0.50	06.56 ± 0.20 [a]	05.02 ± 0.40 [a]	04.27 ± 0.33 [b]
AST (µ/L)	45.30 ± 0.40	65.00 ± 0.80 [a]	56.00 ± 0.60 [a b]	46.50 ± 0.80 [b]
ALP (µ/L)	20.60 ± 0.50	32.00 ± 0.40[a]	28.00 ± 0.45 [a b]	21.90 ± 0.70 [b]
ALT (µ/L)	21.00 ± 0.40	24.20 ± 0.30 [a]	22.50 ± 0.40 [a b]	20.50 ± 0.50 [b]
GSH (µ/L)	16.78 ± 0.40	14.10 ± 0.30 [a]	16.90 ± 0.10 [a b]	16.10 ± 0.40 [b]
MDA (µ/L)	04.30 ± 1.33	09.50 ± 1.60 [a]	06.50 ± 1.00 [b]	05.20 ± 1.30 [b]

3.2. The Effects of E&PPP on the Total Protein, Globulin, and Albumin Levels

Table 1 showed significant differences decrease ($P > 0.05$) in all of Total protein, Globulin and Albumin in E&PPP 75% group compare to E&PPP 30% group and ethanol groups, and no significant differences in E&PPP 75% group compare to the control group. Perhaps the reason is due to the effect of the high concentration of food containing pomegranate peels, which in turn contain many effective antioxidants and anti-ethanol substances such as gallic acid, ellagic acid, punicalagin, luteolin, catechin, rutin, hydrobenzoic acid, quercetin, punicalins) and caffeic acid (Mahmood A. M. & Jabar H. L., 2023).

Continuous exposure of the liver to a specific quantity of ethanol prompts hepatocytes to progressively release proteins (Vildhede A. et al., 2015) to mitigate the effects of ethanol or other oxidizing agents encountered, because of hepatocytes play a pivotal role in liver inflammation (Gong J. et al., 2023) Consequently, the concentrations of total serum proteins, globulin, and albumin elevate, mirroring the increases observed in the ethanol group (Niemelä O., 2001) . In the in E&PPP 30% and in E&PPP 75% groups, pomegranate peel powder effectively restored the usual amounts of these proteins, aiming to rehabilitate liver functions (Faddladdeen K. A. & Ojaimi A. A., 2019) . Consequently, we observed that the PPP 30% group, administered pomegranate powder at a concentration of 30%, could not restore normal liver functions, in contrast to the PPP 80%group, which received a greater concentration of 75%. The data unequivocally demonstrated a reduction in the concentration of total proteins, albumin, and globulin.

3.3. The Effects Of E&PPP on the AST, ALT, ALP Levels

Table 1 showed significant differences decrease ($P > 0.05$) in all of AST, ALT and ALP in E&PPP 75% group compare to E&PPP 30% group and ethanol groups, and no significant differences in E&PPP 75% group compare to the control group. AST, ALP and ALT, are important biomarkers of liver function (Akanya O. H. et al., 2015). The levels of these enzymes rise significantly when the liver is exposed to inflammatory substances such as sebastin (Palipoch S. & Punsawad C., 2013), CCL4 (Kostic T. et al., 2022), and ethanol (Høiseth G. et al., 2022) After giving ethanol to the ethanol group, we saw that the levels of these enzymes went up, while they went down in the PPP 30% and 80% treatment groups. Still, the higher amount of pomegranate peels in the fourth group (PPP 80%) had a big effect on getting protein levels back to normal. ALT is an enzyme typically found in hepatic and cardiac cells. Elevated ALT levels in the blood indicate liver or cardiac impairment when either organ is compromised. In hepatocellular damage, enzymes typically found in the cytosol are liberated into the bloodstream. Their presence in plasma serves as valuable indicators for assessing the degree and nature of hepatocellular injury (Pari L. & Murugan P., 2004).

We use ALT and AST to assess the hepatocellular integrity of liver tissue. ALT is mostly located in the liver, whereas AST is typically present in comparable concentrations in the liver, heart, muscle, kidney, and brain. Consequently, ALT exhibits more specificity for the liver compared to AST. The normal range for both ALT and AST in humans is 25 U/L to 50 U/L (Dollah M. A. et al., 2013). ALP increase by ethanol according to the table , Ethanol exposure results in alcoholic fatty liver, inflammation, necrosis, fibrosis and cirrhosis (Rostami H. et al., 2020) , Alkaline phosphatase (ALP) is a principal liver enzyme and a significant indicator of hepatic physiological health (Xue M. et al., 2017). In 1920, it was discovered that this enzyme elevated in hepatic disorders (Kaneko J. J. et al., 2018) . Alkaline phosphatase (EC3.1.3.1) facilitates the hydrolysis of organic phosphates, including proteins, nucleotides, and alkaloids, in an alkaline environment. The enzyme exists in several forms inside the bloodstream. It is also prevalent in the liver and bones (Fischbach F. & Zawta B., 1992) . It is important to know that pharmaceutical drugs, like vitamin E and corticosteroids, which are often anti-inflammatory and antioxidant, are often used to treat liver damage caused by drinking too much alcohol. However, using them for too long or in the wrong Excessive quantities may lead to complications. A high intake of vitamin E elevates the hazard of prostate cancer in men (Klein E. et al., 2012).

3.4. The Effects of E&PPP on the GSH and MDA Levels

The alterations in GSH content across various groups are presented in Table 1, demonstrating that rats treated Ethanol alone demonstrated a substantial decrease in plasma glutathione (GSH) levels. PPP supplementation elevated plasma glutathione levels. This outcome corresponds with that of (Ashoush I. S. et al., 2013) and (Oh S. I. et al., 1998) (Xue M. et al., 2022) . Glutathione (GSH) is essential for the detoxification of xenobiotics and the maintenance of cellular redox balance (Georgiou-Siafis S. K. & Tsiftsoglou A. S., 2023) . A decrease at the cellular level is often viewed as a sign of oxidative stress. It is clear that this lower level of this natural antioxidant is linked to oxidative stress caused by ethanol, which is shown by the production of harmful acetaldehyde and other reactive molecules inside the cell. The observed increase in GST activity seems to be a planned response aimed at blocking the harmful byproducts produced during the metabolism of ethanol (Macdonald I. O. et al., 2010) . PPP, an agricultural by-product with bioactive polyphenols, to prevent oxidative stress-related pathogenesis (Al-Gubory K. H. et al., 2010). The effect of the PPP in the two treatment groups (E&PPP 80% and E&PPP 30%) was apparent, with an increase in GSH levels in the lower concentration group E&PPP 30%. However, the significant differences removed in the higher concentration group E&PPP 30% compared to the control group.

The significant increase (09.50 ± 1.60) in MDI in the ethanol group compared to the control group was due to high concentration and continuous ethanol dosing (Aggul A. G. et al., 2022). This elevation was due to a rise in oxidants, which then increased free radicals caused by ethanol-damaged liver cells [15]. Research demonstrates that ethanol can provoke lipid peroxidation in cellular membranes via the generation of reactive oxygen species (ROS), resulting in cellular damage (Arthur I., 2001) . The treatment group with the lower concentration E&PPP 30% endeavored to diminish these oxidants utilizing PPP 06.50 ± 1.00. However, it appears that the brief treatment duration and the low PPP concentration precluded the restoration of normal levels of this substance in comparison to the treatment group with the higher concentration E&PPP 80%, which successfully reinstated normal levels 05.20 ± 1.30, exhibiting no significant differences from the control group 04.30 ± 1.33. Without a doubt, the results reveal that PPP therapy improves the antioxidant defense system when ethanol causes oxidative damage (Kumar D. et al., 2013)

4. CONCLUSION

The findings indicate that the mechanisms contributing to heightened oxidative stress following ethanol ingestion encompass the excessive generation of free radicals, a decrease in endogenous antioxidants, and an elevation in MDA release. This work demonstrates that the protective effect of PPP against ethanol-induced liver damage is dependent on the antioxidant activities of phenolic components, including gallic acid, ellagic acid, punicalagin, luteolin, catechin, rutin, hydrobenzoic acid, and potentially glycosides and coumarin derivatives found in pomegranate peel. As the concentration of PPP rises, the dietary levels of these chemicals increase, hence enhancing the protective effect of PPP. The principal mechanism via which PPP alleviates hepatocyte damage is by scavenging free radicals generated by ethanol and its synergistic effects, resulting in elevated levels of GSH and reduced levels of MDA, total protein, globulin, albumin, AST, ALT, ALP proteins, alongside diminished levels of ROS.

5. ACKNOWLEDGEMENTS

I wish to express my gratitude to the Faculty of Nursing and the Faculty of Pharmacology at the University of Kerbala, Iraq.

REFERENCES

Abd Elsabor, R. G., Sadeek, R. A., & Hassan, H. M. (2018). Protective role of juice and peel powder of pomegranate (*Punica granatum* L.) in reducing the hepatic and renal complications caused by paracetamol. In *Tenth Annual International Scientific Conference (Specific scientific conference in Egypt and the Arab world in the light of sustainable development strategies)*.

Abdel-Kawi, S. H., Hashem, K. S., Saad, M. K., Fekry, G., & Abdel-Hameed, E. M. M. (2023). The ameliorative effects of cinnamon oil against ethanol-induced gastric ulcer in rats by regulating oxidative stress and promoting angiogenesis. *Journal of Molecular Histology*, *53*, 573–587. https://doi.org/10.1007/s10735-022-00720-y

Abdulzahra, A. A., & Al-Salih, H. A. A. (2022). Anti-ulcer activity of *Pistacia atlantica* and *Punica granatum* hydroalcoholic extract in comparison with omeprazole in male wister rats. *International Journal of Health Sciences*. https://doi.org/10.53730/ijhs.v53736ns53732.55159

Aggul, A. G., Demir, G. M., & Gulaboglu, M. (2022). Ethanol extract of myrtle (*Myrtus communis* L.) berries as a remedy for streptozotocin-induced oxidative stress in rats. *Applied Biochemistry and Biotechnology*, *194*, 1645–1658. https://doi.org/10.1007/s12010-021-03753-z

Ajibo, D. N., Georgewill, U. O., & Georgewill, O. A. (2023). Investigating the Gastro Protective Effects of Tadalafil on Ethanol- Induced and Reserpine –Induced Gastric Ulcer in Rats. In *Research Developments in Medicine and Medical Science* (pp. 89–99). https://doi.org/10.9734/bpi/rdmms/v9739/6802F

Akanya, O. H., Peter, S., Ossamulu, I., Oibiokpa, I., & Adeyemi, Y. H. (2015). Evaluation of the changes in some liver function and haematological parameters in MSG fed rats. *International Journal of Biochemistry Research & Review*, *6*(3), 113–120. https://doi.org/10.9734/IJBcRR/2015/15433

Al-Gubory, K. H., Laher, I., & Garrel, C. (2010). Pomegranate peel attenuates dextran sulfate sodium-induced lipid peroxidation in rat small intestine by enhancing the glutathione/glutathione disulfide redox potential. *Journal of the Science of Food and Agriculture*, *101*(10), 4278–4287. https://doi.org/10.1002/jsfa.11067

Alsaif, M. A. (2007). Effect of thymoquinone on ethanol-induced hepatotoxicity in Wistar rats. *Journal of Medical Sciences*, *7*(7), 1164–1170.

Arumugam, M. K., Chava, S., Perumal, S. K., Paal, M. C., Rasineni, K., Ganesan, M., Donohue Jr, T. M., Osna, N. A., & Kharbanda, K. K. (2022). Acute ethanol-induced liver injury is prevented by betaine administration. *Frontiers in Physiology*, *13*, 940148. https://doi.org/10.3389/fphys.2022.940148

Arthur, I. (2001). Introduction-serial review: alcohol, oxidative stress and cell injury. *Free Radical Biology and Medicine*, *31*, 1524–1526.

Ashoush, I. S., El-Batawy, O., & El-Shourbagy, G. A. (2013). Antioxidant activity and hepatoprotective effect of pomegranate peel and whey powders in rats. *Annals of Agricultural Sciences*, *58*(1), 27–32. https://doi.org/10.1016/j.aoas.2013.01.005

Bachoual, R., Talmoudi, W., Boussetta, T., Braut, F., & El-Benna, J. (2011). An aqueous pomegranate peel extract inhibits neutrophil myeloperoxidase *in vitro* and attenuates lung inflammation in mice. *Food and Chemical Toxicology*, *49*(6), 1224–1228. https://doi.org/10.1016/j.fct.2011.02.024

Badawi, M. E., & Gomaa, A. M. (2016). Influence of diets supplemented with pomegranate peel extract. *Japanese Journal of Veterinary Research*, *64*(2), S87–S94.

Beiranvand, M., Bahramikia, S., & Dezfoulian, O. (2021). Evaluation of antioxidant and anti-ulcerogenic effects of *Eremurus persicus* (Jaub & Spach) Boiss leaf hydroalcoholic extract on ethanol-induced gastric ulcer in rats. *Inflammopharmacology*, *29*, 1503–1518. https://doi.org/10.1007/s10787-021-00868-x

Caliri, A. W., Tommasi, S., & Besaratinia, A. (2021). Relationships among smoking, oxidative stress, inflammation, macromolecular damage, and cancer. *Mutation Research/Reviews in Mutation Research*, *787*, 108365. https://doi.org/10.1016/j.mrrev.2021.108365

Dollah, M. A., Parhizkar, S., Latiff, L. A., & Hassan, M. H. B. (2013). Toxicity effect of *Nigella sativa* on the liver function of rats. *Advanced Pharmaceutical Bulletin*, *3*(1), 97–102. https://doi.org/10.5681/apb.2013.016

El-Houseiny, W., Mansour, M. F., Mohamed, W. A., Al-Gabri, N. A., El-Sayed, A. A., Altohamy, D. E., & Ibrahim, R. E. (2021). Silver nanoparticles mitigate *Aeromonas hydrophila*-induced immune suppression, oxidative stress, and apoptotic and genotoxic effects in *Oreochromis niloticus*. *Aquaculture*, *535*, 736430. https://doi.org/10.1016/j.aquaculture.2021.736430

Faddladdeen, K. A., & Ojaimi, A. A. (2019). Protective effect of pomegranate (*Punica granatum*) extract against diabetic changes in adult male rat liver: histological study. *Journal of Microscopy and Ultrastructure*, *7*(4), 165–170. https://doi.org/10.4103/JMAU.JMAU_106_19

Fischbach, F., & Zawta, B. (1992). Age-dependent reference limits of several enzymes in plasma at different measuring temperatures. *Klin Lab*, *38*, 555–561.

Georgiou-Siafis, S. K., & Tsiftsoglou, A. S. (2023). The key role of GSH in keeping the redox balance in mammalian cells: mechanisms and significance of GSH in detoxification via formation of conjugates. *Antioxidants*, *12*(11), 1953. https://doi.org/10.3390/antiox12111953

Ghazizadeh, H., Saberi-Karimian, M., Aghasizadeh, M., Sahebi, R., Ghazavi, H., Khedmatgozar, H., Timar, A., Rohban, M., Javandoost, A., & Ghayour-Mobarhan, M. (2020). Pro-oxidant–antioxidant balance (PAB) as a prognostic index in assessing the cardiovascular risk factors: a narrative review. *Obesity Medicine*, *19*, 100272. https://doi.org/10.1016/j.obmed.2020.100272

Gong, J., Tu, W., Liu, J., & Tian, D. (2023). Hepatocytes: A key role in liver inflammation. *Frontiers in Immunology*, *13*, 1083780. https://doi.org/10.3389/fimmu.2022.1083780

Gugliandolo, E., Cordaro, M., Fusco, R., Peritore, A. F., Siracusa, R., Genovese, T., D'Amico, R., Impellizzeri, D., Di Paola, R., & Cuzzocrea, S. (2021). Protective effect of snail secretion filtrate against ethanol-induced gastric ulcer in mice. *Scientific Reports*, *11*, 3638. https://doi.org/10.1038/s41598-021-83170-4

Hamed, H. S., & Abdel-Tawwab, M. (2021). Dietary pomegranate (*Punica granatum*) peel mitigated the adverse effects of silver nanoparticles on the performance, haemato-biochemical, antioxidant, and immune responses of Nile tilapia fingerlings. *Aquaculture*, *540*, 736742. https://doi.org/10.1016/j.aquaculture.2021.736742

Hanani, Z. N., Yee, F. C., & Nor-Khaizura, M. (2019). Effect of pomegranate (*Punica granatum* L.) peel powder on the antioxidant and antimicrobial properties of fish gelatin films as active packaging. *Food Hydrocolloids*, *89*, 253–259. https://doi.org/10.1016/j.foodhyd.2018.10.007

Høiseth, G., Hilberg, T., Trydal, T., Husa, A., Vindenes, V., & Bogstrand, S. T. (2022). The alcohol marker phosphatidylethanol is closely related to AST, GGT, ferritin and HDL-C. *Basic & Clinical Pharmacology & Toxicology*, *130*(1), 182–190. https://doi.org/10.1111/bcpt.13662

Hossen, M. A., Reza, A. A., Ahmed, A. A., Islam, M. K., Jahan, I., Hossain, R., Khan, M. F., Maruf, M. R. A., Haque, M. A., & Rahman, M. A. (2021). Pretreatment of *Blumea lacera* leaves ameliorate acute ulcer and oxidative stress in ethanol-induced Long-Evan rat: A combined experimental and chemico-biological interaction. *Biomedicine & Pharmacotherapy*, *135*, 111211. https://doi.org/10.1016/j.biopha.2020.111211

Ibrahium, M. (2010). Efficiency of pomegranate peel extract as antimicrobial, antioxidant and protective agents. *World Journal of Agricultural Sciences*, *6*(4), 338–344.

Jedidi, S., Aloui, F., Selmi, S., Selmi, H., Sammari, H., Ayari, A., Abbes, C., & Sebai, H. (2022). Antioxidant properties of *Salvia officinalis* decoction extract and mechanism of its protective effects on ethanol-induced liver and kidney injuries. *Journal of Medicinal Food*, *25*(5), 546–556. https://doi.org/10.1089/jmf.2021.0134

Kaneko, J. J., Harvey, J. W., & Bruss, M. L. (2018). *Clinical biochemistry of domestic animals*. Academic Press.

Klein, E., Thompson, I., Tangen, C., Lucia, M., Goodman, P., Minasian, L., Ford, L., Parnes, H., & Gaziano, J., Karp, D. (2012). *Vitamin E and the risk of prostate cancer: Updated results of the Selenium and Vitamin E Cancer Prevention Trial*. Philpapers.

Kostic, T., Popović, D., Perisic, Z., Stanojevic, D., Dakic, S., Saric, S., Radojkovic, D. D., Apostolovic, S., Bozinovic, N., & Zdravkovic, S. C. (2022). The hepatoprotective effect of aminoguanidine in acute liver injury caused by CCl4 in rats. *Biomedicine & Pharmacotherapy*, *156*, 113918. https://doi.org/10.1016/j.biopha.2022.113918

Kumar, D., Singh, S., Singh, A. K., & Rizvi, S. I. (2013). Pomegranate (*Punica granatum*) peel extract provides protection against mercuric chloride-induced oxidative stress in Wistar strain rats. *Pharmaceutical Biology*, *51*(4), 441–446. https://doi.org/10.3109/13880209.2012.738333

Liu, Q., Zhao, Y., Dong, S., Bai, X., Chen, B., Liu, X., Shen, J., & Zhu, D. (2024). Characteristics of Neutrophil Migration and Function in Acute Inflammation Induced by Zymosan and Carrageenan in the Mice Air Pouch Model. *Inflammation*, *47*, 1–14. https://doi.org/10.1007/s10753-024-02064-9

Macdonald, I. O., Olusola, O. J., & Osaigbovo, U. A. (2010). Effects of chronic ethanol administration on body weight, reduced glutathione (GSH), malondialdehyde (MDA) levels and glutathione-s-transferase activity (GST) in rats. *New York Science Journal*, *3*(4), 39–47.

Mahmood, A. M., & Jabar, H. L. (2023). Characterization of biochemical compounds in different accessions of pomegranate (*Punica granatum* L.) peels in Iraq. *Passer Journal of Basic and Applied Sciences*, *5*(2), 382–390. https://doi.org/10.24271/psr.2023.40973

Niemelä, O. (2001). Distribution of ethanol-induced protein adducts *in vivo*: relationship to tissue injury. *Free Radical Biology and Medicine*, *31*(12), 1533–1538. https://doi.org/10.1016/S0891-5849(01)00744-0

Ofusori, A. E., Moodley, R., & Jonnalagadda, S. B. (2020). Antiulcerogenic effects of *Celosia trigyna* plant extracts on ethanol-induced gastric ulcer in adult Wistar rats. *Journal of Traditional and Complementary Medicine*, *10*(6), 586–593. https://doi.org/10.1016/j.jtcme.2019.11.004

Oh, S. I., Kim, C.-I., Chun, H. J., & Park, S. C. (1998). Chronic ethanol consumption affects glutathione status in rat liver. *The Journal of Nutrition*, *128*(4), 758–763. https://doi.org/10.1093/jn/128.4.758

Palipoch, S., & Punsawad, C. (2013). Biochemical and histological study of rat liver and kidney injury induced by cisplatin. *Journal of Toxicologic Pathology*, *26*(3), 293–299. https://doi.org/10.1293/tox.2012-0026

Pari, L., & Murugan, P. (2004). Protective role of tetrahydrocurcumin against erythromycin estolate-induced hepatotoxicity. *Pharmacological Research*, *49*(5), 481–486. https://doi.org/10.1016/j.phrs.2003.11.005

Preedy, V. R., Duane, P., & Peters, T. J. (1988). Comparison of the acute effects of ethanol on liver and skeletal muscle protein synthesis in the rat. *Alcohol and Alcoholism*, *23*(2), 155–162. https://doi.org/10.1093/oxfordjournals.alcalc.a044778

Rostami, H., Hematfar, A., & Samavati Sharif, M. A. (2020). Interactive Effects of Endurance Swimming and Curcumin Supplementation on Serum Levels of Liver Alkaline Phosphatase in Male Rats Following Ethanol Abuse. *Journal of Advanced Sport Technology*, *4*(1), 29–36.

Salama, A. A., Ismael, N. M., & Bedewy, M. (2021). The anti-inflammatory and antiatherogenic *in vivo* effects of pomegranate peel powder: From waste to medicinal food. *Journal of Medicinal Food*, *24*(2), 145–150. https://doi.org/10.1089/jmf.2019.0269

Schlorff, E., Husain, K., & Somani, S. M. (1999). Dose-and time-dependent effects of ethanol on plasma antioxidant system in rat. *Alcohol*, *17*(2), 97–105. https://doi.org/10.1016/S0741-8329(98)00031-0

Suzuki, H., Nishizawa, T., Tsugawa, H., Mogami, S., & Hibi, T. (2011). Roles of oxidative stress in stomach disorders. *Journal of clinical Biochemistry and Nutrition*, *50*(1), 35–39. https://doi.org/10.3164/jcbn.10-115SR

Vildhede, A., Wisniewski, J. R., Noren, A., Karlgren, M., & Artursson, P. (2015). Comparative proteomic analysis of human liver tissue and isolated hepatocytes with a focus on proteins determining drug exposure. *Journal of Proteome Research*, *14*(8), 3305–3314. https://doi.org/10.1021/acs.jproteome.5b00334

Xu, H., Meng, L., & Xu, Y. (2024). Early-life inflammation increases ethanol consumption in adolescent male mice. *Neuroscience Letters*, *832*, 137815. https://doi.org/10.1016/j.neulet.2024.137815

Xue, M., Liu, Y., Lyu, R., Ge, N., Liu, M., Ma, Y., & Liang, H. (2017). Protective effect of aplysin on liver tissue and the gut microbiota in alcohol-fed rats. *PloS One*, *12*(6), e0178684. https://doi.org/10.1371/journal.pone.0178684

Xue, M., Tian, Y., Sui, Y., Zhao, H., Gao, H., Liang, H., Qiu, X., Sun, Z., Zhang, Y., & Qin, Y. (2022). Protective effect of fucoidan against iron overload and ferroptosis-induced liver injury in rats exposed to alcohol. *Biomedicine & Pharmacotherapy*, *153*, 113402. https://doi.org/10.1016/j.biopha.2022.113402

Yang, J. (2011). Research of diagnosis value of level of serum glutamine transferase and glutamine transferase/ALT and AST/ALT ratio conjoint analysis to primary liver cancer. *Chinese Medicine*, *5*(4), 328–329.

Yoo, J.-H., Lee, J.-S., Lee, Y.-S., Ku, S., & Lee, H.-J. (2018). Protective effect of bovine milk against HCl and ethanol–induced gastric ulcer in mice. *Journal of Dairy Science*, *101*(5), 3758–3770. https://doi.org/10.3168/jds.2017-13872

Zamanian, M. Y., Sadeghi Ivraghi, M., Khachatryan, L. G., Vadiyan, D. E., Bali, H. Y., & Golmohammadi, M. (2023). A review of experimental and clinical studies on the therapeutic effects of pomegranate (*Punica granatum*) on non-alcoholic fatty liver disease: Focus on oxidative stress and inflammation. *Food Science & Nutrition*, *11*(12), 7485–7503. https://doi.org/10.1002/fsn3.3713

Zhao, H., Liu, S., Zhao, H., Liu, Y., Xue, M., Zhang, H., Qiu, X., Sun, Z., & Liang, H. (2021). Protective effects of fucoidan against ethanol-induced liver injury through maintaining mitochondrial function and mitophagy balance in rats. *Food & Function*, *12*(9), 3842–3854. https://doi.org/10.1039/D0FO03220D

PURE SCIENCES
International Journal of Kerbala

Pure Sciences International Journal of Kerbala

Year: 2025 Volume : 2 Issue : 7 ISSN: 6188-2789 Print 3005 -2394 Online

2025,Volume 2 , Issue 7 , PSIJK (29-34)

Pure Sciences International Journal of Kerbala

The Multi-Attribute Decision-Making Problem Using Single-Valued Neutrosophic Numbers

Noorulhuda Hussein Qandeel [a*]

[a] Department of Mathematics, College of Education, University of Kerbala, Kerbala, Iraq

P A P E R I N F O

Received: 29.04.2025
Accepted: 11.06.2025
Published: 30.09.2025

Keywords:
intuitionistic fuzzy numbers, single-valued triangular, neutrosophic numbers, multi-attribute decision-making.

A B S T R A C T

In this paper, an extension of intuitionistic fuzzy numbers is presented.The researcher proposes single-valued triangular neutrosophic numbers (SVTNNs). These SVTNNs represent ordinary numbers but possess a level of uncertainty from a philosophical perspective. Additionally, the researcher introduces a modified operator termed the single-valued triangular neutrosophic weighted aggregation (SVTNWA) operator. This operator is utilized in multi-attribute decision-making (MADM) situations, enabling the management of many attribute to facilitate informed decisions. For this SVTNWA operator, examples are offered.

DOI: 10.53851/psijk.v2i7. 29–34

1. INTRODUCTION

In everyday content, most of the issues involve imprecise concepts (Shahoodh, Ali, & Adwan, 2025). The traditional approach of set theory and numbers is inadequate to handle the imprecise idea and it must be expanded to include some additional concepts. The fuzzy concept is one of the concepts for this purpose.

Neutrosophic set theory is a mathematical framework that extends the concepts of classical set theory, fuzzy set theory, and intuitionistic fuzzy set theory. It was introduced by Smarandache in the 1990s as a way to incomplete, handle uncertain, and indeterminate information in a more flexible manner (Deli & Subas, 2014). Neutrosophic sets allow for the representation of three different types of membership degrees: truth, falsity, and indeterminacy. Unlike classical sets where an element is either a member or a non-member, and fuzzy sets where an element has a degree of membership between 0 and 1, neutrosophic sets recognize the existence of an indeterminate region where the membership status cannot be determined with certainty(Ansari, Biswas, & Aggarwal, 2013) (Ashbacher, 2014).

The multi-attribute decision-making (MADM) problem is a common challenge in various domains where decision-makers need to evaluate and compare alternatives based on multiple attribute. Conventional approaches to decision-making frequently take the attribute and their weights to be represented as clear-cut or fuzzy values. However, in practical situations, making decisions may involve ambiguity, insufficient information, and uncertainty(Taherdoost & Madanchian, 2023) (Bhole & Deshmukh, 2018). Current advances in MADM have progressively employed single-valued neutrosophic numbers (SVNNs) to address uncertainty and inaccuracy.

In (Xu & Zhao, 2025), the author presented a multi-attribute group decision-making technique that uses SVNNs in conjunction with extended power average operators and the Dombi operator. In (Liu, Shen, & Zhang, 2024), researchers presented a fresh distance metric for SVNNs, improving the Technique for Order of Preference by Similarity to Ideal Solution (TOPSIS) approache to enhance decision-making accuracy. A more versatile foundation for MADM applications was also provided by the introduction of the idea of single-valued neutrosophic multiple sets (SVNMS) to expand standard SVNNs (Radhakrishnan & Thankachan, 2025). Notwithstanding these advancements, numerous current methodologies either concentrate on particular aggregation operators or lack holistic frameworks to address the intricacies of real-world decision-making

*Corresponding Author Institutional Email:
noorkendel89@gmail.com (Noorulhuda Hussein Qandeel)

contexts. In this paper, The single-valued triangular neutrosophic weighted aggregate (SVTNWA) is employed in multi-attribute decision-making (MADM) contexts, allowing for the management of several attribute to support informed decision-making.

1.1. Fuzzy Set (FS) FS theory is a mathematical framework that facilitates the description and management of uncertain or ambiguous notions (Hussein, 2024). Conversely, fuzzy set theory allows for varying degrees of membership, enabling components to partially belong to a set. The FSs are employed to represent and manage imprecise and uncertain information prevalent in real-world scenarios. They offer a robust instrument for addressing ambiguity and encapsulating the intrinsic vagueness in human reasoning (Yanar & Akyürek, 2006). FSs can convey nuances between full membership and non-membership by permitting incremental membership.

The membership values might vary from $0\ to\ 1$, where 0 indicates non-membership and 1 signifies full membership. Values ranging from $0\ to\ 1$ indicate partial membership. FS theory serves as a significant mathematical instrument, utilizing vagueness and uncertainty to create a framework for modeling and reasoning about imprecise concepts in a more adaptable and realistic way (Kahraman, 2008). In (Atanassov, 1988),the researcher suggested the Intuitionistic Fuzzy Set (IFS) as an extension of the fuzzy set within a universe A. The IFS includes a degree of non-membership $\nu_{X(a)} \in [0,1]$ in addition to the degree of membership $\mu_{X(a)} \in [0,1]$ for each element $a \in A$ belonging to a set X. To maintain this degree of non-membership, the following conditions must be met:

$$\forall\, a \in A, \quad \mu_{X(a)} + \nu_{X(a)} \leq 1 \tag{1}$$

1.2. Neutrosophic Set (NS)

The NS concept was initially introduced by(Smarandache, 1998). Smarandache defined the degree of indeterminacy as an autonomous component. In an NS, every element within the universe of discourse is linked to three values: the truth (T), the indeterminacy (I), and the false (F). These values denote the membership, non-membership, and indeterminacy of an element within a specified set, respectively(Smarandache, 2019) in contrast to fuzzy sets, which have membership values confined to the interval $[0,1]$, the NS permits membership, non-membership, and indeterminacy values to fluctuate within the range $[0,1]$. The degree of truth (T) indicates the extent of an element's membership in a set, the degree of falsity (F) denotes the extent of an element's non-membership in a set, and the degree of indeterminacy (I) signifies the extent of uncertainty regarding an element's membership status (Dubois & Prade, 2012). Collectively, these three values offer more thorough ambiguous information and depiction of unclear.

When the available knowledge is either contradictory or inadequate, NSs serve as a valuable instrument. They can manage scenarios in which it is difficult to ascertain the exact membership or non-membership of components in a set due to ambiguity or uncertainty (Habib, Akram, & Kahraman, 2022). By incorporating the concept of indeterminacy, NSs allow for conflicting data or a more nuanced representation of incomple teness.

Assuming A is a universe of discourse and a represents a generic element in A, the NS set can be defined as an entity that takes on the following structure:

$$X = \{(a, (\mu_X(a), \omega_X(a), \vartheta_X(a)) : a \in A\} \tag{2}$$

1.3. Multi-Attribute Decision Making

The approach of Multi-Attribute Decision Making (MADM) entails assessing and choosing the optimal alternative from a range of options based on various attribute or qualities. It is employed when decision-makers must evaluate and balance various factors concurrently to make informed and rational decisions. In MADM, each alternative is evaluated based on a set of pertinent traits or attribute relevant to the choice being made(Deli & Şubaş, 2017). These features may be quantifiable (e.g., cost, time, or performance measures) or qualitative (e.g., reputation, customer satisfaction, or environmental impact). The decision-maker allocates weights or significance values to each characteristic to represent their relative relevance.

2. SINGLE-VALUED TRIANGULAR NEUTROSOPHIC

Let a triangular neutrosophic number $\tilde{\alpha}$ be defined as $\tilde{\alpha} = ((\boldsymbol{x_1}, \boldsymbol{x_2}, \boldsymbol{x_3}), \boldsymbol{X_{\alpha^-}}),\ ((\boldsymbol{y_1}, \boldsymbol{y_2}, \boldsymbol{y_3}), \boldsymbol{Y_{\alpha^-}}),$ $((\boldsymbol{z_1}, \boldsymbol{z_2}, \boldsymbol{z_3}),\ \boldsymbol{Z_{\alpha^-}})$. An NS is defined on the real number set $\mathbb{R}$, with truth-membership, indeterminacy-membership, and false-membership functions. These functions are given by the following:

$$\mu_{\alpha^-}(\beta) = \begin{cases} (\beta - x_1) X_{\alpha^-} / (x_2 - x_1) & (x_1 \leq \beta < x_2) \\ X_{\alpha^-} & (\beta = x_2) \\ (x_3 - \beta) X_{\alpha^-} / (x_3 - x_2) & (x_2 \leq \beta \leq x_3) \\ 0 & otherwise \end{cases} \tag{3}$$

$$v_{\alpha^{\sim}}(\beta) = \begin{cases} (y_2 - \beta + Y_{\alpha^{\sim}}(\beta - y_1))/(y_2 - y_1) & (y_1 \le \beta < y_2 \\ Y_{\alpha^{\sim}} & (\beta = y_2) \\ (\beta - y_2 + Y_{\alpha^{\sim}}(y_3 - \beta))/(y_3 - y_2) & (y_2 \le \beta < y_3 \\ 1 & otherwise \end{cases} \quad (4)$$

$$\lambda_{\alpha^{\sim}}(\beta) = \begin{cases} (z_2 - \beta + Z_{\alpha^{\sim}}(\beta - z_1))/(z_2 - z_1) & (z_1 \le \beta < z_2 \\ Z_{\alpha^{\sim}} & (\beta = z_3) \\ (\beta - z_2 + Z_{\alpha^{\sim}}(z_3 - \beta))/(z_3 - z_2) & (z_2 \le \beta < z_3 \\ 1 & otherwise \end{cases} \quad (5)$$

If $x_1,\ y_1,\ z_1 \ge 0$ and at least $x_3, y_3, z_3 > 0$, then $\alpha^{\sim}$ is referred to as a positive Single-Valued Triangular Neutrosophic Number (SVTrNN), which is represented as $\alpha^{\sim} > 0$. Likewise, if $x_2, y_2, z_2 \le 0$ and at least $x_1,\ y_1,\ z_1 < 0$, then $\alpha^{\sim}$ is referred to as a negative SVTrNN, which is represented as $\alpha^{\sim} < 0$. A triangular neutrosophic number denoted as $\alpha^{\sim} = ((x_1, x_2, x_3), X_{\alpha^{\sim}})$, $\left((y_1, y_2, y_3), Y_{\alpha^{\sim}}\right)$, $((z_1, z_2, z_3),\ Z_{\alpha^{\sim}})$, can represent a vague or uncertain value related to the variable $\alpha^{\sim}$, which is approximately equivalent to $\alpha^{\sim}$.

3. TWO SINGLE-VALUED TRIANGULAR NEUTROSOPHIC NUMBERS

Let $\alpha^{\sim} = ((x_1, x_2, x_3), X_{\alpha^{\sim}})$, $\left((y_1, y_2, y_3), Y_{\alpha^{\sim}}\right)$, $((z_1, z_2, z_3),\ Z_{\alpha^{\sim}})$ and $\beta^{\sim} = \left((x_1, x_2, x_3), X_{\beta^{\sim}}\right)$, $\left((y_1, y_2, y_3), Y_{\beta^{\sim}}\right)$, $((z_1, z_2, z_3),\ Z_{\beta^{\sim}})$ be two SVTrNNs and $\eta \neq 0$, then

3.1. Addition

$$\alpha^{\sim} + \beta^{\sim} = ((x_1 + y_1,\ x_2 + y_2, x_3 + y_3)\ X_{\alpha^{\sim}}\ min X_{\beta^{\sim}}, Y_{\alpha^{\sim}}\ max\ Y_{\beta^{\sim}},\ Z_{\alpha^{\sim}} max\ Z_{\beta^{\sim}})$$

3.2. Subtraction

$$\alpha^{\sim} - \beta^{\sim} = ((x_1 - y_1,\ x_2 - y_2, x_3 - y_3)\ X_{\alpha^{\sim}}\ min X_{\beta^{\sim}}, Y_{\alpha^{\sim}}\ max\ Y_{\beta^{\sim}},\ Z_{\alpha^{\sim}} max\ Z_{\beta^{\sim}})$$

3.3. Multiplication

$$\alpha^{\sim}\beta^{\sim} = \begin{cases} ((x_1 y_1,\ x_2 y_2, x_3 y_3);\ X_{\alpha^{\sim}}\ min X_{\beta^{\sim}}, Y_{\alpha^{\sim}}\ max\ Y_{\beta^{\sim}},\ Z_{\alpha^{\sim}} max\ Z_{\beta^{\sim}})(x_3 > 0, y_3 > 0) \\ ((x_1 y_3,\ x_2 y_2, x_3 y_1);\ X_{\alpha^{\sim}}\ min X_{\beta^{\sim}}, Y_{\alpha^{\sim}}\ max\ Y_{\beta^{\sim}},\ Z_{\alpha^{\sim}} max\ Z_{\beta^{\sim}})(x_3 < 0, y_3 > 0) \\ ((x_3 y_3, x_2 y_2, x_1 y_1);\ X_{\alpha^{\sim}}\ min X_{\beta^{\sim}}, Y_{\alpha^{\sim}}\ max\ Y_{\beta^{\sim}},\ Z_{\alpha^{\sim}} max\ Z_{\beta^{\sim}})(x_3 < 0, y_3 < 0) \end{cases}$$

3.4. Division

$$\alpha^{\sim}/\beta^{\sim} = \begin{cases} ((x_1/y_1,\ x_2/y_2, x_3/y_3);\ X_{\alpha^{\sim}}\ min X_{\beta^{\sim}}, Y_{\alpha^{\sim}}\ max\ Y_{\beta^{\sim}},\ Z_{\alpha^{\sim}} max\ Z_{\beta^{\sim}})(x_3 > 0, y_3 > 0) \\ ((x_1/y_3,\ x_2/y_2, x_3/y_1);\ X_{\alpha^{\sim}}\ min X_{\beta^{\sim}}, Y_{\alpha^{\sim}}\ max\ Y_{\beta^{\sim}},\ Z_{\alpha^{\sim}} max\ Z_{\beta^{\sim}})(x_3 < 0, y_3 > 0) \\ ((x_3/y_3, x_2/y_2, x_1/y_1);\ X_{\alpha^{\sim}}\ min X_{\beta^{\sim}}, Y_{\alpha^{\sim}}\ max\ Y_{\beta^{\sim}},\ Z_{\alpha^{\sim}} max\ Z_{\beta^{\sim}})(x_3 < 0, y_3 < 0) \end{cases}$$

3.5. Multiplication by a constant

$$\eta\alpha^{\sim} = \begin{cases} ((\eta x_1, \eta x_2, \eta x_3);\ X_{\alpha^{\sim}}, Y_{\alpha^{\sim}},\ Z_{\alpha^{\sim}})(\eta > 0) \\ ((\eta x_3, \eta x_2, \eta x_1);\ X_{\alpha^{\sim}}, Y_{\alpha^{\sim}},\ Z_{\alpha^{\sim}})(\eta < 0) \end{cases}$$

3.6. Inverse

$$\alpha^{\sim -1} = ((1/x_1, 1/x_2, 1/x_3);\ X_{\alpha^{\sim}}, Y_{\alpha^{\sim}},\ Z_{\alpha^{\sim}})\ (\alpha^{\sim} \neq 0)$$

It can be demonstrated that the outcomes derived from the multiplication and division operations involving two SVTrNNs do not consistently yield SVTrNNs. Nevertheless, it is common practice to utilize SVTrNNs as a means of approximating and expressing these computational findings.

3.7. Example

Let $\alpha^{\sim} = ((3,4,6); 0.3, 0.4, 0.6)$ and $\beta^{\sim} = ((2,4,7); 0.5, 0.6, 0.7)$ represent two single-valued triangular neutrosophic numbers.

1. $\alpha^{\sim} + \beta^{\sim} = \left((5,8,13); 0.3, 0.6, 0.7\right)$
2. $\alpha^{\sim} - \beta^{\sim} = \left((1,0,-1); 0.3, 0.6, 0.7\right)$
3. $\alpha^{\sim}\beta^{\sim} = \left((6,16,42); 0.3, 0.6, 0.7\right)$
4. $\alpha^{\sim}\backslash\beta^{\sim} = \left(\left(\frac{3}{7}, \frac{4}{4}, \frac{6}{2}\right); 0.3, 0.6, 0.7\right)$
5. $\alpha^{\sim -1} = \left(\left(\frac{1}{6}, \frac{1}{4}, \frac{1}{3}\right); 0.3, 0.4, 0.6\right)$
6. $3\alpha^{\sim} = ((9,12,18); 0.3, 0.4, 0.6)$

3.8. Remark

If $0 \le X_{\alpha^{\sim}}, Y_{\alpha^{\sim}}, Z_{\alpha^{\sim}} \le 1, 0 \le X_{\alpha^{\sim}} + Y_{\alpha^{\sim}} + Z_{\alpha^{\sim}} \le 1, Z_{\alpha^{\sim}} = 0$ and $0 \le X_{\beta^{\sim}}, Y_{\beta^{\sim}}, Z_{\beta^{\sim}} \le 1, 0 \le X_{\beta^{\sim}} + Y_{\beta^{\sim}} + Z_{\beta^{\sim}} \le 1, Z_{\beta^{\sim}} = 0$, then the SVTrNNs $\alpha^{\sim} = ((x_1, x_2, x_3), X_{\alpha^{\sim}})$, $\left((y_1, y_2, y_3), Y_{\alpha^{\sim}}\right)$, $((z_1, z_2, z_3),\ Z_{\alpha^{\sim}})$ and $\beta^{\sim} = \left((x_1, x_2, x_3), X_{\beta^{\sim}}\right)$, $\left((y_1, y_2, y_3), Y_{\beta^{\sim}}\right)$, $((z_1, z_2, z_3),\ Z_{\beta^{\sim}})$ The concept of degeneracy can be extended to the space of intuitionistic triangular fuzzy numbers $\alpha^{\sim} = ((x_1, x_2, x_3), X_{\alpha^{\sim}})$, $\left((y_1, y_2, y_3), Y_{\alpha^{\sim}}\right)$, (0) and $\beta^{\sim} = \left((x_1, x_2, x_3), X_{\beta^{\sim}}\right)$, $\left((y_1, y_2, y_3), Y_{\beta^{\sim}}\right)$, (0), respectively. As previously stated, the mathematical operations were developed to simplify them.

4. EXAMPLE OF EVALUATING TEACHING

The example we will focus on involves evaluating the quality of teaching and drawing inspiration from the application discussed. Suppose a government organization is seeking to fill a position, and they have

identified five candidates ($X = (x_1, x_2, x_3, x_4)$ for evaluation. The assessment process will be conducted by a panel of experts from Management Science, who will evaluate the candidates based on three specific aspects: teaching attitude (y_1), ability (y_2), and content (y_3).
The teaching attitude of the candidates holds a significant importance in this evaluation, as those who exhibit a positive attitude are likely to have a substantial impact when teaching. Evaluating teaching ability comprises assessing the candidates' professional knowledge and their practical experience in the field. Lastly, the content of their teaching is examined to ensure that it aligns closely with teaching guidance. To establish the relative importance of these attributes, a weight vector is assigned, with the values $(0.4,0.4,0.2)^T$, representing the respective weights for teaching attitude, ability, and content.

Step 1. The teachers were assessed by experts, and the outcomes of their evaluations are presented in Table 1.

	y_1	y_2	y_3
x_1	((0.2,0.3,0.4,0.6);0.6,0.5,0.1)	((0.1,0.2,0.4,0.5);0.4,0.2,0.6)	((0.1,0.3,0.6,0.7);0.8,0.1,0.4)
x_2	((0.3,0.6,0.7,0.9);0.9,0.3,0.5)	((0.3,0.5,0.6,0.8);0.2,0.3,0.4)	((0.3,0.4,0.7,0.7);0.6,0.4,0.8)
x_3	((0.3,0.5,0.7,0.7);0.7,0.3,0.1)	((0.3,0.6,0.7,0.9);0.3,0.6,0.8)	((0.3,0.5,0.5,0.4);0.7,0.3,0.6)
x_4	((0.4,0.5,0.6,0.8);0.8,0.2,0.4)	((0.2,0.4,0.7,0.9);0.8,0.9,0.6)	((0.5,0.6,0.8,0.7);0.4,0.3,0.2)

Step 2. For $\zeta = 1, 2, 3, \text{and } 4$, the table displays the aggregated obtained by the SVTNWA.

	$\zeta = 1$	$\zeta = 2$
x_1	((0.140, 0.260, 0.440, 0.580);0.4, 0.5, 0.6)	((0.022, 0.070, 0.200, 0.342); 0.4, 0.5, 0.6)
x_2	((0.300, 0.520, 0.660, 0.820);0.2, 0.4,0.8)	((0.090, 0.276, 0.438, 0.678); 0.2,0.4,0.8)
x_3	((0.300, 0.540, 0.660, 0.720);0.3, 0.6,0.8)	((0.090, 0.294, 0.442, 0.552); 0.3,0.6,0.8)
x_4	((0.340, 0.480, 0.680, 0.820);0.4, 0.9,0.6)	((0.130, 0.236, 0.468, 0.678); 0.4,0.9,0.6)

	$\zeta = 3$	$\zeta = 4$
x_1	(0.004, 0.019, 0.094, 0.205); 0.4, 0.5, 0.6)	(0.001, 0.006, 0.046, 0.125); 0.4, 0.5, 0.6)
x_2	(0.027, 0.149, 0.292, 0.565); 0.2,0.4,0.8)	(0.008, 0.082, 0.196, 0.474); 0.2,0.4,0.8)
x_3	(0.027, 0.161, 0.299, 0.442); 0.3,0.6,0.8)	(0.008, 0.089, 0.205, 0.364); 0.3,0.6,0.8)
x_4	(0.054, 0.119, 0.326, 0.565); 0.4,0.9,0.6)	(0.023, 0.061, 0.230, 0.474); 0.4,0.9,0.6)

Step 3. The score values of the respective alternatives are shown in table.

	$S_1(x_1)$	$S_2(x_2)$	$S_3(x_3)$	$S_4(x_4)$
$\zeta = 1$	0.1846	0.1438	0.1248	0.1305
$\zeta = 2$	0.0514	0.0926	0.0774	0.0850
$\zeta = 3$	0.0262	0.0646	0.0522	0.0598
$\zeta = 4$	0.0144	0.0475	0.0374	0.0044

Step 4. The accuracy degrees of the respective alternatives are shown in table.

	$\boldsymbol{AC_1(x_1)}$	$\boldsymbol{AC_2(x_2)}$	$\boldsymbol{AC_3(x_3)}$	$\boldsymbol{AC_4(x_4)}$
$\zeta = 1$	0.2219	0.3738	0.3469	0.3045
$\zeta = 2$	0.0991	0.2408	0.2153	0.1985
$\zeta = 3$	0.0503	0.1679	0.1510	0.1397
$\zeta = 4$	0.0278	0.1235	0.1041	0.1034

Step 5. The alternatives are ranked based on these scores and their accuracy degrees.

	The score	**The accuracy degrees**
$\zeta = 1$	$x_1 > x_2 > x_4 > x_3$	$x_2 > x_3 > x_4 > x_1$
$\zeta = 2$	$x_2 > x_4 > x_3 > x_1$	$x_2 > x_3 > x_4 > x_1$
$\zeta = 3$	$x_2 > x_4 > x_3 > x_1$	$x_2 > x_3 > x_4 > x_1$
$\zeta = 4$	$x_2 > x_3 > x_1 > x_4$	$x_2 > x_3 > x_4 > x_1$

By determining the score and accuracy values, a comprehensive candidate ranking can be established. Aligning these scores and accuracy degrees enhances the effectiveness of candidate evaluations using MADM methods. It is easy to see that x_2 has the highest values of score and accuracy degrees. The alignment between our objective and the outcomes is readily discernible.

Our objective revolves around creating a versatile framework capable of accommodating diverse

decision attribute, enabling decision-makers to effectively assess and prioritize factors based on their relative significance. The clarity achieved through this approach becomes evident in the results, as they vividly highlight the comprehensive representation, we aimed to provide for the decision problem. This alignment enhances the robustness and informed nature of the decision outcomes, reinforcing the purpose behind our efforts to ensure a more effective decision-making process.

The assessment of candidates based on their teaching attitude, ability, and content holds significant importance when considering weighted attribute. By increasing the value of ζ, the process of determining the highest-ranking candidate becomes more straightforward, as it enables a clearer distinction in terms of score and accuracy degrees.

In this context, evaluating candidates necessitates a comprehensive examination of various factors, such as their teaching attitude, ability, and content. Each of these attribute is assigned a weight to denote its relative importance in the overall assessment. The weight assigned to a criterion signifies the degree of significance it holds in the evaluation process.
We implemented this example using MATLAB to obtain the presented results as in Figure 1.

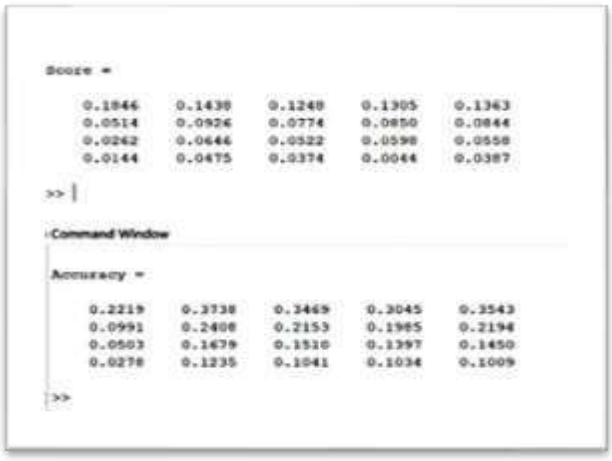

Figure 1. MATLAB results (example of evaluating teaching)

5. CONCLUSIONS

As a conclusion, the employment of SVTNWAs in multi-attribute decision-making has been demonstrated to be an effective method for handling decision problems that are characterized by uncertainty, vagueness, and indeterminacy. In this research, we have explored the theoretical foundations of SVTNWA and its application in MADM, particularly in the context of multiple attribute decision-making scenarios.

The SVTNWA operator-based MADM has been shown to be applicable in a real-world context through the use of the practical example that has been offered in this scientific investigation. The example demonstrated how decision-makers can utilize SVTNWA to assess options, gain significant insights into complicated decision-making circumstances, and make educated choices. The SVTNWA can also be used to have more sophisticated decision-making scenarios in the real world that involve large-scale or dynamic data.

REFERENCES

Ansari, A. Q., Biswas, R., & Aggarwal, S. (2013). Neutrosophic classifier: An extension of fuzzy classifer. *Applied soft computing*, *13*(1), 563–573.

Ashbacher, C. (2014). *Introduction to Neutrosophic logic*. Infinite Study.

Atanassov, K. (1988). Review and new results on intuitionistic fuzzy sets. *Preprint Im-MFAIS-1-88, Sofia*, *5*(1).

Bhole, G. P., & Deshmukh, T. (2018). Multi-criteria decision making (MCDM) methods and its applications. *International Journal for Research in Applied Science & Engineering Technology (IJRASET)*, *6*(5), 899–915.

Deli, I., & Subas, Y. (2014). Single valued neutrosophic numbers and their applications to multicriteria decision making problem. *Neutrosophic Sets Syst*, *2*(1), 1–13.

Deli, I., & Şubaş, Y. (2017). A ranking method of single valued neutrosophic numbers and its applications to multi-attribute decision making problems. *International journal of machine learning and cybernetics*, *8*(4), 1309–1322.

Dubois, D., & Prade, H. (2012). Gradualness, uncertainty and bipolarity: making sense of fuzzy sets. *Fuzzy sets and Systems*, *192*, 3–24.

Habib, A., Akram, M., & Kahraman, C. (2022). Minimum spanning tree hierarchical clustering algorithm: A new Pythagorean fuzzy similarity measure for the analysis of functional brain networks. *Expert Systems with Applications*, *201*, 117016.

Hussein, A. M. (2024). Using Triple Simple Elliptic Absolute Orlicz Function Defined by Triple Sequences Spaces (l∞)F3(Θ) with Fuzzy Metric. *Pure Sciences International Journal of Kerbala*, *1*(1), 60–68.

Kahraman, C. (2008). Multi-criteria decision making methods and fuzzy sets. In *Fuzzy multi-criteria*

decision making: Theory and Applications with Recent Developments (pp. 1–18).

Liu, P., Shen, J., & Zhang, P. (2024). Multi-attribute group decision-making method using single-valued neutrosophic credibility numbers with the Dombi extended power aggregation operator and its application in intelligent transportation system data collection scheme selection. *Engineering Applications of Artificial Intelligence*, *133*, 108639.

Radhakrishnan, S., & Thankachan, B. (2025). Single-Valued Neutrosophic Multiple sets and its Application in Multi-Criteria Decision-Making. *Neutrosophic Sets and Systems*, *86*, 312–331.

Shahoodh, M. K., Ali, O. K., & Adwan, M. I. (2025). On Pure Ideals: A Review. *Pure Sciences International Journal of Kerbala*, *2*(5), 55–61.

Smarandache, F. (1998). *Neutrosophy: neutrosophic probability, set, and logic: analytic synthesis & synthetic analysis*.

Smarandache, F. (2019). Neutrosophic set is a generalization of intuitionistic fuzzy set, inconsistent intuitionistic fuzzy set (picture fuzzy set, ternary fuzzy set), pythagorean fuzzy set, spherical fuzzy set, and q-rung orthopair fuzzy set, while neutrosophication is a generalization of regret theory, grey system theory, and three-ways decision (revisited). *Journal of New Theory*, (29), 1–31.

Taherdoost, H., & Madanchian, M. (2023). Multi-criteria decision making (MCDM) methods and concepts. *Encyclopedia*, *3*(1), 77–87.

Yanar, T. A., & Akyürek, Z. (2006). The enhancement of the cell-based GIS analyses with fuzzy processing capabilities. *Information Sciences*, *176*(8), 1067–1085.

Xu, D., & Zhao, Y. (2025). A new distance measure for single-valued neutrosophic set and an improved method based on TOPSIS and TODIM to multi-attribute decision-making. *International Journal of Knowledge-Based and Intelligent Engineering Systems*.

PURE SCIENCES
International Journal of Kerbala

Pure Sciences International Journal of Kerbala

Year: 2025 Volume : 2 Issue : 7 ISSN: 6188-2789 Print 3005 -2394 Online

2025,Volume 2 , Issue 7 , PSIJK (35-39)

Pure Sciences International Journal of Kerbala

Phytochemicals Screening and Antimicrobial Activity of Veronica Agrastis Extract

Jihan Hussein AL-Masoudi [a*] , Neepal Imtair Al Garaawi [a]

[a] *Biology of Department, College of Education for Pure Science, University of Kerbala, Kerbala, Iraq*

P A P E R I N F O

Received: 29.04.2025
Accepted: 11.06.2025
Published: 30.09.2025

Keywords:
Veronica agrestis gas chromatography–mass spectrometry , bioactive phytochemical, antibacterial activity , antifungal activity, Pproteus mirabilis ,Candida albicans,

A B S T R A C T

Phytochemical compounds are of medical importance for many diseases, including inhibitory activity against bacterial and fungal pathogens. In this paper , multiple phytochemicals were isolated from *Veronica agrestis* in Iraq by subjecting the stem and leaves to gas chromatography-mass spectrometry (GC-MS). The study aims to identify the active compounds of the vegetative parts of the species and test their inhibitory activity against pathogens. The analysis revealed the presence of ten biologically active phytochemicals: benzeneacetonitrile, 3-hydroxy; (E)-4-(3-hydroxyprop-1-en-1-yl)-2;methoxyphenol; phytol; 9,12,15,-octadecatetrienoic acid (Z,Z,Z); 13,17Seco-5 pregn-13(18)-n-20-one; stigmasterol; octatriacontyl pentafluoropropionate; 5-(7a-isopropyl-4,5-dimethyl-octahydroindin-4-yl)-3-methyl-penta-2,4-dien-1-ol; cholestan-3-ol; 2-Methylenediamine-,(3β,5α)-. These compounds showed high inhibitory activity against the pathogenic fungus *Candida albicans* and the bacteria *Proteus mirabilis*. Six concentrations of the extract were used (5 ,10, 20 ,40 ,60 ,80)mg/ml showed results (00.00, 0.00, 0.00, 6.00,10.00,16.00) mm diameter of colonies in *Candida albicans* whil the diameter of colonies in *Proteus mirabilis* presented results (0.00,0.00, 10.00, 14.00, 22.00, 30.00) mm respectivly .

DOI: 10.53851/psijk.v2.i7. 35-39

1. INTRODUCTION

The genus *Veronica* is an important plant genera belonging to the Plantaginaceae family (Albach D. C., 2006) , and includes a large number of species that are rich in biologically active phenolic compounds. This genus has attracted the attention of researchers due to its potential uses in various fields, including pharmaceuticals, cosmetics, and natural products used in food preservation (Brčić A., 2024).Studies have shown that some Veronica species, such as *V. rosea*, contain flavonoids with antioxidant activity. These compounds have also been shown to be effective in protecting against sun exposure and reducing heat-induced hemolysis, reflecting their potential role in supporting skin health and reducing muscle tension (Chaira S. et al., 2022).

As for *V. amygdalina*, leaf analysis has revealed a wide range of active plant compounds, such as alkaloids, flavonoids, tannins, saponins, and others, which have demonstrated cholesterol-lowering, antioxidant, and anticancer properties, as well as their effectiveness in lowering blood sugar levels (Great I. et al., 2023).Studies have also been conducted on *V. biloba*, where active compounds such as dichloromethane, ethyl acetate, and n-hexane were extracted. (Hassan A. M. I. R., 2019). These extracts demonstrated remarkable activity against a range of bacteria and fungi, particularly due to the presence of ginkolic acid, known for its antibacterial properties (Hassan A. et al., 2019) Other species of the genus, such as *V. officinalis* (Rajakumar S. et al., 2022) *V. orchidea*, and *V. teucrium,* have also proven effective as antimicrobials, particularly against Gram-positive bacteria such as *Bacillus cereus* and *Listeria spp*. (Nazlić M. et al., 2023) . Some Veronica species also contain compounds such as benzaldehyde, known for its role in fungicidal resistance (Ebrahimzadeh M. & Navaei N., 2024). On the other hand, extracts of *V. montana* have demonstrated activity against *Escherichia coli* and *Staphylococcus aureus*. This activity is attributed to the

*Corresponding Author Institutional Email:
neepal.i@uokerbala.edu.iq (Jihan Hussein AL-Masoudi)

effect of flavonoids and tannins in disrupting bacterial cell membranes (Brčić A., 2024).
Many other species, such as *V. persica*, *V. hederifolia*, *V. polita poir*, and *V. anagallis*-aquatica, have been observed to be rich in phenolic compounds with diverse health effects, including antimicrobial activity (Bačič K., 2024) . Despite this significant research on the various species of the genus, insufficient information is available on the phytochemical composition of *Veronica agrestis*, highlighting the need for a detailed study of this species. Therefore, this study aims to identify the active compounds in the vegetative parts of this species and test their inhibitory activity against certain pathogens, such as bacteria and fungi, particularly the genus *Candida.*

2. MATERIAL AND METHODES

2.1. Study Area and Sample Collection

The samples used in this study were obtained from a number of infected patients, in collaboration with the University of Karbala. The samples were collected under sterile conditions and then transported to the laboratory for isolation. Fungi and bacteria were isolated from the biological samples, and the species under study were identified after obtaining pure cultures using standard microbiological methods.

2.2 Collection and Preparation of Plant Materials

sciences college laboratory, Kerbala

The plant known as "*Veronica agrastis*" was found in several locations throughout Iraq. After that, the plants were cleaned and allowed to dry at room temperature. After absorbing 100 milliliters of ethanol, 10 grams of powdered plants were filtered.

2.3. Plant Extract preperation

The dried stem and leaves were pulverized and extracted in a Soxhlet. The polar compounds were extracted with 1.5 liters of eythanol, then filtered and evaporated. After that, the compounds were weighed, and their yield percentage, expressed as a percentage of their dry weight, was calculated. The yield of the dark green extract from eythanol was 10 grams (0.095%), the plant extracts were placed in the °C. (Wahid A. Z. & Jafar F. N., 2005) dark and refrigerated at a temperature of 4

2-4-Testing the Effect of the Alcoholic Extract of Veronica agrestis on the Growth of Fungi and Bacteria

The effectiveness of the alcoholic extract of V. agrestis against pathogenic strains of fungi and bacteria (Proteus spp. and Candida spp.) was evaluated using the well diffusion method on Mueller-Hinton agar

PROCEDURE

1. Preparation of Inoculum:
   - Inoculate a single colony of Proteus and Candidain sterile broth and incubate overnight at 37°C (for Proteus) and 30°C (for Candida).
   - Adjust the inoculum to match a 0.5 McFarland standard.
2. Inoculating the Plates:
   - Pour Mueller-Hinton agar into sterile Petri dishes and allow it to solidify.
   - Use a sterile swab to evenly spread the inoculum across the surface of the agar plates.
3. Creating Wells:
   - Once the agar is inoculated and dried, use a sterile cork borer or well-maker to create wells in the agar plates.
4. Adding Plant Extracts and Controls:
   - Using a micropipette, add 100 µL of each concentration of the plant extract (80, 60, 40, 20, 10, and 5) mg/ml into separate wells.
   - Add 100 µL of ciprofloxacin into one well as the positive control and 100 µL of distilled water into another well as the negative control.
5. Incubation:
   - Incubate the plates at the appropriate temperature (37°C for Proteus and 30°C for Candida) for 24-48 hours.
6. Measuring Inhibition Zones
   - After incubation, measure the diameter of the inhibition zones around each well using a ruler or caliper.
   - Record the results for each concentration of the plant extract and the controls.

2- Using gas chromatography and mass spectrometry (GC/MS) to identify the chemical components of the extract, GC-MS analysis was used to chemically identify the compounds of *V. agrastis*. At Al-Zahraa Center for Medical and Pharmaceutical Sciences Research, the sample was prepared according to the method (Abu-Serag N. A. et al., 2019) (Al-Zahraa Center for Medical and Pharmaceutical Research Sciences, n.d.)

2.5. Statistical Analysis

Data were analyzed using STATGRAPHICS Centurion XV (version 20.1.16). ANOVA and LSD tests were employed at a 95% confidence level.

3. RESULTS AND DISCUSSION

3.1 These results are consistent with (Ertas A. et al., 2014), when they studied the activity of the family species against the obtained pathogens. It was found that the ethanolic extract of V. agrestis parts inhibited the fungi causing candidiasis and other skin diseases and that some of the secondary metabolites had antifungal properties. Six concentrations of the extract (5, 10, 20, 40, 60, 80) g/ml were used. The colony diameter of Candidia albicans showed results (0.00, 0.00, 0.00, 6.00, 10.00, 16.00) mm, respectively. Therefore, the results are presented in Table (1) figure (1) . The alcoholic extract showed high antibacterial activity against Proteus mirabilis, which causes urinary tract infections. Six concentrations of the extract (5, 10, 20, 40, 60, 80) g/ml were used. The colony diameter of Proteus mirabilis showed results of (0.00, 0.00, 10.00, 14.00, 22.00, 30.00) mm, respectively. Therefore, the results are shown in Table (2) and figure (2). These results are consistent with the results of Salehi (Salehi B. et al., 2019), when they studied the activity of the family species against some secondary metabolites that act as antimicrobials and they found that.

Table 1. Antifungal activity of ethanol extracts from *V.agrastis* against *Candida albicans*

Table (1)	Mean of Inhibition zone (mm)						
Comparison with distilled water (0.00) mg/ml	Comparison with Nystatin 10mg	Concentration (5mg/ml)	Concentration (10mg/ml)	Concentration (20mg/ml)	Concentration (40mg/ml)	Concentration (60mg/ml)	Concentration (80mg/ml)
0.00	8.00	0.00	0.00	0.00	6.00	10.00	16.00

Table 2. Antibacteral activity of ethanol extracts from *V.agrastis* against *P. mirabilis*

Comparison with distilled water (0.00) mg/ml	Comparison with Ciproflox acin 10mg	Concentration (5mg/ml)	Concentration (10mg/ml)	Concentration (20mg/ml)	Concentration (40mg/ml)	Concentration (60mg/ml)	Concentration (80mg/ml)
0.00	8.00	0.00	0.00	10.00	14.00	22.00	30.00

When reviewing the results of the current study on the chemical compounds of Veronica, it is noted that the percentage of compounds with fungal growth inhibitory properties is high, such as steroids, sticasterol, lanosterol, organofluoro ester compounds, unsaturated fats, in addition to phenols and diterpenes, all of which play a role in the inhibitory action against Candida (Alqurashi A. S. et al., 2022).

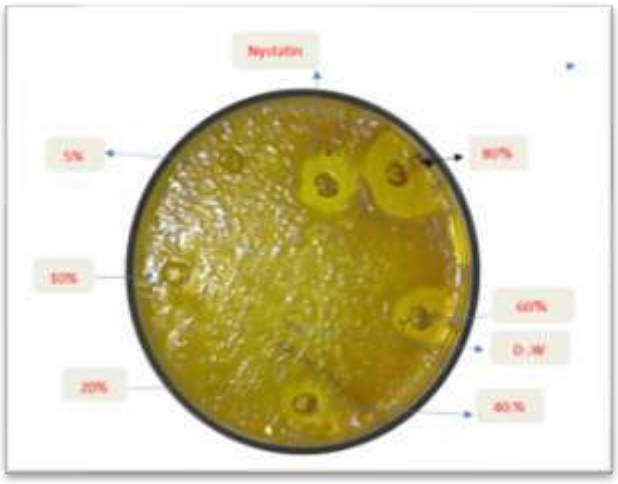

Figure 1. *Candida albicans* growth grown in varying concentrations of *V. agrestis* ethanol extract.

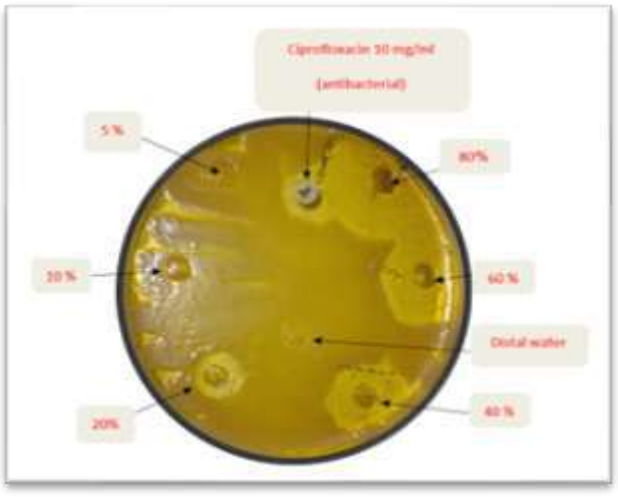

Figure 2. Growth of Proteus mirabilis cultured in varying concentrations of *V. agrestis* ethanol extract

3.1. Gas chromatography-mass spectrometry (GC-MS)

The ethanolic extract of the vegetative parts of Veronica agrestis was analyzed using gas chromatography-mass spectrometry (GC-MS). Ten major chemical compounds were detected, as shown in Table (3).

Table 3. Major phytochemical compounds in ethanolic extract *V. agrastis.*

No.	R. t. (min)	Area	%Total	M. wt	Prob %	Name
1	18.347	1.005e+8	2.036	133	68.8 %	Benzeneacetonitrile, 3-hydroxy
2	18.788	1.544e+8	3.129	133	68.7 %	Benzeneacetonitrile, 3-hydroxy
3	24.536	7.685e+7	1.557	180	51.0 %	(E)-4-(3-Hydroxyprop-1-en-1-yl)-2-methoxyphenol
4	31.788	1.850e+8	3.749	296	64.6 %	Phytol
6	41.327	1.752e+7	0.355	400	15.3 %	Cholestan-3-ol, 2-methylene-, (3β,5α)-
7	43.501	3.723e+8	7.543	302	8.12 %	13,17-Seco-5α-pregn-13(18)-en-20-one
8	44.628	1.179e+9	23.887	412	57.1 %	Stigmasterol
9	45.998	7.685e+7	1.557	696	5.06 %	Octatriacontyl pentafluoropropionate
10	48.737	3.119e+7	0.632	288	12.8 %	5-(7a-Isopropenyl-4,5-dimethyl-octahydroinden-4-yl)-3-methyl-penta-2,4-dien- 1-ol

Table 4. Classification and Biological Relevance of Phytochemicals Isolated from the ethanolic extract *V. agrastis.*

No.	Compound Name	Compound Type	
1	Benzeneacetonitrile, 3-hydroxy	Aromatic nitrile	Antimicrobial, antioxidant
2	(E)-4-(3-Hydroxyprop-1-en-1-yl)-2-methoxyphenol (Coniferyl alcohol)	Phenylpropanoid	Antioxidant, anti-inflammatory, anticancer
3	Phytol	Diterpene alcohol	Antimicrobial, antioxidant, anticancer,
4	9,12,15-Octadecatrienoic acid, (Z,Z,Z)- (α-Linolenic acid)	Omega-3 fatty acid	Anti-inflammatory, antioxidant
5	Cholestan-3-ol, 2-methylene-, (3β,5α)-	Plant sterol	Cholesterol-lowering, anti-inflammatory, anticancer
6	13,17-Seco-5α-pregn-13(18)-en-20-one	Steroid derivative	Hormonal activity, anti-inflammatory effect
7	Stigmasterol	Plant sterol	Antioxidant, anti-inflammatory, cholesterol-lowering
8	Octatriacontyl pentafluoropropionate	Long-chain ester	antibacterial
9	5-(7a-Isopropenyl-4,5-dimethyl-octahydroinden-4-yl)-3-methyl-penta-2,4-dien-1-ol	Unsaturated cyclic terpenoid	Antifungal, antibacterial, antioxidant

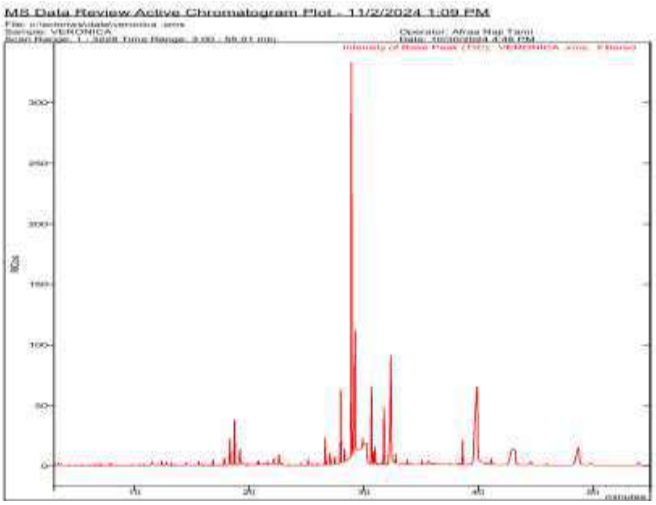

Figure 3. GC-MS chromatogram of ethanolic extract the leaves and stem for *V. agrestis*

4. CONCLUSION

The ethanolic aroma of *V. agrestis* leaves and stems exhibits potent antifungal activity against the fungus Candidia albicans and the bacterium Protus mirabilis. Gas chromatography-mass spectrometry (GC-MS) analysis revealed that the extracts contained a variety of bioactive plant compounds, including aromatic compounds, phenols, steroids, and terpenes, which likely contribute to their antimicrobial properties. This suggests *V. agrestis* as a natural source of antifungal and antibacterial properties.

REFERENCES

Abu-Serag, N. A., Al-Garaawi, N. I., & Ali, A. M. (2019). Analysis of bioactive phytochemical compound of (Cyperus aucheri Jaub.) by using gas chromatography–mass spectrometry. IOP Conference Series: Earth and Environmental Science, 388(1), 012063.

Albach, D. C. (2006). Evolution of Veronica (Plantaginaceae) on the Balkan Peninsula. Phyton: Annales Rei Botanicae, 12(2), 231–244.

Alqurashi, A. S., Al Masoudi, L. M., Hamdi, H., & Abu Zaid, A. (2022). Chemical Composition and Antioxidant, Antiviral, Antifungal, Antibacterial and Anticancer Potentials of Opuntia ficus-indica Seed Oil. Molecules, 27(17), 5453. https://doi.org/10.3390/molecules27175453

Al-Zahraa Center for Medical and Pharmaceutical Research Sciences (ZCMPRS). (n.d.). Email: zcmprs@alzahraa.edu.iq

Bačič, K. (2024). Investigation of the optimal yield of phenolic compounds from the genus Veronica using different extraction techniques and solvents [MSc Thesis, Faculty of Science, University of Split, Croatia].

Brčić, A. (2024). Rod Veronica – izvor fenolnih spojeva, njihova biološka aktivnost i primjena [PhD Dissertation, University of Split, Faculty of Science].

Chaira, S., Ben Moussa, M. T., Hanfer, M., Ouache, R., Kadd, I., Pale, P., & Harkat, H. (2022). Veronica rosea biomolecule profiling, antioxidant potential, dermoprotective effect, anti-inflammatory and hemostatic activities and zyme inhibitory action. European Journal of Integrative Medicine, 56, 1876–3820.

Ebrahimzadeh, M., & Navaei, N. (2024). Review of the ethnopharmacology, phytochemistry, and pharmacology of the Veronica officinalis: An update (2020–2024). Tabari Biomedical Student Research Journal, 6(1), 35–43.

Ertas, A., Boga, M., Kizil, M., Ceken, B., Goren, A. C., Hasimi, N., & Kolak, U. (2014). Chemical profile and biological activities of Veronica thymoides subsp. pseudocinerea. Pharmaceutical Biology, 53(3), 334–339. https://doi.org/10.3109/13880209.2014.919326

Great, I., Oghenekeno, S. L. P., Agatha, N., Favour, O., Laura, I., Promise, O., Ajiri, R., Joy, E., Victor, O., Chinenye, F., & Eunice, D. (2023). Biological and bioactive components of bitter leaf (Vernonia amygdalina)—Insight on health and nutritional benefits: A review. Food Chemistry Advances, 3, 2772–753X.

Hassan, A., Ullah, H., & Bonomo, M. G. (2019). Antibacterial and antifungal activities of the medicinal plant Veronica biloba. Journal of Chemistry, 2019(1), Article ID 5264943.

Hassan, A. M. I. R. (2019). Antibacterial and Antifungal Activities of the Medicinal Plant Veronica biloba. Journal of Chemistry. https://doi.org/10.1155/2019/5264943

Nazlić, M., Vrca, I., Čikeš Čulić, V., Lozić, M., Dunkić, N., Kremer, D., Ruščić, M., & Dunkić, V. (2023). Isolation of volatile compounds by microwave-assisted extraction from six Veronica species and testing of antiproliferative and apoptotic activities. Plants (Basel), 12(18), 3244.

Rajakumar, S., Revanth, M. P., Kasi, A., & Sujitha, P. (2022). Evaluating the antibacterial efficacy and minimal bactericidal concentration (MBC) of three different herbal extracts on recalcitrant endodontic pathogens: An in vitro study. Journal of International Oral Health, 14(3), 266–272.

Salehi, B., Shetty, M. S., Kumar, V. A. N., Živković, J., Calina, D., Docea, A. O., Emamzadeh-Yazdi, S., Kılıç, C. S., Goloshvili, T., Nicola, S., Pignata, G., Sharopov, F., Contreras, M. del M., Cho, W. C., Martins, N., & Sharifi-Rad, J. (2019). Veronica plants—Drifting from farm to traditional healing, food application, and phytopharmacology. Molecules, 24(13), 2454.

Wahid, A. Z., & Jafar, F. N. (2005). Test of life effectiveness of Carthamus tinctorius extract toward germ and fungi. Al-Basrah Research Journal, 31(3B), 39–47.

PURE SCIENCES
International Journal of Kerbala

Pure Sciences International Journal of Kerbala

Year: 2025 Volume : 2 Issue : 7 ISSN: 6188-2789 Print 3005 -2394 Online

2025,Volume 2 , Issue 7 , PSIJK (40-45)

Pure Sciences International Journal of Kerbala

The Phytochemical Compounds and the Antimicrobial Activity of Portulaca grandiflora Aqueous & Methanol Extracts in Iraq

Mahasen Abid –Ali Alkafaji [a] , Neepal Imtair Al Garaawi [a*] , Fatima Karim Khudair [a]

[a] *Biology of Department, College of Education for Pure Science, University of Kerbala, Kerbala, Iraq*

P A P E R I N F O

Received: 04.05.2025
Accepted: 02.07.2025
Published: 30.09.2025

***Keywords*:**
Portulaca grandiflora,
gas chromatography–mass spectrometry,
bioactive phytochemical,
antibacterial activity,
Proteus mirabilis,
antifungal activity,
Candida albicans

A B S T R A C T

Inhibitory activity against bacterial and fungal pathogens is one of the many diseases for which phytochemical compounds are useful in medicine. By using gas chromatography-mass spectrometry (GC-MS) on the floral parts of ***Portulaca grandiflora*** s in Iraq, several phytochemicals were extracted for this study. The study's objective is to determine the active substances found in the species' vegetative parts and evaluate their ability to inhibit pathogens. In the current study, various medical phytochemical compounds that have been isolated from *Portulaca grandiflora* from the floral parts that showed antifungal activity as *Candida albicans* and antibacterial as *Proteus mirabilis*. The phytochemicals of *Portulaca grandiflora* floral parts were exposed to gas chromatography–mass spectrometry (GC-MS) analysis. The results revealed the highest activity against fungal and bacteria. The study used six concentrations of the floral parts (5,10,20,40,60,80) mg/ml for both aqueous and methanolic extracts. The aqueous extract showed high inhibition against Candida fungi, It was (0.00mm, 0.00mm, 0.00mm, 0.00mm, 12.00mm, 22.00mm) respectively in the diameter of colonies Thus, the aqueous extract indicated high inhibition against bacteria *Proteus mirabilis* . It was (0.00mm, 0.00mm, 0.00mm, 10.00mm, 14.00mm, 18.00mm) separately in the diameter of colonies. The methanolic extracts of floral parts have lower inhibition rates compared to the aqueous extract.which was giving results against Candida fungi (0.00mm, 0.00mm, 4.00mm, 6.00mm, 10.00mm, 24.00mm) respectively in the diameter of colonies, so that in a result with the inhibition against bacteria *Proteus mirabilis* . It was (0.00mm ,3.00mm, 6.00mm,10.00mm, 15.00mm, 25.00mm) respectively in the diameter of colonies. The analysis of compounds to *P. grandiflora* floral parts by GC-MS showed the presence of five bioactive phytochemical compounds as: Benzaldehyde : Cyclohexene , 1-methyl-4-(1-methylethenyl)-: (S), Linalool : Naphthalene : and Cyclohexanol, 1-methyl-4-(1-methylethenyl)-, acetate.

DOI: 10.53851/psijk.v2.i7. 40-45

1. INTRODUCTION

Microbes cause many diseases and increase the mortality rate worldwide. Their resistance to conventional medicines has been a major reason for the interest in medicinal plants as a reliable alternative for managing diseases resulting from bacterial infections in recent times. Many research efforts have been directed towards exploring plant components with antimicrobial potential that are used as antimicrobial agents due to their high therapeutic performance, low toxicity and reasonable prices (Ojah EO , 2021).

The family Portulacaceae consists of one genus and 116 species (Christenhusz MJ& Byng JW, 2016) based on previous molecular studies that reduced the family to a single monophyletic group, which included one genus, *Portulaca L.*, and 100 species (Nyffeler R & Eggli U, 2010). The word genus is taken from a Latin word composed of two syllables; the first is Portare, which means carry, and the syllable Lak, which means milk and gives the meaning of the milky liquid secreted by the plant. Its types are commonly used in general to treat infections, ulcers, colds, coughs, urinary tract diseases, and many others (Philips SM, 2000). The ancient Egyptians and the English in the Middle Ages used plants of this genus medicinally, as food, or as vegetables (Boulos L, El-Hadidi MN, 1984) .

Portulaca grandiflora is a plant that is cultivated by humans for its beautiful colorful flowers. It is widely spread due to its rapid reproductive property. In Iraq flora, it has been established as a cultivated plant and its original homeland is South America. In Iraq, it is called Yaldis, after its Turkish name Aldoz. It is known in

*Corresponding Author Institutional Email:
(neepal.i@uokerbala.edu.iq) (Neepal Imtair Al Garaawi)

Europe and America as the eleven O' clock rose, moss rose, sun plant and in India lyauiya and Goddu pavelli, and Sokkare Kamma in Canada(Netala S, Pravallika R,et al., 2015)

It was found that the chemical extracts of *P. grandiflora* samples contain alkaloids, hydroquinols, phenols, flavonoids, saponins, tannins, terpenoids and steroids, as the different effectiveness of these complex compounds leads to significant variations in antioxidant capacity(Aisyah SI, et al., 2023). In addition, *P. grandiflora* plants showed antioxidant activities, indicating that they would have variable flavonoid content and therefore they had variable wound healing activity depending on flower color(Budiawan A,et al., 2023). A similar study also revealed that n-hexane extract of *P. grandiflora* significantly enhances wound healing by increasing cell migration and wound closure compared to wounds treated with MEBO ointment(Mus'hib HK, Abdul-Jalil TZ, 2024). The use of methanolic, ethanolic and n-hexane extracts of the *P. grandiflora* plant contains antibacterial, antifungal, anticancer and antioxidant properties(Salahuddin H,et al.,2024). A study showed that flavonoids, one of the compounds of *P. grandiflora*, can protect the skin from ultraviolet UV rays. Accordingly, it was possible to develop a sunscreen that protects the skin from the risk of skin cancer and prevents premature skin aging(Kirana BC,et al., 2023). And as stated by experiment that the methanolic extract of the green parts of the morning flower *P. grandiflora* contains a high percentage of flavonoids, which act as an antihyperlipidemic agent induced by a high-fat diet (HFD) and as an antioxidant(Wang X,et al.,2023).

Candida albicans is a fungus that lives in the human body in normal conditions, in the intestines and oral cavity. It then turns into an opportunistic organism in special cases, such as weak immunity, or when dealing with some animals, such as birds, cows, cats, dogs, and pigs, if hygiene conditions are not observed, as it is a fungus present in their bodies(Edelmann A,et al.,2005).

Proteus bacteria, including *Proteus mirabilis*, form a symbiotic relationship between higher organisms, including humans and some animals. This is indicated by the contamination of soil and water with the feces of infected animals, which constitutes a source of infection for humans when consuming this water or marine organisms contaminated with the feces of these infected animals(Drzewiecka D,2016).

2. MATERIALS AND METHODS

2.1. Study Area And Sampling

The studied fungi and bacteria were isolated from some infected patients in Karbala, the fungi and the bacteria were identified in the pure sciences college laboratory, Kerbala university.

2.2. Plant Extract Preparation

The dried aerial parts were pulverized and extracted in a Soxhlet. The polar compounds were extracted with 1.4 ml methanol + 60ml distal water for the alcoholic extraction and 200ml of distal water for the aqueous extract, then filtered and evaporated. After that, the compounds were weighed, and their yield percentage expressed as a percentage of their dry weight, was calculated. The yield of the dark green extract from methanol was 60 grams (0.095%). The plant extracts were placed in the dark and refrigerated at a temperature of 4 °C, Wahid & Jafar method(Wahid AZ & Jafar FN, 2005)

2.3. Cultivated Method of Aqueous & Alcoholic Extract *P. Grandiflora* of Plant on Pathogenic Fungi Growth

To perform the inhibition zone assay for *Proteus* and *Candida* using your plant extract and nanoparticles in a Mueller-Hinton agar setup, follow these steps:

Materials Needed

-Mueller-Hinton agar plates
-Plant extract at concentrations of 80 mg, 60 mg, 40 mg, 20 mg, 10 mg, and 5 mg
-Ciprofloxacin (positive control)
-Distilled water (negative control)
-Sterile wells or cork borer
-Inoculating loop
-Sterile swabs
-Incubator

PROCEDURE

1 .Preparation of Inoculum:

- Inoculate a single colony of Proteus and Candidain sterile broth and incubate overnight at 37°C (for *Proteus*) and 30°C (for *Candida*).
- Adjust the inoculum to match a 0.5 McFarland standard.

2 .Inoculating the Plates:

- Pour Mueller-Hinton agar into sterile Petri dishes and allow it to solidify.
- Use a sterile swab to evenly spread the inoculum across the surface of the agar plates.

3 .Creating Wells:
- Once the agar is inoculated and dried, use a sterile cork borer or well-maker to create wells in the agar plates.

4 .Adding Plant Extracts and Controls:
- Using a micropipette, add 100 µL of each concentration of the plant extract (80 mg, 60 mg, 40 mg, 20 mg, 10 mg, and 5 mg) into separate wells.
- Add 100 µL of ciprofloxacin into one well as the positive control and 100 µL of distilled water into another well as the negative control.

5 .Incubation:
- Incubate the plates at the appropriate temperature (37°C for Proteus and 30°C for Candida) for 24-48 hours.

6 .Measuring Inhibition Zones
- After incubation, measure the diameter of the inhibition zones around each well using a ruler or caliper.
- Record the results for each concentration of the plant extract and the controls.

Data Analysis
-Analyze the inhibition zones to determine the effectiveness of the plant extract at different concentrations.
- Compare the inhibition.

2.4. Collection And Preparation of Plant Materials

P. grandiflora plant were located from various places from Karbala city in Iraq. Then plants were well washed and dried at room temperature. 10gm of plant powdered had taken in 1.4L methanol and 60ml distal water for the alcoholic extract solution and then filtered, and 10gm of plant powdered in 200ml of distal water and also had been filtered.

2.5. Constituents Identification Of Extract By Gas Chromatography – Mass Spectrum (GC/MS)

Phytochemical identification of *P. grandiflora* were carried out by GC-MS analysis in (Scion Instruments Company.Model: SCiON 436) GC-MS Column: SCION-5MS { ID = 0.25mm, length = 15m, df = 0.25µm } Carrier gas : Helium. Instrument under computer designed control at 60eV. About 1µL of them ethanol extract was injected into the GC-MS column using a micro syringe and the scanning was done for 10 minutes. Column oven : initial temperature is 50 ℃ increase by 5 ℃ / min to 240 ℃, Sample Preparation : 50 µL of the sample is diluted with 2.5ml of Methanol (HPLC-Grade) before injection. Gas flow ratio : 1 ml/min. Pressure : 10 psi. Range :1 – 2000 m/z, split ratio 1:40. (This method is innovative in Al-Zahraa Center for Medical and Pharmaceutical Research Sciences (ZCMPRS)) (Purwanto A,et al.,2022).

3. RESULTS AND DISCUSSION

3.1. Antifungal Activity

The current study *Candida albicans* was selected to test the activity of the aqueous and methanol extract of *P. grandiflora* partss.The extract showed a high antifungal activity against *Candidia albicans*. Six concentrations of extract (5,10,20,40 ,60,80 mg/ml) were used for the floral parts of the plant each as aqueous and methanol extracts. The results showed (00.00 , 0.00, 0.00 , 0.00, 12.00, 22.00 mm) diameter of colonies in *Candida albicans* for aqueous extract, the results showed in Table 1, and (00.00 , 0.00, 4.00 , 6.00, 10.00, 24.00 mm) diameter of colonies in *Candida albicans* for alcoholic extract. Table 2 offered the results . We conclude from the results of our current experiment that the inhibitory ability of the alcoholic extracts of the floral parts of the plant against *Candida albicans* was higher than the inhibitory ability of the aqueous extracts of the same parts against *Candida albicans*.

Table 1. Antifungal activity of aqueous extracts from *P. grandiflora* floral parts against *Candida albicans*

Mean of Inhibition zone (mm							
Comparison with distilled water (0.00) mg/ml	Comparison with Nystatin 10mg	Concentration (5mg/ml)	Concentration (10mg/ml)	Concentration (20mg/ml)	Concentration (40mg/ml)	Concentration (60mg/ml)	Concentration (80mg/ml)
0.00	8.00	0.00	0.00	0.00	0.00	12.00	22.00

Table 2. Antifungal activity of methanolic extracts from *P. grandiflora* floral parts against *Candida albicans*

Mean of Inhibition zone (mm							
Comparison with distilled water (0.00) mg/ml	Comparison with Nystatin 10mg	Concentration (5mg/ml)	Concentration (10mg/ml)	Concentration (20mg/ml)	Concentration (40mg/ml)	Concentration (60mg/ml)	Concentration (80mg/ml)
0.00	8.00	0.00	0.00	4.00	6.00	10.00	24.00

In support, scientists proved in an experimental laboratory study using the disk diffusion method that the extract of the morning glory plant *P. grandiflora* had different inhibition rates against the growth of the fungus

*C. albicans(*Purwanto A,et al.,2024). Based on differences in polarity of extract of *P. grandiflora* (aqueous, ethanolic, distilled water, ethyl acetate, n-hexane) the aqueous extract had the strongest effect against *C. albicans* based on disc diffusion method(Abu-Serag NA et al., 2019).

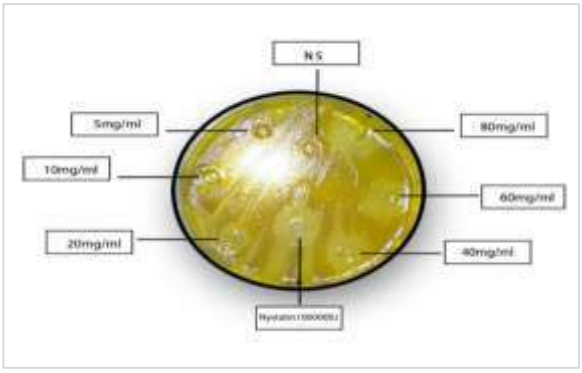

Figure 1 :*Candida albicans* growth grown in varying concentrations of *P. grandiflora* ethanol extract.

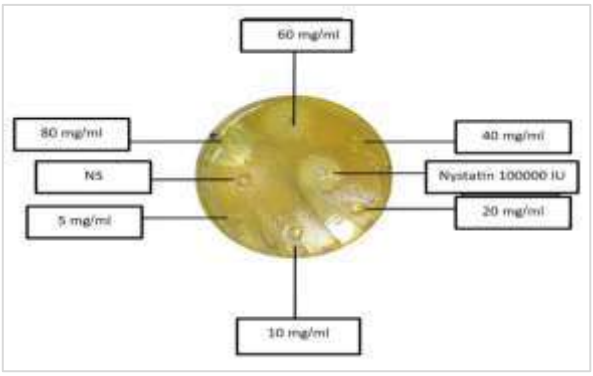

Figure 2 : Antifungal activity of aqueous extracts from *P. grandiflora* floral parts against *Candida albicans*

3.2. Antibacterial Action

In this study *Proteus mirabilus* was selected to test the activity of the aqueous and methanolic extracts of *P. grandiflora* floral parts.The extracts showed a high antibacterial activity against *Proteus mirabilus*. Six concentrations of extract (5,10,20,40 ,60,80 mg/ml) were used for the floral parts of the plant each as aqueous and methanol extracts. The results indicated (00.00mm , 0.00mm, 0.00mm , 10.00mm, 14.00mm, 18.00 mm) diameter of colonies in *Proteus mirabilus* for aqueous extract.The results were displayed in Table 3, and they wrer (00.00 mm, 3.00mm, 6.00 mm, 10.00mm, 15.00mm, 25.00 mm) diameter of colonies in *Proteus mirabilus* .For alcoholic extract, the results wre showed in Table 4.

We conclude from the results of our current experiment that the inhibitory ability of the alcoholic extracts of the floral parts of the plant against *Proteus mirabilus* was higher than the inhibitory ability of the aqueous extracts of the same parts against *Proteus mirabilus*.Further, the alcoholic extracts showed inhibitions even at low concentrations.

Table 3. Antibacterial activity of aqueous extracts from *P. grandiflora* floral parts against *Proteus mirabilus*

Mean of Inhibition zone (mm)							
Comparison with distilled water (0.00) mg/ml	Comparison with Ciprofloxacin 10mg	Concentration (5mg/ml)	Concentration (10mg/ml)	Concentration (20mg/ml)	Concentration (40mg/ml)	Concentration (60mg/ml)	Concentration (80mg/ml)
0.00	8.00	0.00	0.00	0.00	10.00	14.00	18.00

Table 4. Antibacterial activity of methanolic extracts from *P. grandiflora* floral parts against *Proteus mirabilus*

Mean of Inhibition zone (mm)							
Comparison with distilled water (0.00) mg/ml	Comparison with Ciprofloxacin 10mg	Concentration (5mg/ml)	Concentration (10mg/ml)	Concentration (20mg/ml)	Concentration (40mg/ml)	Concentration (60mg/ml)	Concentration (80mg/ml)
0.00	8.00	0.00	3.00	6.00	10.00	15.00	25.00

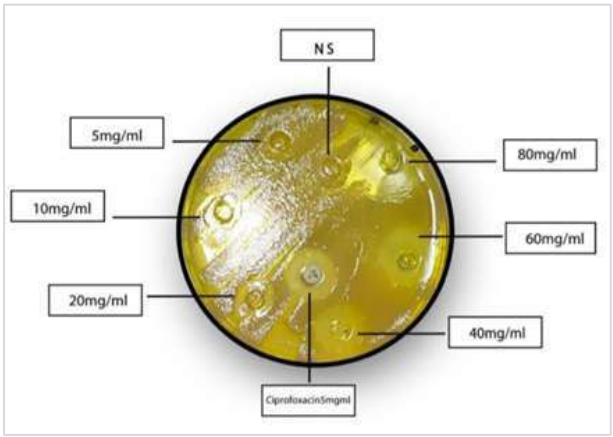

Figure 3 : Antibacterial activity of aqueous extracts from *P. grandiflora* floral parts against *Proteus mirabilus*

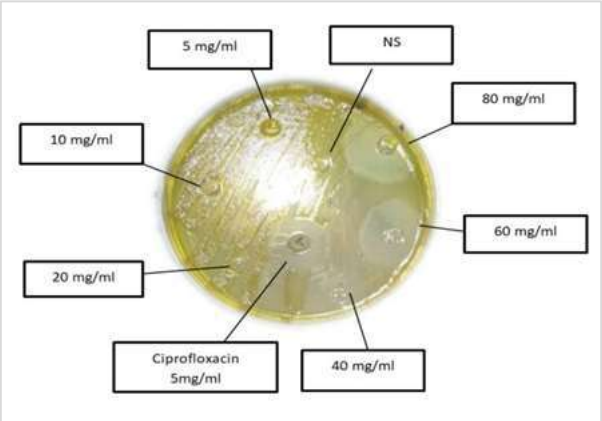

Figure 4: Antibacterial activity of methanolic extracts from *P. grandiflora* floral parts against *Proteus mirabilus*

4. ASSESSMENT OF BIOCHEMICAL COMPOUNDS OF *P. grandiflora*

The analysis GC-MS ethanolic extract of *P. grandiflora* floral (Figure 1) partsrevealed the presence of five components found in Table 5 as: Benzaldehyde, Cyclohexene, 1-methyl-4-(1-methylethenyl)-, (S), Linalool, Naphthalene, and Cyclohexanol, 1-methyl-4-(1-methylethenyl)-, acetate.

It is noted that the percentage of terpene compounds is high (Cyclohexene, 1-methyl-4-(1-methylethenyl)-, (S : Linalool : Cyclohexanol, 1-methyl-4-(1-) and it is considered to be one of the highly efficient compounds in inhibiting microbes, especially pathogenic ones in the experimental samples, such as Candida *(Candida albicans)* and bacteria *(Proteus mirabilus)* (AlAmery SF & Al-Garaawi NI,2020).

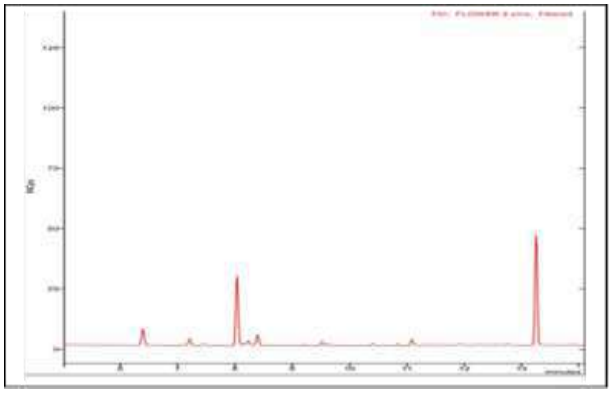

Figure 6. Chromatography plot of *P. grandiflora* floral parts

Table 5. Major phytochemical composites in ethanolic extra of P. grandiflora floral parts

No.	R. t. (min)	Area	%Total	M.wt	Prob %	Name
1	6.399	2.214e+7	13.713	63.0	106	Benzaldehyde
2	8.041	9.134e+7	19.067	20.4	136	Cyclohexene, 1-methyl-4-(1-methylethenyl)-, (S)
3	9.522	4.645e+6	12.359	33.6	154	Linalool
4	10.842	2.181e+6	12.169	16.4	128	Naphthalene
5	13.257	1.371e+8	22.606	13.8	196	Cyclohexanol, 1-methyl-4-(1-methylethenyl)-, acetate

REFERENCES

Abu-Serag, N. A., Al-Garaawi, N. I., & Ali, A. M. (2019). Analysis of bioactive phytochemical compound of (*Cyperus aucheri Jaub.*) by using gas chromatography–mass spectrometry. *IOP Conf Ser Earth Environ Sci*, *388*(1), 012063.

Aisyah, S. I., Oktavia, A. W. P., Ayuningtyas, A. A., Putra, R. P., Prassiska, S., Jamilah, S., et al. (2023). Differences in phytochemical compounds and antioxidant activity of *Portulaca oleracea* and *Portulaca grandiflora*. *Biodiversitas J Biol Divers*, *24*(3).

AlAmery, S. F., & Al-Garaawi, N. I. (2020). Phytochemical profile and antifungal activity of stems and leaves methanol extract from the *Juncus maritimus* Linn. (Juncaceae family) against some dermatophytes fungi. *AIP Conf Proc*, *2290*, 020034-1–020034-17.

Boulos, L., & El-Hadidi, M. N. (1984). *The weed flora of Egypt*. The American University in Cairo Press.

Budiawan, A., Purwanto, A., Puradewa, L., Cahyani, E. D., & Purwaningsih, C. E. (2023). Wound healing activity and flavonoid contents of purslane (*Portulaca grandiflora*) of various varieties. *RSC Adv*, *13*(15), 9871–9877.

Christenhusz, M. J., & Byng, J. W. (2016). The number of known plant species in the world and its annual increase. *Phytotaxa*, *261*(3), 201–217.

Drzewiecka, D. (2016). Significance and roles of *Proteus spp*. bacteria in natural environments.

Microb Ecol, *72*(4), 741–758. https://doi.org/10.1007/s00248-015-0720-6

Edelmann, A., Krüger, M., & Schmid, J. (2005). Genetic relationship between human and animal isolates of *Candida albicans*. *J Clin Microbiol*, *43*(12), 6164–6166. https://doi.org/10.1128/JCM.43.12.6164-6166.2005

Kirana, B. C., Cahyani, E. D., & Budiawan, A. (2023). Protective factor evaluation of purslane (*Portulaca grandiflora*) magenta flower variety herbs extract cream formula. *Pharm Pharm Sci J*, *10*(3).

Mus'hib, H. K., & Abdul-Jalil, T. Z. (2024). *Portulaca grandiflora* phytochemicals as a potential source for wound healing activity: *in vitro* and *in vivo* studies. *Plant Sci Today*, *10*(2), 123–130. https://doi.org/10.14719/pst.4209

Netala, S., Pravallika, R., Md S. S., & Kumari, N. (2015). Comparative pharmacognostic studies on three species of *Portulaca*. *Int J Pharmacogn Phytochem Res*, *6*(4), 806–816.

Nyffeler, R., & Eggli, U. (2010). Disintegrating Portulacaceae: a new familial classification of the suborder Portulacineae (Caryophyllales) based on molecular and morphological data. *Taxon*, *59*(1), 227–240.

Ojah, E. O., et al. (n.d.). Phytochemical and antibacterial properties of root extracts from *Portulaca oleracea* Linn. (purslane) utilised in the management of diseases in Nigeria. *J Med Plants Econ Dev*. Retrieved from

Philips, S. M. (2000). Notes on *Portulaca* L. (Portulacaceae) in tropical East Africa. *Kew Bull*, *55*, 687–698.

Purwanto, A., Nugroho, C. A., & Indriasari, C. (2024). Aktivitas antifungi *in vitro* berdasarkan perbedaan polaritas pelarut ekstrak herba krokot (*Portulaca grandiflora*). *JIIP-J Ilm Ilmu Pendidik*, *7*(1), 181–187.

Purwanto, A., Purwaningsih, C. E., & Indriasari, C. (2022). Aktivitas anticandida herba krokot (*Portulaca grandiflora*). *Florea J Biol Pembelajarannya*, *9*(2), 110–117.

Salahuddin, H., Batool, R., Sabri, S., Mansoor, Q., Akhtar, M. S., & Mahmood, T. (2024). Phytochemical and *in vitro* biological profiling of *Portulaca grandiflora* whole plant extracts. *Lahore Garrison Univ J Life Sci*, *8*(1), 32–49.

Wahid, A. Z., & Jafar, F. N. (2005). Test of life effectiveness of *Carthamus tinctorius* extract toward germ and fungi. *Al-Basrah Res J*, *31*(3B), 39–47.

Wang, X., Hao, W., Kumar, M., Gupta, R., Kushwah, A. S., & Kaur, G. (2023). Flavonoid-rich extract of *Portulaca grandiflora* Hook. attenuates oxidative stress, biochemical changes and vascular dysfunction in atherogenic model. *Lat Am J Pharm*, *42*(6), 1164–1175.

PURE SCIENCES
International Journal of Kerbala

Pure Sciences International Journal of Kerbala

Year: 2025 Volume : 2 Issue : 7 ISSN: 6188-2789 Print 3005 -2394 Online

2025,Volume 2 , Issue 7 , PSIJK (46-52)

Pure Sciences International Journal of Kerbala

Synthesis and Characterization of Indium Phosphide by Electrochemical Deposition Method

Imad Kadhim Khudhair [a*]

[a] Ministry of Education, Baghdad Education Directorate of Al- Karkh , Iraq

P A P A R I N F O

Received: 11.05.2025
Accepted: 22.06.2025
Published: 30.09.2025

Keywords:
Indium phosphide, Electrochemical deposition method, X-ray diffraction, Electrical properties, thermoelectric properties.

A B S T R A C T

Three samples of indium phosphide (InP) were prepared by electrochemical deposition method on porous nickel substrates. The results of X-ray diffraction of InP showed that it crystallizes in one direction (220). There is an increase in the intensity of the diffraction peak with increasing deposition time for the prepared samples. By calculating (C-V) at a fixed frequency and drawing the relationship between the (1/C2) and (V), it was found that the slope has a negative value, indicating that the prepared samples are of the p-type, the built-in potential (Vbi) of the samples was determined to be (1.42, 1.54, 1.66)eV.(I-V) was calculated for the samples prepared for InP at different temperatures (303,313,323)ko , the relationship between I and V showed that the current intensity increases with increasing temperatures, and the electrical resistance (R) of the samples decreases with increasing different temperatures, the activation energy (Ea) values of the samples ranged (0.14,0.07,0.06) eV at different temperatures. from the study of the thermoelectric properties, it was found that the best value of the Seebeck coefficient (S) is for the sample with a deposition time of (4h).

DOI: 10.53851/psijk.v2.i7. 46-52

Table 1. Nomenclature and Definitions Used in the Study

InP	Indium phosphide	ε	crystal lattice strain
XRD	X-ray diffraction	δ	dislocation density
FCC	Face centered cubic	Ψ	barrier height of the system
WZ	Wurtzite	V_{bi}	built-in potential
ZB	zincblende	R	electrical resistance
aδ	crystal lattice constant	Ea	activation energy
nm	nanometer	K	Boltzmann constant
d_{hkl}	distance between the crystal planes	S	Seebeck coefficient
N	integer called diffraction order	FWHM	Full Width at Half Maximum
D	crystallite size		

*Corresponding Author Institutional Email:
emadkadhem20@gmail.com (Imad Kadhim Khudhair)

1.INTRODUCTION

Nanostructured semiconductors have attracted much attention due to their good optical properties, especially nanowires belonging to group (III-V) which are well-known electronic and optoelectronic materials (Li, He, et al., 2023) , and can cover important spectral ranges extending from the visible to the infrared range. The direct energy gap is one of the main advantages of most compound semiconductors of group (III-V) (Cipriano, Di Liberto, et al., 2020), making the study of these materials very desirable. Among these compounds is indium phosphide (InP) (Li & Lu, 2008). Indium phosphide has a direct energy gap (1.42-1.35) eV, at 300K^o and has an absorption wavelength between (873-918) nm (Al Hammade, 2022) , in the infrared range (Almeida, Ubbink, et al., 2023) , and has various applications in electronics and optoelectronic devices as it is characterized by high electronic mobility (4000 cm^2/V.S) (Yue, Shi, et al., 2023). The crystal structure of indium phosphide is face-centered cubic (FCC). It exists in two crystal forms (WZ), (ZB) as in Figure (1), and its crystal lattice constant is (a= 5.8687A^o).Its molar mass is (145.792 g/mol) and its density is (4.81g/cm^3).

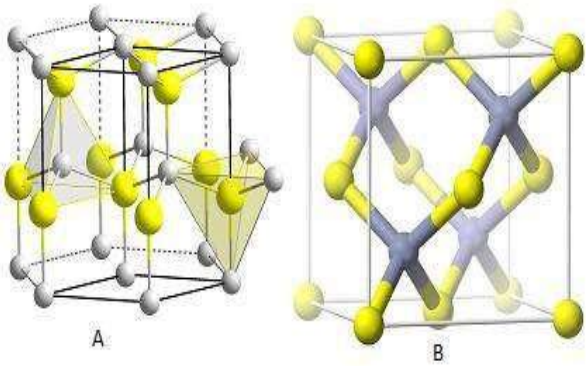

Figure 1. Shows the crystal structure of (InP),(A) Wurtzite and (B) zincblende (Almeida, Ubbink, et al., 2023)

Applications of indium phosphide include solar cells (Lasheer, Fathy, et al., 2023), photodiodes, photosensitive sensors, light-emitting diodes (LEDs) (Sticklus, Hoeher, et al., 2020), transistors (FETS) (Malik & Kharadi, 2020), wireless communications, medical and biological applications (Almeida, Ubbink, et al., 2023) (Bhagya & Kim, 2021) .InP nanowires can be fabricated using several techniques including multiphase (vapor-solid-liquid) method (Jafari Jam, Persson, et al., 2020) , organic complex method (Zhang, Xu, et al., 2017) solution-phase (liquid-solid) method, hot solution method (Wang, Dong, et al., 2016) .laser-assisted growth method (Ahmed, Qi, et al., 2023) , and electrochemical deposition method (Zhang, Feng, et al., 2020). This is the method used in this research. The electrochemical method is a simple and inexpensive method compared to other preparation methods. Many parameters (concentration, temperature, deposition time) can be changed, which ultimately affect the properties of the prepared compound.

2. THEORETICAL CONSIDERATIONS

Based on Bragg's law for X-ray diffraction in relation (1), we can determine the distance between the crystal planes (d_{hkl}). $2d_{hkl}\ Sin(\Theta_{hkl}) = n\lambda$ ……(1)

Where θ= diffraction angle, n= integer called diffraction order, λ= wavelength of X-rays (λ=1.5405A˚). The crystal lattice constant was calculated using the relation (2) which gives the crystal distance of the parallel planes in terms of the crystal lattice constants of the face-centered cubic structure: (Bandoh, Nkrumah, et al., 2021) (Bandoh, Nkrumah, et al., 2021)

$a = d\sqrt{h^2 + k^2 + l^2}$ ……(2),

where a (crystal lattice constant). From the Scherrer equation, the crystallite size (D) was calculated

$$D = \frac{k\lambda}{\beta cos\theta} \text{ ……(3),}$$

where k= constant (0.9), β =Full Width at Half Maximum (FWHM) of the diffraction peak, θ= diffraction angle, λ= wavelength of X-rays (Ravi & Chitra, 2020). The crystal lattice strain (ε) and the dislocation density (δ) in the crystal lattice were calculated using the two relationships. (Filipovic, Obradovic, et al., 2018),

$$\varepsilon = \frac{\beta Cos\theta}{4} \text{ …….(4) ,}$$

$$\delta = \frac{n}{D^2} \text{ ……..(5), where (n=1).}$$

The type of semiconductor can be determined from the Schottky relationship. (Ashajyothi & Reddy, 2021) , $\left(\frac{1}{C} - \frac{1}{2C_0}\right)^2 = \frac{2}{e\,\epsilon_o \cdot \epsilon_r\,(N_d - N_a)}(\psi + V)$ ……(6), where (e) electron or elementary charge, (ε_r) relative permittivity, (ε_o) permittivity of free space, (N_d) density of donor atoms, (N_a) density of acceptor atoms , (Ψ) barrier height of the system. (C_o), (C) are the capacitance per unit area of a grain boundary biased and (V) volts. We find from the relationship (6) that when the density of the acceptor atoms is greater than the density of the donor atoms, (N_a>> N_d). the density of donor atoms can be neglected, and therefore when plotting the changes in ($1/C^2$) in terms of the applied voltage (V) on the prepared samples, we obtain a graph with a negative slope. This means that the semiconductor is of the p-type, and if (N_d>> N_a) then when plotting the changes in ($1/C^2$) in terms of (V), we get a

graph with a positive slope, so the semiconductor is of the N-type

The activation energy (Ea) was calculated based on the following relationship:

$I = I_o e^{-Ea/kT}$……(7) (Filipovic, Obradovic, et al., 2018) (Schubert, 2022) where I= current intensity at temperature (T), I_o = current intensity at absolute zero, k= Boltzmann constant. Taking the (lnI) of relation (7) we get

$\ln I = \ln I_o - Ea/kT$ ……..(8).

The Seebeck coefficient (S) (which is the basis for choosing the material in power generation devices) was found for the samples prepared using the electrical circuit shown in figure (2) within the range of temperature changes of (310-430) k^o through the following equation.

$S = \frac{\Delta V}{\Delta T}$ ……..(9) (Van & Mitterhuber, 2023) .

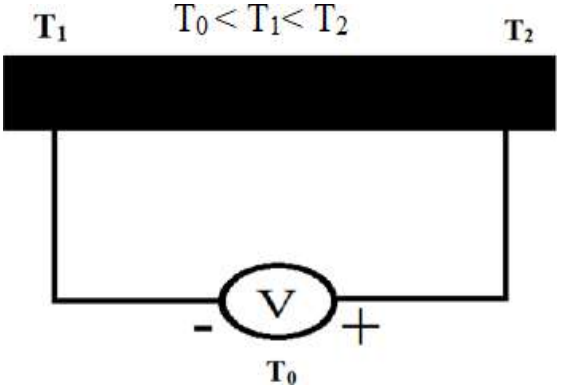

Figure 2. Electrical circuit (Seebeck coefficient)

3. EXPERIMENTAL PART

A high purity nickel substrate was taken and its surface was smoothed with sandpaper of different sizes to obtain a mirror-smooth surface. The substrate was cleaned with a solution of (CH_3COOH) and (CH_3COCH_3) using an ultrasonic device to enhance the surface quality of the substrate, after which the surface was oxidized under a constant voltage of (40)V at (0.3)mol/L of oxyacetylene as an electrolyte for 30min. The substrate was used as anode and the temperature was maintained at 25°C during oxidation. After that, the oxide layer was etched with 0.5% of HCL at a temperature of 65°C for 20minutes. Thus, a large number of surface pores were obtained in the Ni substrate, which is suitable for Indium phosphide (InP) deposition. After that, the oxide layer was removed from the back part of the slide and attached with an insulating tape to prevent the deposition of (InP) on the back part, but the deposition was only on the front part that contains the surface pores.

Indium chloride ($InCl_3$) solution was prepared by dissolving (0.482)gm in indium oxide (In_2O_3) in 50 ml of distilled water and placing it on a magnet, then add a few drops of (HCl) until complete dissolutionm, after that a solution of indium chloride ($InCl_3$) and phosphorus acid (H_3PO_4) was prepared.

The surface-porous nickel substrate were washed with ethanol and then washed with distilled water. A nickel substrate was used as a cathode and a platinum electrode was used as an anode. They were placed in the prepared electrolyte solution where the distance between the two electrodes was (3cm) under a voltage (5)V. The deposition process continued for two hours for the first substrate, denoted as (2h), three hours of deposition for the second substrate denoted as (3h), and four hours of deposition for the third substrate denoted as (4h). The samples were washed several times with distilled water and placed under a temperature of 200 ^{o}C for two hours. Thus three samples of InP were obtained

4. RESULTS AND DISCUSSION

Figure (3) shows the X-ray diffraction of the prepared (InP) samples. The crystal planes formed follow the cubic structure and they are face centered cubic (FCC), with the appearance of three peaks for nickel and one peak for (InP) in the direction (220). This indicates that InP crystallizes in one direction when

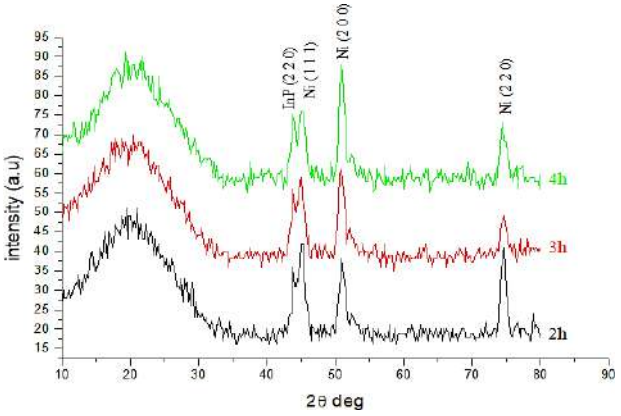

Figure 3. X-ray diffraction of prepared InP samples.

growing on a nickel substrate with surface pores. It is also clear that the intensity of the diffraction peak increases with increasing deposition time. This means that the

growth of the samples increases with deposition time. Based on Bragg's law for X-ray diffraction in relation (1), we can determine the distance between the crystal planes (d_{hkl}). The crystal lattice constant was calculated using the relation (2) which gives the crystal distance of the parallel planes in terms of the crystal lattice constants of the face-centered cubic structure. From the Scherrer equation, the crystallite size (D) was calculated using the relation (3). The crystal lattice strain (ε) and the dislocation density (δ) in the crystal lattice were calculated using the two relationships. (4), (5). The table (2) reveals the values of the distance between crystal planes, crystal lattice constanat, crystallite size, crystal lattice strain and dislocation density for InP wires prepared on nickel substrates with surface pores in the (220) direction where there is an increase in the values of (ε) and (δ) and a decrease in the values of (D).This indicates the presence of crystal distortion

Table 2. Shows the results of X-ray diffraction of the prepared InP wires.

	2θ	d(A^0)	a(A^0)	β (rad)	D (nm)	$\varepsilon \times 10^{-4}$ (lines^{-2}.m^{-4})	$\delta \times 10^{14}$ (lines/m^2)
2h	43.8	2.065	5.83	0.0034	45.90	7.88	4.74
3h	43.8	2.065	5.83	0.0061	25.58	14.14	15.28
4h	43.8	2.065	5.83	0.0087	17.93	20.18	31.10

To determine the type of semiconductor, the capacitance was measured with a device (LCR- meter) with a variable voltage (0.1-2)V at a fixed frequency (1KHZ) at room temperature. From the relationship between ($1/C^2$) and (V) for the prepared samples, the graphs shown in figure (4) showed linear relationships with negative slopes. This indicates that the semiconductor formed is of the p-type. Even at voltage (0.5)V the slope is negative and at values greater than (0.5)V the slope is also negative. Thus, the total slope is negative. As shown in the figure (4) there is a large decrease in capacitance at (0.22)V and a small decrease in capacitance that is almost constant when the voltage increases to (2)V.

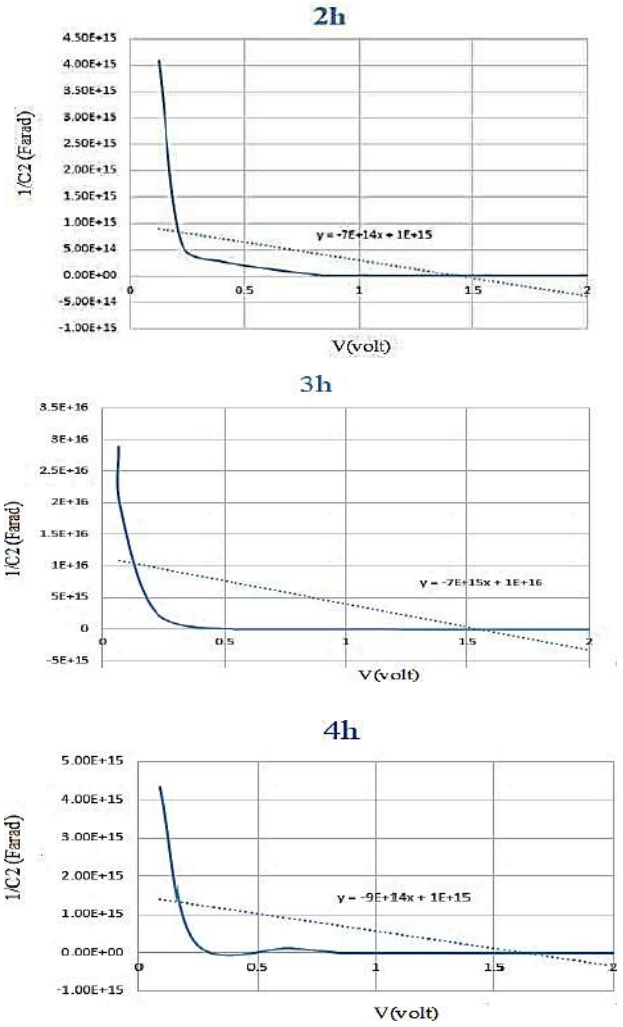

Figure 4. Variations of ($1/C^2$) with respect to (V) for prepared samples

Figure (4), we find the built-in potential (V_{bi}) of the samples prepared from the point of intersection of the slope line with the V-axis, we notice that increases the deposition time of the prepared samples increases the values of (V_{bi}) as shown in table (3)

Table 3. V_{bi} values for prepared samples.

Deposition time	2h	3h	4h
V_{bi} (eV)	1.42	1.54	1.66

To identify the electrical properties of the prepared samples of (InP), the (I-V) characteristics were studied at different temperatures (303, 313, 323) k^o As shown in figure (5), the relationship between current and voltage is a linear relationship, and the current intensity increases with increasing temperature, which in turn increases the

movement of charge carriers, leading to an increase in electrical conductivity.

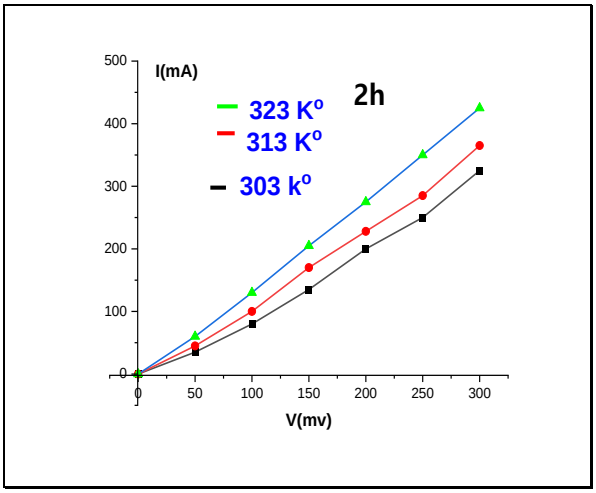

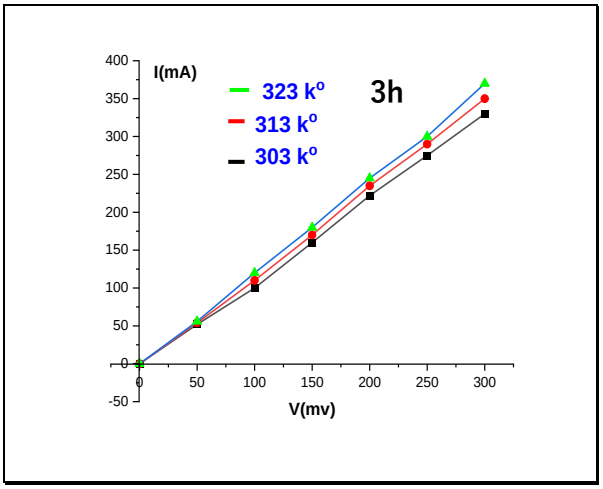

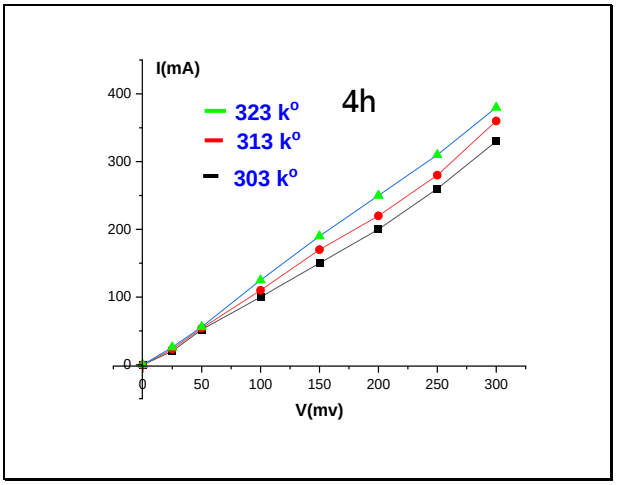

Figure 5. (I-V) For samples prepared InP at different temperatures.

By studying changes in electrical resistance with temperature changes of (303, 313, 323) k° for the samples prepared at (300)mV, and as they are shown in figure (6)

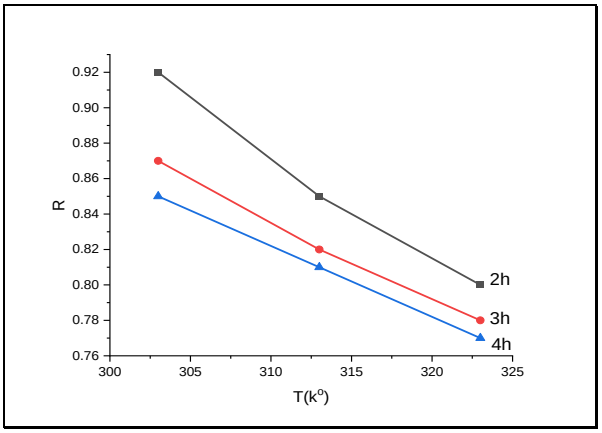

Figure 6. Shows the decrease in electrical resistance (R) of InP with increasing temperatures.

The data exhibits an approximately linear relationship. This is due to the increase in the movement and density of charge carriers thermally, which indicates that the behavior of InP is a natural behavior for semiconductors, as the electrical resistance of the prepared samples decreases with increasing temperatures according to table (4).

Table 4. Showing the decrease in electrical resistance of InP samples with increasing temperatures

	2h	**3h**	**4h**
T(k⁰)	**R(Ω)**	**R(Ω)**	**R (Ω)**
303	0.92	0.87	0.85
313	0.85	0.82	0.80
323	0.80	0.78	0.77

The relationship between (lnI) and (1/T) is shown in the figure (7).

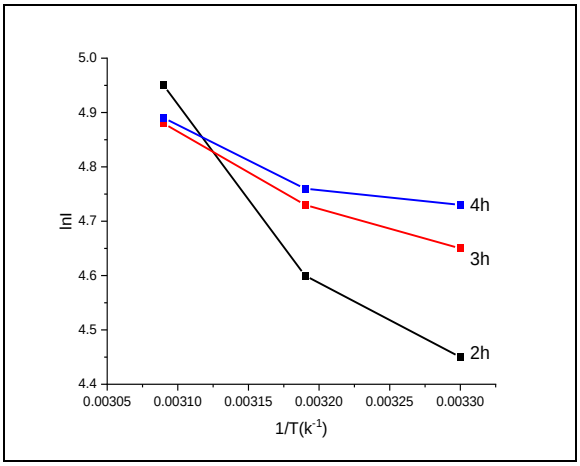

Figure 7. Shows the changes in (lnI) as a function of (1/T) for InP.

From the slope of the straight line in the curves resulting from figure (7) and by applying the relationships (7),(8) the (E_a) values for InP were calculated at temperatures of (303, 313, 323) k^o as shown in table (5).

Table 5. Shows the (E_a) values of InP.

Depositin time	E_a(eV)
2h	0.14
3h	0.07
4h	0.06

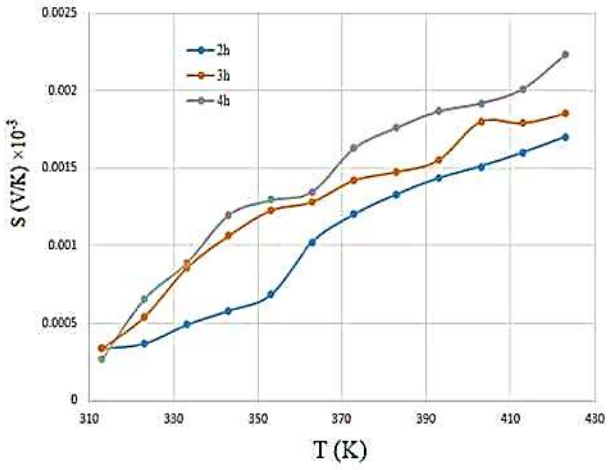

Figure 8. Shows the changes in (S) as afunction of temperature changes for InP.

Using relation (9) the Seebeck coefficient (S) was found. Figure (8) shows that (S) has a positive value. This confirms that the formed semiconductor is of the p-type. The best value of (S) for the sample is InP at a deposition time of (4h).

5. CONCLUSION

The results of X-ray diffraction of InP showed that it crystallizes in one direction (220), and increase in the intensity of the diffraction peak with increasing deposition time for the prepared samples. It was found from the calculation of (C-V) that the slope is negative value. This indicates that the prepared samples are of the p-type. (V_{bi}) which was determined to be (1.42, 1.54, 1.66) eV. This increases the deposition time of the prepared samples and increases the values of (V_{bi}). (I-V) was calculated for the samples prepared for InP at different temp (303,313,323) k^o .The relationship between I and V showed that the current intensity increases with increasing temp, and electrical resistance (R) of the samples decreases with increasing different temp. (Ea) values of the samples ranged (0.14,0.07,0.06) eV at different temp. Seebeck coefficient (S) is positive for prepared samples. This confirms that the formed semiconductor is of the p-type. The best value of (S) for the sample is InP at a deposition time of (4h).

REFERENCES

Ahmed, N. M., Qi, L. X., et al. (2023). Investigating the Role of Temperature in Laser Assisted Chemical Bath Deposition for ZnO Growth for Photodetector Application. *Photonics*, *10*(8), 910. https://doi.org/10.3390/photonics10080910

Almeida, G., Ubbink, R. F., et al. (2023). InP colloidal quantum dots for visible and near-infrared photonics. *Nature Reviews Materials*, *8*, 742–758. https://doi.org/10.1038/s41578-023-00596-4

Ashajyothi, S., & Reddy, V. R. (2021). Influence of tin oxide (SnO2) interlayer on the electrical and reverse current conduction mechanism of Au/n−InP Schottky junction and its microstructural properties. *Thin Solid Films*, *740*, 139001. https://doi.org/10.1016/j.tsf.2021.139001

Bandoh, C. K., Nkrumah, I., et al. (2021). Effect of annealing on the structure and optical properties of lead selenide and cadmium selenide thin film

prepared by chemical bath deposition. *Chalcogenide Letters*, *18*(2), 81–89.

Bhagya, H., & Kim, E. B. (2021). Safe synthesis of InP quantum dots for Biological applications. *The Electrochemical Society*, *MA01*(23). https://doi.org/10.1149/MA2021-0123915mtgabs

Cipriano, L. A., Di Liberto, G., et al. (2020). Quantum confinement in group III-V semiconductor 2D nanostructures. *Nanoscale*, *12*, 17494–17501. https://doi.org/10.1039/D0NR03577G

Faroz A. Malik, G., & Kharadi, M. A. (2020). Performance analysis of indium phosphide channel based sub-10 nm double gate spin field effect transistor. *Physics Letters A*, *384*(19), 126498. https://doi.org/10.1016/j.physleta.2020.126498

Filipovic, S., Obradovic, N. N., et al. (2018). Physical properties of sintered alumina doped with different oxides. *Science of Sintering*, *50*(4), 409–419. https://doi.org/10.2298/SOS1804409F

Jafari Jam, R., Persson, A. R., et al. (2020). Template-assisted vapour–liquid–solid growth of InP nanowires on (001) InP and Si substrates. *Nanoscale*, *12*, 888–894. https://doi.org/10.1039/C9NR08025B

Lasheer, D., Fathy, M., et al. (2023). Synthesis and characterization of InP quantum dots for photovoltaics applications. *Journal of Materials Science*, *34*. https://doi.org/10.1007/s10854-023-10179-2

Li, G.-R., & Lu, X.-H. (2008). Electrochemical reduction synthesis of In–Sb nanoropes and terraced micropyramids. *Electrochemistry Communications*, *10*(1), 127–130. https://doi.org/10.1016/j.elecom.2007.11.007

Li, Z., He, Z., et al. (2023). Review on III–V Semiconductor Nanowire Array Infrared Photodetectors. *Advanced Materials Technologies*, *8*(13), 2202126. https://doi.org/10.1002/admt.202202126

Ravi, K., & Vchitra. (2020). Structural and Surface morphology of Lead Selenide (PbSe) thin films. *Materials Science and Engineering*, *932*, 012133. https://doi.org/10.1088/1757-899X/932/1/012133

Schubert, F. E. (2022). *Physical Foundations of Solid-State Devices* (e-book).

Sticklus, J., Hoeher, P. A., et al. (2020). Experimental Characterization of Single-Color Power LEDs Used as Photodetectors. *Sensors*, *20*(18), 5200. https://doi.org/10.3390/s20185200

T. B. Al Hammade, H. (2022). Theoretical study of the conduction band and energy gap of *GaInNAs/InP* quantum well structure. *Nanosystems, Nanomaterials, Nanotechnologies*, *20*(1), 15–23. https://doi.org/10.15407/nnn.20.01.015

Van, H. J., Mitterhuber, L., et al. (2023). Nanostructured Thermoelectric Films Synthesised by Spark Ablation and Their Oxidation Behaviour. *Nanofabrication and Nanomanufacturing*, *13*(11), 1778. https://doi.org/10.3390/nano13111778

Wang, F., Dong, A., et al. (2016). Solution–Liquid–Solid Synthesis, Properties, and Applications of One-Dimensional Colloidal Semiconductor Nanorods and Nanowires. *Chemical Reviews*, *116*(18), 10888–10933. https://doi.org/10.1021/acs.chemrev.5b00701

Yue, L.-Q., Shi, Y.-L., et al. (2023). InP Low-Dimensional Nanomaterials for Electronic and Optoelectronic Device Application. *Advanced Sensor Research*, *2*(10), 2200101. https://doi.org/10.1002/adsr.202200101

Zhang, J., Xu, W., et al. (2017). Organic Donor–Acceptor Complexes as novel organic semiconductors. *American Chemical Society*, *50*(7), 1654–1662. https://doi.org/10.1021/acs.accounts.7b00124

Zhang, Z., Fengm, C., et al. (2020). Electrochemical deposition as a universal route for fabricating single-atom catalysts. *Nature Communications*, *11*(1), 1215. https://doi.org/10.1038/s41467-020-14917-6

PURE SCIENCES
International Journal of Kerbala

Pure Sciences International Journal of Kerbala

Year: 2025 Volume : 2 Issue : 7 ISSN: 6188-2789 Print 3005 -2394 Online

2025,Volume 2 , Issue 7 , PSIJK (53-57)

Pure Sciences International Journal of Kerbala

R-Al Tememe Transformation for Solving Ordinary Differential Equations with Constant Coeffecients

Ruaa Hussain Ali [a] , Ali Hassan Mohammed [a*]

[a] *Department of Mathematics, College of Education for Women, University of Kufa, Najaf, IRAQ*

P A P E R I N F O

Received: 11.05.2025
Accepted: 30.06.2025
Published: 30.09.2025

Keywords:
Applied Mathematics, Constant Coefficients, Analytical Solutions, Al-Zughair Method, R. Al-Tememe Transform.

A B S T R A C T

Solving (LODEs) with constant coefficients is a core engineering and applied mathematics task. For a long time, several differential transform and integral methods have been developed to facilitate these equations and to get accurate analytical solutions, such as Laplace [1–5], Al-Zughair [6], and other research. In this research, we explore the new application of the R. Al-Tememe transform to examine the capability in solving (LODEs) with constant coefficients.

DOI: 10.53851/psijk.v2.i7. 53-57

Table 1. Nomenclature and Definitions Used in the Study

RA	R.Al–Tememe Transform
$(RA)^{-1}$	The inverse of R.Al–Tememe transform
eq.	equation
LODEs	Linear Ordinary Differential Equations
ODEs	Ordinary Differential Equations

1. INTRODUCTION

In many scientific and technical fields, differential equations both ordinary (ODEs) and partial (PDEs) are crucial instruments for simulating dynamic processes. Their answers are essential to comprehending mechanical, biological, and physical phenomena. However, it is frequently difficult to find analytical solutions to these equations, particularly for complex or nonlinear systems. This has spurred the creation and use of a number of integral transforms that reduce the complexity of solving differential equations by transforming them into algebraic forms. This has traditionally been accomplished using classical transforms like the Laplace and Fourier transforms. Analytical or semi-analytical solutions for linear and nonlinear differential equations with both constant and variable coefficients have been successfully obtained using these methods.

To solve linear ordinary differential equations with constant coefficients, a number of genuine integral transforms have been proposed recently: Kumar and Prasad's (2025) New Integral Transform is specifically used for ODEs with constant coefficients. Effective for ODEs and PDEs, the Shehu Transform generalizes both the Laplace and Sumudu transforms (Maitama & Zhao, 2019). (April 2025) examined dual Shehu Transform variations, connecting Shehu to other traditional transforms for fractional ODEs (Mlaiki et al., 2025). Higher-order linear ODEs with constant coefficients are the focus of the two-parameter MAHA Transform (2024) (AlSaoudi et al., 2024). For first- and second-order linear ODEs with constant coefficients, the Kamal Transform (2024) was examined in relation to Hyers-Ulam stability (Anderson, 2024). These reliable sources highlight new developments in analytical tools for solving ODEs with constant coefficients and highlight the growing interest in specialized integral transforms.

The purpose of this study is to present and investigate the characteristics of a new integral transform called the R. Al-Tememe Transform. Its formulation, inverse, and application to the solution of linear ordinary differential equations with constant coefficients will all be covered. Our objective is to show how this cutting-edge tool might function as a useful substitute for conventional transforms, possibly providing improved accuracy and application simplicity.

which has a kernel $\left(\frac{(\ln(ln\mathcal{M}))^{\hat{r}-1}}{\mathcal{M}(ln\mathcal{M})}\right)$, and the general form of it:

$$RA(\dot{S}(\ln(ln\mathcal{M}))) = \int_e^{e^e} \frac{(\ln(ln\mathcal{M}))^{\hat{r}-1}}{\mathcal{M}(ln\mathcal{M})}\, \dot{S}(\ln(ln\mathcal{M}))d\mathcal{M}$$

*Corresponding Author Institutional Email:
prof.ali57hussan@gmail.com (Ali Hassan Mohammed)

Where $\mathcal{M} \in [e, e^e]$, $\hat{r} > 0, \hat{r} \neq 1$

2. R. A. TRANSFORM FOR THE FUNDAMENTAL FUNCTIONS

Table 2. This table represents the relation of R.Al–Tememe with some functions

Function	$R.A(f(\ln(lns))) = \int_e^{e^e} \frac{(\ln(lns))^{p-1}}{s(lns)} f(\ln(lns))ds = F(p)$	Region of Convergence
1	$\frac{1}{p}$	$p > 0$
ɱ, ɱ a is constant	$\frac{ɱ}{p}$	$p > 0$
$(\ln(lns))^n$ $n = 1,2,3, \ldots.$	$\frac{1}{p+n}$	$p > -n$
$(\ln(\ln(lns)))^n$ $n = 1,2,3 \ldots.$	$\frac{(-1)^n\, n!}{p^{n+1}}$	$p > 0$
$\cos(a(ln(\ln(\ln(lns)))))$ a is a constant	$\frac{p}{p^2+a^2}$	$p > -a$
$\sin(a(\ln(\ln(lns))))$ a is a constant	$\frac{-a}{p^2+a^2}$	$p > -a$
$\cosh(a(\ln(\ln(lns))))$ a is a constant	$\frac{p}{p^2-a^2}$	$\lvert p - a\rvert > 0$
$\sinh(a(\ln(\ln(lns))))$ a is a constant	$\frac{-a}{p^2-a^2}$	$\lvert p - a\rvert > 0$

R.Al–Tememe transform for deriving

Theorem:

Let us consider that $y = y(\ln(\ln(lns)))$ so, we define the R.Al–Tememe Transform $(RA)$for y as the following:

$$RA(y(\ln(\ln(lns))) = \int_e^{e^e} \frac{(\ln(lns))^{p-1}}{s(lns)}\, y(\ln(\ln(lns)))ds,$$

This integration will be defective and $p > 0, p \neq 1$ and we consider $y(-\infty) = y'(-\infty) = \cdots y^n(-\infty) = 0$ then:

1. $\boldsymbol{RA[y'(\ln(\ln(lns)))] = y(0) - py(\ln(\ln(lns)))}$

Proof:

$RA[y'(\ln(\ln(lns)))] =$

$\int_e^{e^e} \frac{(\ln(lns))^{p-1}}{s(lns)}\, y'(\ln(\ln(lns)))\, ds$

By part integration to solve the above integration

Let

$u = (\ln(lns))^p \rightarrow du = p\left(\frac{(\ln(lns))^{p-1}}{s(lns)}\right) ds$

$dv = \frac{y'(\ln(\ln(lns)))}{s(lns)(\ln(lns)}\, ds \rightarrow v = y(\ln(\ln(lns)))$

$RA[y'(\ln(\ln(lns)))] = (\ln(lns))^p y(\ln(\ln(lns)))|_e^{e^e} - p\int_e^{e^e} \frac{(\ln(lns))^{p-1}}{s(lns)}\, y(\ln(\ln(lns)))ds$

$= y(0) - py(\ln(\ln(lns)))$

2. $\boldsymbol{RA[y''(\ln(\ln(lns)))] = y'(0) - py(0) + p^2 RA[y(\ln(\ln(lns)))]}$

Proof:

$RA[y''(\ln(\ln(lns)))] =$

$\int_e^{e^e} \frac{(\ln(lns))^{p-1}}{s(lns)}\, y''(\ln(\ln(lns)))\, ds$

By part integration to solve the above integral

$u = (\ln(lns))^p \rightarrow du = p\left(\frac{(\ln(lns))^{p-1}}{s(lns)}\right) ds$

$dv = y''(\ln(\ln(lns)))ds \rightarrow v = y'(\ln(\ln(lns)))$

$RA[y''(\ln(\ln(lns)))] = (\ln(lns))^p y'(\ln(\ln(lns)))|_e^{e^e} - p\int_e^{e^e} \frac{(\ln(lns))^{p-1}}{s(lns)}\, y'(\ln(\ln(lns)))ds$

$= y'(0) - p\int_e^{e^e} \frac{(\ln(lns))^{p-1}}{s(lns)}\, y'(\ln(\ln(lns)))ds$

Let

$u = (\ln(lns))^p \rightarrow du = p\frac{(\ln(lns))^{p-1}}{s(lns)}\, ds$

$dv = \frac{y'(\ln(\ln(lns)))}{s(lns)(\ln(lns))} \rightarrow v = y(\ln(\ln(lns)))$

$= y'(0) - p\left[(\ln(lns))^p y(\ln(\ln(lns)))\,\right|_e^{e^e} - p\int_e^{e^e} \frac{(\ln(lns))^{p-1}}{s(lns)}\, y(\ln(\ln(lns)))\Big]$

$RA[y''(\ln(\ln(lns)))] = y'(0) - p\big[y(0) - pRA[y(\ln(\ln(lns)))]\big]$

$= y'(0) - py(0) + p^2 RA[y(\ln(\ln(lns)))]$

3. $\boldsymbol{RA[y'''(\ln(\ln(lns)))] = y''(0) - py'(0) + p^2 y(0) - p^3 RA[y(\ln(\ln(lns)))]}$

Proof:

$RA[y'''(\ln(\ln(lns)))] =$

$\int_e^{e^e} \frac{(\ln(lns))^{p-1}}{s(lns)}\, y'''(\ln(\ln(lns)))ds$

By using partial integration to solve the above integration

$u = (\ln(lns))^p \rightarrow du = p(\frac{(\ln(lns))^{p-1}}{s(lns)})ds$

$dv = \frac{y'''(\ln(\ln(lns)))}{s(lns)(\ln(lns))} ds \rightarrow v = y''(\ln(\ln(lns)))$

Then

$RA[y'''(\ln(\ln(lns)))] =$
$(\ln(lns))^p y''(\ln(\ln(lns)))|_e^{e^e} -$
$\int_e^{e^e} \frac{(\ln(lns))^{p-1}}{s(lns)}\, y''(\ln(\ln(lns)))ds$
$= y''(0) - p\int_e^{e^e} \frac{(\ln(lns))^{p-1}}{s(lns)} y''(\ln(\ln(lns)))ds$
By part integration to solve the above integral $dv = \frac{y''(\ln(\ln(lns)))}{s(lnd)(\ln(lns))}ds \rightarrow \quad v = y'(\ln(\ln(lns)))$

$$u = (\ln(lns))^p \rightarrow du = p\frac{(\ln(lns))^{p-1}}{s(lns)}\, ds$$
$$= y''(0) - p[(\ln(lns))^p y'(\ln(\ln(lns)))\,|_e^{e^e} -$$
$$p\int_e^{e^e} \frac{(\ln(lns))^{p-1}}{s(lns)} y'(\ln(\ln(lns)))\, ds$$
$$u = (\ln(lns))^p \rightarrow du = p\frac{(\ln(lns))^{p-1}}{s(lns)}\, ds$$
$$dv = \frac{y'(\ln(\ln(lns)))}{s(lns)(\ln(lns))}\, ds \rightarrow$$
$$v = y\,(\ln(\ln(lns)))$$
$$= y'(0) - p\left[(\ln(lns))^p y(\ln(\ln(lns)))\,|_e^{e^e} - p\int_e^{e^e} \frac{(\ln(lns))^{p-1}}{s(lns)}\, y(\ln(\ln(lns)))\right]$$
$= y''(0) - p[y'(0) - py(0) + p^2 RA[y(\ln(\ln(lns)))]]$
$RAy'''(\ln(\ln(lns))) = y''(0) - py'(0) + p^2 y(0) - p^3 RA[y(\ln(\ln(lns)))]$

4. $\boldsymbol{RA[y^{iv}(\ln(\ln(lns)))] = y'''(0) - py''(0) + p^2 y'(0) - p^3 y(0) + p^4 RA[y(\ln(\ln(lns)))]}$
$=$
$\int_e^{e^e} \frac{(\ln(lns))^{p-1}}{s(lns)}\, y^{iv}(\ln(\ln(lns)))\, ds$
Using the partial integration to solve above integration we get
$u = (\ln(lns))^p \rightarrow du = p\left(\frac{(\ln(lns))^{p-1}}{s(lns)}\right) ds$
$dv = \frac{y^{iv}(\ln(\ln(lns)))}{s(lns)(\ln(lns))}\, ds \rightarrow v = y'''(\ln(\ln(lns)))$
$=$
$(\ln(lns))^p y'''(\ln(\ln(lns)))|_e^{e^e} - p\int_e^{e^e} \frac{(\ln(lns))^{p-1}}{s(lns)}\, y'''(\ln(\ln(lns)))ds$
$= y'''(0) - p\int_e^{e^e} \frac{(\ln(lns))^{p-1}}{s(lns)} y'''(\ln(\ln(lns)))\, ds$
$= y'''(0) - p[y''(0) - p\int_e^{e^e} \frac{(\ln(lns))^{p-1}}{s(lns)}\, y''(\ln(\ln(lns)))]ds$
$= y'''(0) - py''(0) - p^2\left[y'(0) - p\int_e^{e^e} \frac{(\ln(lns))^{p-1}}{s(lns)} y'(\ln(\ln(lns)))ds\right]$
$= y'''(0) - py''(0) + p^2 y' - p^3\left[y(0) - p\int_e^{e^e} \frac{(\ln(lns))^{p-1}}{s(lns)}\, y(\ln(\ln(lns)))ds\right]$

$RA[y^{iv}(\ln(\ln(lns)))] = y'''(0) - py''(0) + p^2 y'(0) - p^3 y(0) + p^4 RA[y(\ln(\ln(lns)))]$
In general
$RA[y^n(\ln(\ln(lns)))]$
$= y^{n-1}(0) - py^{n-2} + \ldots\ldots$
$\mp p^{n-1} y(0) \pm p^n RA[y(\ln(\ln(lns)))]$

Example: To solve the differential eq.
$y'(\ln(\ln(lns))) - 3y(\ln(\ln(lns))) = \sin(\ln(\ln(lns)))$, with condition $y(0) = 1$ … (1)
Take RA transform for eq. (1) we get
$y(0) - pRA[y(\ln(\ln(lns))] - 3RA[y(\ln(\ln(lns)))] = \frac{-1}{p^2+1}$
$-(p+3)RA[y(\ln(\ln(lns)))] = \frac{-2-p^2}{p^2+1}$
$RA[y(\ln(\ln(lns)))] = \frac{2+p^2}{(p+3)(p^2+1)}$
… (2)
To find $y(\ln(\ln(lns)))$ take the inverse to RA transform to eq. (2) we get
$y(\ln(\ln(lns))) = (RA)^{-1}\left(\frac{p^2+2}{(p+3)(p^2+1)}\right)$
$\frac{p^2+2}{(p+3)(p^2+1)} = \frac{A}{p+3} + \frac{Bp+C}{p^2+1}$
$= \frac{Ap^2+A+Bp^2+3Bp+Cp+3C}{(p+3)(p^2+1)}$
$A + B = 1, 3B + C = 0, A + 3C = 2$

$A = \frac{11}{10}, B = \frac{-1}{10}, C = \frac{3}{10}$

$y = (RA)^{-1}\left[\frac{\frac{11}{10}}{(p+3)} + \frac{\frac{-1}{10}p + \frac{3}{10}}{p^2+1}\right]$

$y = \frac{11}{10}(\ln(lns))^3 - \frac{1}{10}\cos(\ln(\ln(lns))) - \frac{3}{10}\sin(\ln(\ln(lns)))$

Example: To solve the differential eq.

$y'(\ln(\ln(lns))) + 2y(\ln(\ln(lns))) = \sinh(ln(ln(lns)))$ with condition $y(0) = 0$ … (3)

Using RA transform for eq. (3) we get

$y(0) - pRA[y(\ln(\ln(lns)))] + 2RA[y(\ln(\ln(lns)))] = \frac{-1}{p^2-1}$

$-(p-2)RA[(\ln(\ln(lns)))] = \frac{-1}{p^2-1}$

$RA[y(\ln(\ln(lns)))] = \frac{1}{(p-2)(p^2-1)}$
… (4)

To find $y(\ln(\ln(lns)))$ take $(RA)^{-1}$ for the eq. (4) we get

$y(\ln(\ln(lns))) = (RA)^{-1}\left(\frac{1}{(p-2)(p^2-1)}\right)$

$\frac{1}{(p-2)(p^2-1)} = \frac{Ap+B}{p^2-1} + \frac{C}{p-2}$

$= \frac{Ap^2-2Ap+Bp-2B+Cp^2-C}{(p-2)(p^2-1)}$

$A + C = 0$,$-2A + B = 0$, $-2B - C = 1$

$A = -\frac{1}{3}, B = -\frac{2}{3}, C = \frac{1}{3}$

$y(\ln(\ln(lns))) = (RA)^{-1}\left[\frac{-\frac{1}{3}p-\frac{2}{3}}{p^2-1} + \frac{\frac{1}{3}}{p-2}\right]$

$= -\frac{1}{3}\cosh(\ln(\ln(lns))) + \frac{2}{3}\sinh(\ln(\ln(lns))) + \frac{1}{3}(\ln(lns))^{-2}$

Example: To solve the differential eq.

$y''(\ln(\ln(lns))) + y(\ln(\ln(lns))) = (\ln(\ln(lns)))$
with conditions $y(0) = 1, y'(0) = 0$ … (5)

Take RA transform for eq. (5) we get

$y'(0) - py(0) + p^2RA[y(\ln(\ln(lns)))] + RA[Y(\ln(\ln(lns)))] = -\frac{1}{p^2}$

$-p + (p^2+1)RA[y(\ln(\ln(lns)))] = -\frac{1}{p^2}$

$(p^2+1)RA[y(\ln(\ln(lns)))] = \frac{p^3-1}{p^2}$

$RA[y(\ln(\ln(lns)))] = \frac{p^3-1}{p^2(p^2+1)}$
… (6)

To find $y(\ln(\ln(lns)))$ take inverse of RA transform for eq. (6)

$y(\ln(\ln(lns))) = (RA)^{-1}\left[\frac{p^3-1}{p^2(p^2+1)}\right]$

$\frac{p^3-1}{p^2(p^2+1)} = \frac{Ap+B}{p^2} + \frac{Cp+D}{p^2+1}$

$= \frac{Ap^3+Ap+Bp^2+B+Cp^3+Dp^2}{p^2(p^2+1)}$

$A + C = 1, B + D = 0$

$A = 0, B = -1, D = 1, C = 1$, then

$y(\ln(\ln(lns))) = (RA)^{-1}\left[-\frac{1}{p^2} + \frac{p+1}{p^2+1}\right]$

$= (\ln(\ln(lns))) + \cos(\ln(\ln(lns))) - \sin(\ln(\ln(lns)))$

Example: To solve the differential eq.

$y''(\ln(\ln(lns))) = (\ln(\ln(lns)))^3 + 3$, with conditions $y(0) = 0, y'(0) = 1$ … (7)

Take RA Transform for the eq. (7) we get

$y'(0) - py(0) + p^2RA[y(\ln(\ln(lns)))] = -\frac{6}{p^4} + \frac{3}{p}$

$p^2RA[y(\ln(\ln(lns)))] = \frac{-6+3p^3-p^4}{p^4}$

$RA[y(\ln(\ln(lns)))] = \frac{-p^4+3p^3-6}{p^6}$ … (8)

Take the inverse of RA Transform for eq. (8) to get $y(\ln(\ln(lns)))$

$y(\ln(\ln(lns))) = (RA)^{-1}\left(\frac{-p^4+3p^3-6}{p^6}\right)$

$y(\ln(\ln(lns))) = (RA)^{-1}\left(\frac{-1}{p^2} + \frac{3}{p^3} - \frac{6}{p^6}\right)$

$= (\ln(\ln(lns))) - \frac{3}{2}(\ln(\ln(lns)))^2 + \frac{1}{20}(\ln(\ln(lns)))^5$

Example: To solve the differential eq.

$y'''(\ln(\ln(lns))) - y''(\ln(\ln(lns))) = \sinh(2\ln(\ln(lns)))$ … (9)

with condition $y''(0) = y'(0) = y(0) = 0$

Take RA Transform for eq. (9) we get

$y''(0) - py'(0) + p^2y(0) - p^3RA[y(\ln(\ln(lns)))] - y'(0) + py(0) - p^2RA[y(\ln(\ln(lns)))] = \frac{-2}{p^2-4}$

$-p^2(p+1)RA[y(\ln(\ln(lns)))] = \frac{-2}{p^2-4}$

$RA[y(\ln(\ln(lns)))] = \frac{2}{p^2(p^2-4)(p+1)}$
… (10)

To find $y(\ln(\ln(lns)))$ we take the inverse of RA Transform for the eq. (10) we get

$$y(\ln(\ln(lns))) = (RA)^{-1}\left[\frac{2}{p^2(p+1)(p^2-4)}\right]$$

$$\frac{2}{p^2(p+1)(p^2-4)} = \frac{Ap+B}{p^2} + \frac{C}{p+1} + \frac{Dp+E}{p^2-4}$$

$$= \frac{Ap^4+Ap^3-4Ap^2-4Ap+Bp^3+Bp^2-4Bp-4B+Cp^4-4Cp^2+Dp^4+Dp^3+Ep^3+Ep^2}{p^2(p^2-4)(p+1)}$$

$$A + C + D = 0, A + B + D + E = 0, -4A + B - 4C + E = 0, \ -4A - 4B = 0$$

$$B = -\frac{1}{2}, A = \frac{1}{2}, C = -\frac{2}{3}, D = \frac{1}{6}, E = -\frac{1}{6}$$

$$y(\ln(\ln(lns))) = (RA)^{-1}\left[\frac{\frac{1}{2}p-\frac{1}{2}}{p^2} + \frac{-\frac{2}{3}}{p+1} + \frac{\frac{1}{6}p-\frac{1}{6}}{p^2-4}\right]$$

$$= \frac{1}{2} + \frac{1}{2}(\ln(\ln(lns))) - \frac{2}{3}(\ln(lns)) + \frac{1}{6}\cosh(2\ln(\ln(lns))) + \frac{1}{12}\sinh(2\ln(\ln(lns))$$

3. CONCLUSION

In this study, linear ordinary differential equations with constant coefficients are solved using the R. Al–Tememe Transform, which is essential for mathematical modeling in many scientific and engineering domains. Its promise as a potent analytical tool that streamlines the process of solving such equations is demonstrated by the creation and application of this innovative transformation. By defining, inverting, and applying the R. Al–Tememe Transform, we have demonstrated how this technique can be used to simplify differential equation solving, especially when more conventional transforms might not be sufficient or become unwieldy. According to our research, this transformation is a useful supplement to the current collection of mathematical tools utilized in analytical and computational procedures since it provides simplicity, accuracy, and flexibility.

REFERENCES

AlSaoudi, M., et al. (2024). New Two Parameter Integral Transform "MAHA Transform" and Its Applications. *WSEAS Journal of Mathematics*.

Anderson, D. R. (2024). Integral Transforms and the Hyers–Ulam Stability of Linear Differential Equations with Constant Coefficients. *Symmetry*, *16*(2), 135. https://doi.org/10.3390/sym16020135

Fahmi, A. M. (2017). *Al-Zughair Transform*. LAP Lambert Academic Publishing.

Kumar, N. K., & Prasad, K. S. (2025). The New Integral Transform. *The Academia: An Interdisciplinary Research Journal*, *5*(1), 1–20.

Maitama, S., & Zhao, W. (2019). New Integral Transform: Shehu Transform – a generalization of Sumudu and Laplace Transform for Solving Differential Equations. *International Journal of Analysis and Applications*.

Mlaiki, N., et al. (2025, April 29). Duality of Shehu transform with other well-known transforms and application to fractional order differential equations.

PURE SCIENCES
International Journal of Kerbala

Pure Sciences International Journal of Kerbala

Year: 2025 Volume : 2 Issue : 7 ISSN: 6188-2789 Print 3005 -2394 Online

2025,Volume 2 , Issue 7 , PSIJK (58-64)

Pure Sciences International Journal of Kerbala

A Secure Hybrid Symmetric Cryptosystem Combining Huffman Coding, Affine Transformation, and Cartesian Graphs

Ihsan Mezher Rasheed [a*], Kawthar Abdulabbas Hassoon [a]

[a] *Department of Mathematics,, College of Education for Pure Sciences, University of Kerbala , Karbala, Iraq*

P A P E R I N F O

Received: 05.08.2025
Accepted: 16.09.2025
Published: 30.09.2025

***Keywords*:**
Symmetric cryptography, Huffman coding, affine transformation, cartesian product, graphs, encryption, decryption.

A B S T R A C T

We present in this research a new data symmetric cryptography model that combines three techniques: Huffman coding for compression, affine transformation for value obfuscation, and the Cartesian product of graphs to create a complex encrypted graph. The suggested model demonstrates enhanced cryptographic strength and adaptability across various document types. It also provides a high level of security due to to owing to the structural complexity of the generated graph and the multi-layered encryption method.

DOI: 10.53851/psijk.v2.i7. 58-64

Table 1. Nomenclature and Definitions Used in the Study

NOMENCLATURE			
k_i	length of words of plaintext M	Z_{127}	Indices to the ring of integers modulo 127
M	plaintext	P_j	Plaintext block i (matrix form)
A	Invertible transformation matrix (2×2)	x	the padding character
B	Offset matrix (2×2)	V(graph)	represents the vertex set of a graph.
G	Graph used in the Cartesian product	**Subscripts**	
H	A secret keyword-generating Graph that is used in the Cartesian product graph.	i	Indices (words)
C_j	Ciphertext block j	j	Indices (blocks)
$\|H\|$	The length of H	n	Indices total words in the plaintext.

1. INTRODUCTION

The exponential expansion of digital communication and the growing complexity of cyber-attacks have rendered traditional encryption methods insufficient. Consequently, modern research increasingly favors hybrid encryption models that combine multiple layers of protection, aiming to enhance complexity and security without significantly impacting performance. Traditional schemes such as Affinity ciphers, Huffman-based techniques, and graph-theoretic methods are examples of traditional systems that only partially answer the cryptography problem. None of them offer a thorough balance of transformation, compression, algebraic processing, and structural complexity. Our work suggests a hybrid symmetric cryptosystem that combines Cartesian product graphs, affine matrix transformations (executed through matrix multiplication), and Huffman coding in order to close this gap. Although it uses matrix multiplication for affine operations, this combination improves computational and structural security, provides

*Corresponding Author Institutional Email: ihsanmrasheed@uokerbala.edu.iq (Ihsan Mezher Rasheed)

greater resistance to statistical and brute-force attacks, and it is still computationally feasible for contemporary communication systems and resource-constrained settings.

2 .PREVIOUS WORKS

One foundational approach is presented by Beena Kittur et al. (Kittur et al., 2022), who proposed a symmetric encryption model based on Huffman coding combined with an affine transformation, achieving initial value obfuscation. In another direction, Marwah Ali Hussein Ali et al. (Hussein Ali et al., 2023) introduced a cryptographic model based on the Cartesian Product of Graphs (CPG), which enhanced structural encryption by mapping plaintext into graph-based representations. Furthermore, Hassan Rashed Yassein and Hadeel Hadi Abo-Alsood (Abo-Alsood & Yassein, 2021) introduced an enhanced NTRU encryption that boosts efficiency and security. To improve performance and defend against lattice-based assaults, their system makes use of sophisticated matrix operations. This connection is especially pertinent to our work because our proposed hybrid cryptosystem extends the reach of matrix-based cryptography into a multi-layered encryption framework by utilizing matrix multiplications, specifically through affine transformations, in conjunction with Huffman coding and Cartesian product graphs. Additional studies, such as that by Khalid Bekkaoui et al. (Bekkaoui et al., 2020), applied Hamiltonian cycles and divide-and-conquer strategies to graph-based encryption, offering a modular and scalable model for lightweight cryptographic applications. Similarly, P.A.S.D. Perera and G.S. Wijesiri (Perera & Wijesiri, 2021) explored encryption based on matrix graph transformations and key mixing, providing another dimension of cryptographic diffusion. Notably, Ahmed A. Omran et al. (Omran et al., 2024) investigated even sum edge domination in graphs, a concept that can inform the development of graph-based encryption schemes.

3. ESSENTIAL FACTS

Table 2. Standard ASCII Table: Complete Sequential Display(127–0)

Dec	Char	Dec	Char
0	NUL	...	...
1	SOH	32	SP (␣)
2	STX	33	!
...	...	...	...
65	A	97	a
...	...	...	...
122	z	125	}
123	{	126	~
124	|	127	DEL

Note: For character representation in this work, we will only use the first 127 characters (from decimal 0 to 126) of the conventional ASCII encoding. The last ASCII character (decimal value 127), which stands for the DEL (Delete) control character, will not be taken into account.

4. PROPOSED CRYPTOSYSTEM

Building upon these foundational works, this paper proposes a novel symmetric encryption model that unifies three independent security principles into a layered structure:

- Huffman coding for statistical compression and frequency masking,
- Affine matrix transformation for mathematical diffusion and value distortion,
- Cartesian product graph encoding for structural complexity and topological obfuscation.

The synergy of these layers results in a model that is computationally secure, structurally ambiguous, and highly adaptable. A comprehensive procedural description, mathematical foundation, and encryption/decryption example (using the word "mathematics") are presented.

The model's security is analyzed and compared to previous schemes to highlight its robustness and adaptability in modern applications such as secure graph communications, embedded systems, and the Internet of Things IoT.

4.1 Encryption Procedure

Shared Secret Keys (k_i, Leaf Levels, A, B, H_i)

PUBLIC PARAMETERS:

- In this scheme, each word in the plaintext is individually encrypted and transmitted along with its corresponding length (denoted by k_i)
- Leaf Levels: Depths of leaf nodes in the Huffman tree

Step 1: using English characters represented in ASCII Table 2., that are represented by numbers. The user can select a plaintext word or an English sentence made up of a few words, with 126 letters available for selection.

Step 2: The length of the plain text (k_i) has been added to each of these quantities individually, Modulo 127.

Step 3: A pseudo-Huffman tree is constructed where values derived from (the numerical output of the preceding encryption layer + k_i mod 127) are treated as frequency weights for symbolic nodes. This ensures that the Huffman tree's structure remains ambiguous to an unauthorized party, as its construction is based on a secret, intermediate encrypted value rather than the plaintext ASCII.

Step 4: Decimal equivalents are created using the prefix codes of the letters that were found to be leaves in the pseudo-Huffman tree.

Step 5: The sender transmits this ciphertext to the recipient by adding (each leaf's level to the decimal equivalent that was determined in step 3) modulo 127.

Step 6: The ciphertext resulting from the previous phase is segmented into multiple 2×2 matrices P_j. In cases where the total number of characters is not divisible by four (the matrix block size), padding is applied to fill the remaining positions in the final matrix. For consistency, the padding character is chosen as 'the letter x', and its corresponding ASCII value according to Table 2. is used during encryption.

Step 7: Using a Matrix Affine Transformation, the sender encrypts the ciphertext that was obtained in step 6 once more.
Matrix Affine Transformation is defined by the following equation:

$$C_j \equiv \left(A \times P_j + B\right) mod\ 127$$

Where:
A: Invertible transformation matrix (2×2).
B: Offset matrix (2×2).
P_i: is the matrix representation of the plaintext or the output from the previous encryption level (step 6).
.
Step 8: The numerical values obtained after encryption are first mapped back to their corresponding characters using the standard ASCII table. These characters are then used to construct the graph structure. Specifically, the encrypted characters are grouped into a primary set G, which represents the first component of the Cartesian product. A secondary set H, which is derived deterministically from a randomly chosen secret keyword, to form a secure foundation for the construction of the Cartesian product graph, by the following steps:

- Each character in the key corresponds to a unique vertex.
- An edge is drawn from each character to the next in sequence.
- This creates a linear path reflecting the exact order of the key characters.

Step 9: Computing the ciphertext as a Cartesian Product of Graphs (CPG) of two graphs, by the following steps:

1. The Cartesian product graph (CPG) of two simple graphs G and H is denoted as GH where: $V(GH) = \{(u, v): u \in V(G) \text{ and } v \in V(H)\}$
2. In this graph, the vertices (u, v) and (u', v') are adjacent if and only if one of the following conditions is satisfied:

   - **Condition 1**: u = u′ and v is adjacent to v' in H.
   - **Condition 2**: $v = v'$ and u is adjacent to u' in G.

Pseudocode Encryption Procedure
Input: Plaintext
Output: Final Ciphertext
Step 1: Convert charters to ASCII
Step 2: Add length of plain text (k_i) mod 127 to each value
Step 3: Build Pseudo-Huffman Tree using encrypted values as weights
Step 4: Convert binary prefix codes to decimals
Step5: Add leaf level to its decimal mod 127
Sept 6: if Length divisible by 4
Segment into 2x2 matrices
else Pad with 'x'
Segment into 2x2 matrices
end if
Step 7: Apply Affine Transform $C_j \equiv A \times P_j + B$ mod 127 to each matrix
Step 8: Map numbers to chars (G) and Construct Graph H from secret keyword
Step 9: Compute Cartesian Product Graph $G * H$ and get the final Ciphertext $GH = G * H$
End.

4.2 Decryption Procedure

To obtain plain text, execute these steps:

1. Extract the G and H sets from the Cartesian product graph.

2. Apply the inverse affine transformation.

3. Subtract leaf levels from numerical values to obtain the original Huffman decimal codes.

4. Convert decimal numbers into binary prefix codes.

5. Restore the original text with the Huffman tree.

5. EXAMPLE

5.1. Encryption Procedure

Step 1: Convert Plaintext to ASCII Values.

Each character in the input plaintext is translated to its matching ASCII code using Table 2.

Plaintext = Mathematics ASCII values:

$[77, 97, 116, 104, 101, 109, 97, 116, 105, 99, 115]$.

Step 2: Add Plaintext Length Modulo 127

length $k = 11$. Add k to each ASCII value (mod 127).

Modified values are:

$[88, 108, 0, 115, 112, 120, 108, 0, 116, 110, 126]$.

Step 3: Build a pseudo-Huffman tree from the values above.

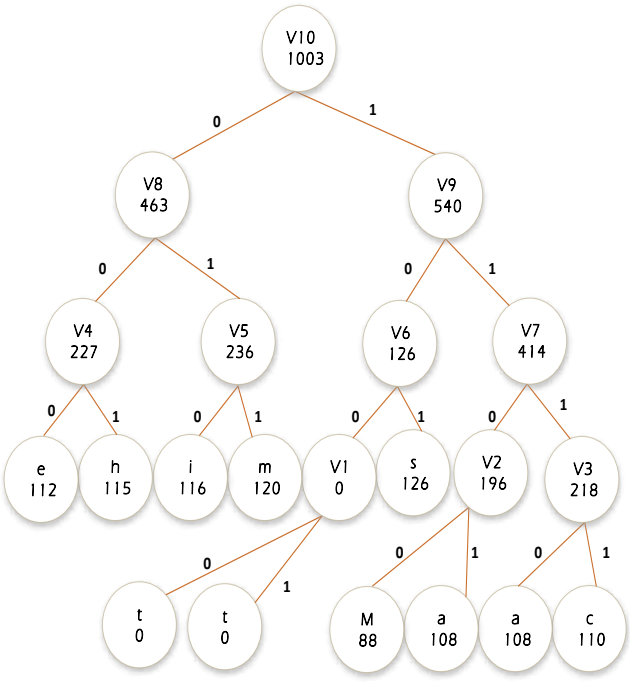

Figure 1. Convert Plaintext to ASCII Values

Table 3. Summarized steps (4 and 5)

Character	Huffman Code	Decimal	Leaf level	Encrypted values
M	1100	12	4	16
A	1101	13	4	17
T	1000	8	4	12
h	001	1	3	4
e	000	0	3	3
m	011	3	3	6
a	1110	14	4	18
t	1001	9	4	13
i	010	2	3	5
C	1111	15	4	19
S	010	5	3	8

Step 6: Form 2×2 Matrices

$$P_1 = \begin{pmatrix} M & a \\ t & h \end{pmatrix} \equiv \begin{pmatrix} 16 & 17 \\ 12 & 4 \end{pmatrix}$$

$$P_2 = \begin{pmatrix} e & m \\ a & t \end{pmatrix} \equiv \begin{pmatrix} 3 & 6 \\ 18 & 13 \end{pmatrix}$$

and $P_3 = \begin{pmatrix} i & c \\ s & x \end{pmatrix} \equiv \begin{pmatrix} 5 & 19 \\ 8 & 120 \end{pmatrix}$

Step 7: Apply Affine Matrix Transformation

Let $A = \begin{pmatrix} 3 & 3 \\ 1 & 2 \end{pmatrix}, B = \begin{pmatrix} 1 & 1 \\ 1 & 1 \end{pmatrix}$

Where $C_i \equiv (A \times P_i + B)\ mod\ 127$

$$C_1 \equiv (A \times P_1 + B)\ mod\ 127$$
$$\equiv \begin{pmatrix} 16 & 17 \\ 12 & 4 \end{pmatrix} \times \begin{pmatrix} 3 & 3 \\ 1 & 2 \end{pmatrix} + \begin{pmatrix} 1 & 1 \\ 1 & 1 \end{pmatrix} \text{ mod } 127$$
$$\equiv \begin{pmatrix} 66 & 83 \\ 41 & 45 \end{pmatrix} \text{ mod } 127$$

$$C_2 \equiv \begin{pmatrix} 3 & 6 \\ 18 & 13 \end{pmatrix} \times \begin{pmatrix} 3 & 3 \\ 1 & 2 \end{pmatrix} + \begin{pmatrix} 1 & 1 \\ 1 & 1 \end{pmatrix}$$
$$\equiv \begin{pmatrix} 16 & 22 \\ 36 & 81 \end{pmatrix} \text{ mod } 127$$

$$C_3 \equiv \begin{pmatrix} 5 & 19 \\ 8 & 120 \end{pmatrix} \times \begin{pmatrix} 3 & 3 \\ 1 & 2 \end{pmatrix} + \begin{pmatrix} 1 & 1 \\ 1 & 1 \end{pmatrix}$$

$$\equiv \begin{pmatrix} 35 & 54 \\ 145 & 265 \end{pmatrix} \bmod 127$$

$$\equiv \begin{pmatrix} 35 & 54 \\ 18 & 11 \end{pmatrix} \bmod 127$$

Therefore

$$C_1 \equiv \begin{pmatrix} B & S \\ ) & - \end{pmatrix}$$

$$C_2 \equiv \begin{pmatrix} DLE & SYN \\ \$ & Q \end{pmatrix}$$

$$C_3 \equiv \begin{pmatrix} \# & 6 \\ v & VT \end{pmatrix}$$

Mathematics → G =BS)DLESYN$Q#vVT

Steps (8 and **9)**

The encryption key H selected is **All2**.

Then, using the Cartesian product of graphs to generate a complicated encrypted graph to send it to the recipient as follows:

$$GH = G * H =$$

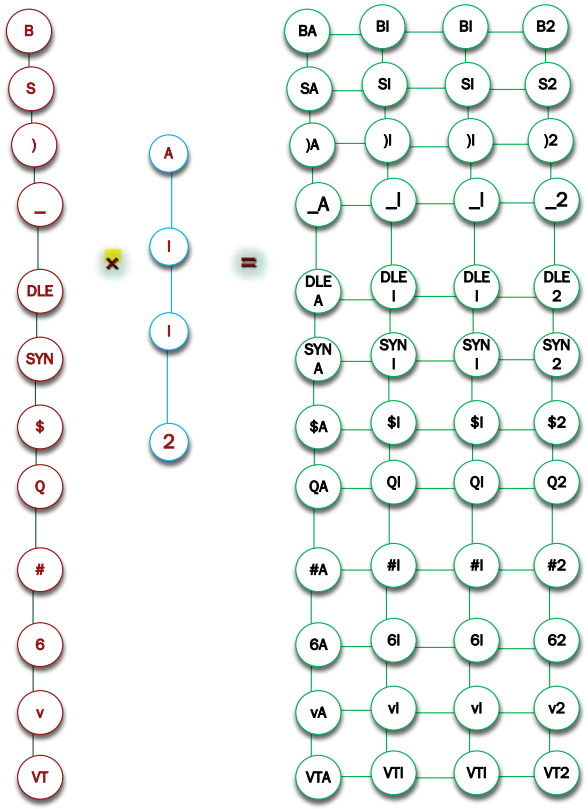

Figure 2. using the Cartesian product of graphs to generate a complicated encrypted graph to send it to the recipient

5.2. Decryption Procedure

Step 1: Retrieve the Cartesian Product GH Graph and decompose it into G and H and extract vertex values: G

Step 2: Convert data to numerical values, then recombine them into a 2×2 matrix from the flat list.

Step 3: Apply Inverse Affine Transformation

$$P_i \equiv (C_i - B) \times A^{-1} \, mod \, 127$$

Such

$$P_1 \equiv (C_1 - B) \times A^{-1} \, mod \, 127$$

$$\equiv \left(\begin{pmatrix} 66 & 83 \\ 41 & 45 \end{pmatrix} - \begin{pmatrix} 1 & 1 \\ 1 & 1 \end{pmatrix} \right) \times 3^{-1} \begin{pmatrix} 2 & -3 \\ -1 & 3 \end{pmatrix} \bmod 127$$

$$\equiv 85 \times \begin{pmatrix} 65 & 82 \\ 40 & 44 \end{pmatrix} \times \begin{pmatrix} 2 & -3 \\ -1 & 3 \end{pmatrix} \bmod 127$$

$$\equiv 85 \begin{pmatrix} 48 & 51 \\ 36 & 12 \end{pmatrix} \bmod 127$$

$$\equiv \begin{pmatrix} 16 & 17 \\ 12 & 4 \end{pmatrix} \bmod 127$$

Continuing the calculations to identify the remaining components.

Step 5: Subtract Leaf Levels

Step 6: Convert Decimal to Huffman Binary

Step 7: Decode Using Huffman Tree

Plaintext = Mathematics

6. SECURITY ANALYSIS

6.1. Resistance to Attacks

The proposed encryption model employs a multi-layered security architecture incorporating Huffman compression, affine matrix transformation, and Cartesian graph structures, which collectively strengthen its resistance to various types of cryptographic attacks:

- **Brute-force attacks** Brute-force attacks are computationally infeasible due to the exponentially large key space introduced by variable-length Huffman leaf levels, invertible affine matrix pairs, and complex graph combinations.
- **Statistical attacks** are mitigated through the Huffman compression step, which removes predictable frequency patterns commonly exploited by attackers.
- **Structural analysis attacks** are complicated by the final encoding into a Cartesian Product Graph (CPG), which effectively obfuscates

direct relationships between ciphertext and plaintext.

6.2. Cryptanalysis Perspective

Assuming the plaintext consists of n words $W_1, W_2,..., W_n$, each encrypted independently, the brute-force key space complexity is calculated as follows:

- Each word W_i has a length k_i, where $1 \leq k_i \leq 126$ (based on the usable ASCII range 0–126).
- The number of possible length combinations for n words is 126^n (since each k_i has 126 as a maximum possible value). This term (126^n) represents only the complexity of guessing the words' lengths, not the actual plaintext.
- In the affine transformation stage, we consider all possible combinations of transformation matrix A and offset matrix B:
  - For B: 127^4 possible 2×2 matrices (each element in $\boldsymbol{Z_{127}}$)
  - For A: The total number of invertible 2×2 matrix structures over $\boldsymbol{Z_{127}}$ (Morrison, 2006) is:

$$(127^2 - 1)(127^2 - 127)$$

Furthermore, the final encryption layer, which employs the Cartesian product of graphs, provides its own key space. If the number of vertices in the second graph H is $|H|$, then the Cartesian key space becomes: $\boldsymbol{126^{|H|}}$

6.3. Assumptions Clarification

Independence of Components: The calculation assumes that the encryption of each word and the transformations applied are independent of one another. This means that the choice of key for one component does not affect the others, allowing for a multiplicative combination of their respective key spaces.

- Choice of n: The variable n represents the number of words in the plaintext. The assumption is that this number can vary, and thus, the total key space scales exponentially with n.
- Choice of |H|: Similarly, |H| refers to the number of vertices in graph H. The assumption is that this can also vary, which impacts the Cartesian key space contribution.

Consequently, the total brute-force key space is the product of these components:

$$\begin{aligned} Total\ Key\ Space &= (Key\ Space\ for\ k_i) \\ &\times (Key\ Space\ for\ A\ and\ B) \\ &\times (Key\ Space\ for\ H) \end{aligned}$$

$$\begin{aligned} Total\ Key\ Space &= 126^n \times ((127^2 - 1)(127^2 \\ &- 127) \times 127^4 \times 126^{|H|} \end{aligned}$$

Such complexity is well beyond the capabilities of current high-performance computing systems.

6.4. Comparative Security Analysis

To strengthen the evaluation, we consider the following metrics:

Resistance to Specific Attacks: Analyzing how each model fares against known attack types, such as brute-force, statistical, and structural attacks.

Structural Complexity: Assessing the depth of structural security provided by each model, particularly in the context of data encoding and transformation.

- **Beena et al. (Affine + Huffman):** This model demonstrates effective compression and initial obfuscation. However, it lacks structural complexity. By introducing a topological encryption layer using CPGs, our model significantly enhances structural security.
- **Marwah et al. (CPG-only):** Their work emphasizes graph-based structural encoding but omits value transformation and frequency masking.
- Our hybrid model brings together all three security dimensions.
- **AES (Advanced Encryption Standard):** Although AES continues to be the gold standard in symmetric cryptography, our model offers specific advantages for scenarios involving structured data, such as encrypted graphs or network communications. Furthermore, it is flexible enough to support future integration with public-key systems or hardware-based enhancements.

7. CONCLUSION

This paper introduced a novel hybrid symmetric encryption scheme combining Huffman coding, affine matrix transformation, and the Cartesian product of graphs. The proposed method delivers high structural and computational security by blending data compression, algebraic transformation, and graph theory. The system proves resilient against brute-force and statistical attacks, and it holds promise for adaptable use in secure communications, structured data protection, and

lightweight cryptographic systems in constrained environments like IoT. Future research can explore how using the tensor product of graphs might improve the security of graph-based cryptographic systems, along with adding additional security mechanisms, and exploring extensions to public-key frameworks or hardware-level integration.

REFERENCES

Abo-Alsood, H. H., & Yassein, H. R. (2021). Design of an alternative NTRU Encryption with High Secure and Efficient. *International Journal of Mathematics and Computer Science*, *16*(4), 1469–1477.

Bekkaoui, K., Ziti, S., & Omary, F. (2020). A robust scheme to improving security of data using graph theory. *International Journal of Advanced Computer Science and Applications*, *11*(5).

Hussein Ali, M. A., Omran, A. A., & Ajeena, R. K. K. (2023). The cartesian product graph for encryption schemes. *AIP Conference Proceedings*, *2591*(1), 1–9.

Kittur, B., Kumari, D. C., Kulkarni, S. G., & KM, M. (2022). Super-Encryption Method using Affine Transform Via Trees. *International Journal of Mathematics Trends and Technology-IJMTT*, *68*(6), 190–194.

Morrison, K. E. (2006). Integer sequences and matrices over finite fields. *Journal of Integer Sequences*, *9*(06.2.1), 1–28.

Omran, A. A., Rasheed, I. M., Obaid, S. A., & Talib, R. H. (2024). Even Sum Edge Domination in Graph. *Pure Sciences International Journal of Kerbala*, *1*(4), 59–63.

Perera, P., & Wijesiri, G. S. (2021). Encryption and decryption algorithms in symmetric key cryptography using graph theory. *Psychology and Education Journal*, *58*(1), 3420–3427.

0096477699201 65
https://journals.uokerbala.edu.iq
Iraq - Holy Karbala